

NACA TM 1369

7940



NATIONAL ADVISORY COMMITTEE FOR AERONAUTICS

TECHNICAL MEMORANDUM 1369

FLAT PLATE CASCADES AT SUPERSONIC SPEED

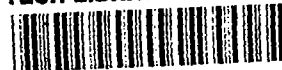
By Rashad M. El Badrawy

Translation of "Ebene Plattengitter bei Überschallgeschwindigkeit."
Mitteilungen aus dem Institut für Aerodynamik
an der E.T.H., no. 19, 1952



Washington

May 1956



	Page
PREFACE	iii
INTRODUCTION	1
CHAPTER I. THE FLAT PLATE	4
1. General Considerations - Stipulations	4
2. Conditions at Expansion Around a Corner	6
3. Conditions of Oblique Compression Shock	8
4. Lift and Drag of an Infinitely Thin Plate (Exact Solution)	10
5. Lift and Drag at High Mach Numbers	13
6. Calculation of Lift and Drag by Linearized Theory	15
7. Comparison of the Results of the Linearized Theory With Those of the Exact Method	18
CHAPTER II. INTERSECTION, OVERTAKING AND REFLECTION OF COMPRESSION SHOCKS AND EXPANSION WAVES	19
1. Introduction	19
2. Small Variations	19
3. Overtaking of Compression Shock and Expansion Wave	22
4. Intersection of Compression Shock and Expansion Wave	26
5. Crossing of Expansion Waves	31
6. Reflection of Compression Shocks and Expansion Waves	33
CHAPTER III. THE CASCADE PROBLEM	34
1. Problem	34
2. Method of Calculation	34
3. Example	35
4. Calculation of Thrust, Tangential Force and Efficiency	37
CHAPTER IV. LINEARIZED CASCADE THEORY	40
1. Assumptions	40
2. Linearization of Cascade Problem	40
3. Calculation of Lift and Drag	41
4. Numerical Example	44
5. Comparison With Exact Method	45
CHAPTER V. SCHLIEREN PHOTOGRAPHS OF CASCADE FLOW	46
1. Cascade Geometry	46
2. Experimental Setup	47
3. Schlieren Photographs	47
CHAPTER VI. THE FLAT PLATE CASCADE AT SUDDEN ANGLE-OF-ATTACK CHANGE	49
1. Problem	49
2. The Unsteady Source	50

	Page
3. Pressure and Velocity of a Periodically Arising Source Distribution	52
4. Single Flat Plate in a Vertical Gust (Biot 1945)	59
5. The Straight Cascade	61
6. Numerical Example	67
CHAPTER VII. EFFICIENCY OF A SUPERSONIC PROPELLER	71
1. Introduction	71
2. Effect of Friction on Cascade Efficiency	71
3. Effect of Thickness	73
4. Appraisal of the Efficiency of a Supersonic Propeller	74
SUMMARY	77
REFERENCES	78
TABLES	79
FIGURES	91

PREFACE

The work on the present report was carried out at the Institute for Aerodynamics of the E.T.H., Zürich, under the direction of Prof. Dr. Ackeret, during the time from December 1949 to June 1951.

I want to express here my deep gratitude to Prof. Ackeret for his suggestions and for the great interest he took in my work.

I am very grateful to Dipl.-Eng. B. Chaix, scientific assistant at the Institute, and to Mr. E. Hurlimann, precision mechanic, for their indispensable help in taking the schlieren pictures.

I should like to acknowledge that the "Faruk University", Alexandria (Egypt) made my studies in Zürich possible.

NATIONAL ADVISORY COMMITTEE FOR AERONAUTICS

TECHNICAL MEMORANDUM 1369

FLAT PLATE CASCADES AT SUPERSONIC SPEED*

By Rashad M. El Badrawy

INTRODUCTION

The cascade problem in the subsonic range can be analyzed under certain assumptions either by mapping or substitution of the blades by singularities - sources, sinks and bound vortices - where the separation of flow from the blades can cause various departures from the obtained results.

Raising the flow velocity to a given value is accompanied by sonic velocity within the cascade, which usually renders the solution of the problem even more difficult. The same complication exists on the cascade in flow at supersonic speed, in which the velocity is retarded to subsonic by shocks.

But when the cascade operates entirely in the supersonic range, the conditions become clearer. All disturbances act downstream only from the sources of disturbance, so that the pressures and velocities at the surface of a sufficiently thin airfoil in the stream can be readily determined.

The present report deals exclusively with problems of cascade flow in the supersonic range. As is known the flat infinitely thin plate is the best airfoil with respect to wave resistance in supersonic flows; hence it is logical to start with the cascade of flat plates. The last chapter deals with the case of finite thickness.

Lift and wave resistance of an isolated plate are computed first since the cascade problem can often be reduced to this special case. The well-known theories of two-dimensional supersonic flow are applied - that is, the laws of oblique compression shocks and the expansion around a corner.

The air forces are then calculated again and compared with the previously obtained exact values by means of Ackeret's formulas of linearized theory.

*"Ebene Plattengitter bei Überschallgeschwindigkeit." Mitteilungen aus dem Institut für Aerodynamik an der E.T.H., no. 19, 1952.

The cascade problem was to be solved in such a way as to be free from the inevitable inaccuracies of the graphical method. For this reason the cases of overtaking, crossing and reflection of compression shocks and expansion waves frequently occurring on supersonic cascade flows, which usually are solved by graphical method, are analyzed in chapter II.

In chapter III the cascade problem is discussed and its solution described in the light of the results obtained in chapter II. A numerical example is also given. The same chapter gives further a definition of the efficiency of the simple supersonic cascade and an evaluation for several angles of stagger and attack.

The small angles of attack involved justified the use of a linearized cascade theory.¹ This is done in chapter IV. The numerical example of chapter III is thus linearized and the results compared with those of the exact solution. The supersonic cascade flow at various angles of attack was recorded by schlieren photographs of the flow between two parallel plates, in the high-speed wind tunnel of the Institute (chapter V).

Chapter VI deals with the specific case of unsteady flow through the cascade, caused by abrupt angle-of-attack changes.

¹According to Ackert's linearized theory, the lift and drag of a double-wedge profile of thickness d and chord l at angle ψ in supersonic flow M is, in the presence of friction (c_f)

$$c_a = \frac{4\psi}{\sqrt{M^2 - 1}} \quad c_w = \frac{4}{\sqrt{M^2 - 1}} \left[\psi^2 + \left(\frac{d}{l} \right)^2 + 2c_f \frac{\sqrt{M^2 - 1}}{4} \right]$$

For the best drag-lift ratio $\epsilon = \frac{c_w}{c_a}$, put $\frac{d\epsilon}{d\psi} = 0$. This means that the wave resistance should be equal to the sum of friction drag and thickness effect. In that event

$$\begin{aligned} \psi_{\text{opt}} &= \sqrt{\left(\frac{d}{l} \right)^2 + 2c_f \frac{\sqrt{M^2 - 1}}{4}} \\ c_{w\text{opt}} &= \frac{8\psi_{\text{opt}}^2}{\sqrt{M^2 - 1}} = \frac{8}{\sqrt{M^2 - 1}} \left[\left(\frac{d}{l} \right)^2 + 2c_f \frac{\sqrt{M^2 - 1}}{4} \right] \\ \epsilon_{\text{opt}} &= 2\psi_{\text{opt}} = 2\sqrt{\left(\frac{d}{l} \right)^2 + 2c_f \frac{\sqrt{M^2 - 1}}{4}} \end{aligned}$$

Assuming possible values for d/l and c_f results in comparatively small optimum angles ψ_{opt} .

In chapter VII the effect of friction and thickness in a special case on the cascade efficiency is analyzed. Since there might be a possible application of the supersonic cascade to the supersonic propeller, a simple evaluation of the efficiency of such a propeller is made. A parallel steady two-dimensional flow is - with exception of chapter VI - postulated.

The conventional notation is used unless specifically stated otherwise in the text.

CHAPTER I. THE FLAT PLATE

1. General Considerations - Stipulations

The general equation of continuity of any compressible flow is

$$\frac{\partial \rho}{\partial t} + \frac{\partial(\rho u)}{\partial x} + \frac{\partial(\rho v)}{\partial y} + \frac{\partial(\rho w)}{\partial z} = 0 \quad (1)$$

The rate of propagation of a small disturbance, that is, the sonic velocity, is, as is known

$$a^2 = \frac{\partial p}{\partial \rho} = \kappa \frac{p}{\rho} \quad (2)$$

where $\kappa = \frac{c_p}{c_v}$.

In flows, in which a flow potential ϕ exists, the continuity equation can be written as

$$\frac{1}{\rho a^2} \left(\frac{\partial p}{\partial t} + \frac{\partial \phi}{\partial x} \frac{\partial p}{\partial x} + \frac{\partial \phi}{\partial y} \frac{\partial p}{\partial y} + \frac{\partial \phi}{\partial z} \frac{\partial p}{\partial z} \right) + \frac{\partial^2 \phi}{\partial x^2} + \frac{\partial^2 \phi}{\partial y^2} + \frac{\partial^2 \phi}{\partial z^2} = 0 \quad (3)$$

The momentum theorem gives the following relations

$$\left. \begin{aligned} -\frac{1}{\rho} \frac{\partial p}{\partial x} &= \frac{\partial^2 \phi}{\partial x \partial t} + \frac{\partial \phi}{\partial x} \frac{\partial^2 \phi}{\partial x^2} + \frac{\partial \phi}{\partial y} \frac{\partial^2 \phi}{\partial x \partial y} + \frac{\partial \phi}{\partial z} \frac{\partial^2 \phi}{\partial x \partial z} \\ -\frac{1}{\rho} \frac{\partial p}{\partial y} &= \frac{\partial^2 \phi}{\partial y \partial t} + \frac{\partial \phi}{\partial x} \frac{\partial^2 \phi}{\partial y \partial x} + \frac{\partial \phi}{\partial y} \frac{\partial^2 \phi}{\partial y^2} + \frac{\partial \phi}{\partial z} \frac{\partial^2 \phi}{\partial y \partial z} \\ -\frac{1}{\rho} \frac{\partial p}{\partial z} &= \frac{\partial^2 \phi}{\partial z \partial t} + \frac{\partial \phi}{\partial x} \frac{\partial^2 \phi}{\partial z \partial x} + \frac{\partial \phi}{\partial y} \frac{\partial^2 \phi}{\partial z \partial y} + \frac{\partial \phi}{\partial z} \frac{\partial^2 \phi}{\partial z^2} \end{aligned} \right\} \quad (4)$$

In two-dimensional flow the potential must therefore satisfy the equation

$$\frac{\partial^2 \phi}{\partial x^2} \left[1 - \frac{1}{a^2} \left(\frac{\partial \phi}{\partial x} \right)^2 \right] + \frac{\partial^2 \phi}{\partial y^2} \left[1 - \frac{1}{a^2} \left(\frac{\partial \phi}{\partial y} \right)^2 \right] - \frac{2}{a^2} \frac{\partial \phi}{\partial x} \frac{\partial \phi}{\partial y} \frac{\partial^2 \phi}{\partial x \partial y} - \frac{2}{a^2} \frac{\partial \phi}{\partial x} \frac{\partial^2 \phi}{\partial x \partial t} - \frac{2}{a^2} \frac{\partial \phi}{\partial y} \frac{\partial^2 \phi}{\partial y \partial t} - \frac{1}{a^2} \frac{\partial^2 \phi}{\partial t^2} = 0 \quad (5)$$

The velocity of sound is then

$$a^2 = a_0^2 - (\kappa - 1) \left\{ \frac{1}{2} \left[\left(\frac{\partial \phi}{\partial x} \right)^2 + \left(\frac{\partial \phi}{\partial y} \right)^2 \right] + \frac{\partial \phi}{\partial t} \right\} \quad (6)$$

where a_0 = velocity of sound in state of rest.

For the steady case, the equation is reduced to

$$\frac{\partial^2 \phi}{\partial x^2} \left[1 - \frac{1}{a^2} \left(\frac{\partial \phi}{\partial x} \right)^2 \right] + \frac{\partial^2 \phi}{\partial y^2} \left[1 - \frac{1}{a^2} \left(\frac{\partial \phi}{\partial y} \right)^2 \right] - \frac{2}{a^2} \frac{\partial \phi}{\partial x} \frac{\partial \phi}{\partial y} \frac{\partial^2 \phi}{\partial x \partial y} = 0 \quad (7)$$

and the flow is completely identified, if the function $\phi(x,y)$, which is to satisfy the boundary conditions, is determined.

This equation is either elliptic, parabolic, or hyperbolic, depending upon

$$(1 - M^2) \lessgtr 0$$

where

$$M = \frac{1}{a} |\text{grad}| \phi \quad (8)$$

is the local Mach number.

The use of this equation is difficult if its type in the particular range, as in the transonic range, is changed. However, the flows analyzed here, are of identical character everywhere, that is, the flow is of the hyperbolic type.

One of the known solutions is the expansion around a corner, developed by Prandtl and Meyer (ref. 1).

2. Conditions at Expansion Around a Corner

The two-dimensional flow past the wall AE at a Mach number M_1 (fig. 1) is deflected by a convex bend at E through an angle Θ , through which an expansion is initiated. The disturbance proceeding from E spreads out solely in the range lying downstream of the Mach line EB_1 , where

$$\angle B_1EA' = \text{Mach angle} \quad \mu_1 = \sin^{-1} \frac{1}{M_1} \quad (9)$$

and stops at the Mach line EB_2 , where

$$\angle B_2ED = \mu_2 = \sin^{-1} \frac{1}{M_2}$$

In it M_2 is the Mach number of the flow after the expansion.

The streamlines in range B_1EB_2 are curved similarly and run parallel to the wall ED downstream of this range.

It can be proved that the Mach lines in this flow are the characteristics of the differential equation which define the potential.

When the expansion proceeds from a Mach number $M_1 = 1$, $\left(\mu_1 = \frac{\pi}{2}\right)$, the following relations can be proved (ref. 2):

$$\tan \mu_2 = \lambda \cot \lambda \alpha \quad (10)$$

$$\left(\lambda = \sqrt{\frac{\kappa - 1}{\kappa + 1}} \right)$$

$$\frac{p_2}{p_0} = \left(\frac{\kappa + 1}{2 \cos^2 \lambda \omega} \right)^{-\frac{\kappa}{\kappa-1}} \quad (11)$$

(p_0 = stagnation pressure)

$$M_2 = \sqrt{\frac{(\kappa + 1) - 2 \cos^2 \lambda \omega}{(\kappa - 1) \cos^2 \lambda \omega}} \quad (12)$$

Obviously

$$\Theta = \omega + \mu_2 - \frac{\pi}{2} \quad (13)$$

As function of M_2 (ref. 3)

$$\Theta = \left[\cos^{-1} \frac{1}{M_2} + \frac{1}{2} \lambda \cos^{-1} \left(1 - \frac{\kappa + 1}{1 + \frac{\kappa - 1}{2} M_2^2} \right) \right] \quad (14)$$

This equation gives a maximum angle of expansion Θ_{\max} , which corresponds to a Mach number $M_2 = \infty$ after expansion ($\kappa = 1.400$)

$$\Theta_{\max} = 130.45^\circ$$

If the Mach number before the expansion M_1 is assumed other than 1, the maximum angle of expansion becomes obviously

$$\Theta_{\max M_1} = \Theta_{\max} - \nu$$

where ν is the angle of expansion from $M = 1$ to M_1 . The values for various Mach numbers of the inflow (M_1) are

M_1	1.00	1.50	2.00	2.50	5	8	10	∞
$\Theta_{\max M_1}^\circ$	130.45	118.55	104.07	91.32	53.55	34.53	28.14	0

3. Conditions of Oblique Compression Shock

The discontinuities that may appear in supersonic flows and across which velocity, pressure, density, temperature, and entropy undergo a discontinuity, while the total energy, thermic and mechanical, remains constant, were predicted by Riemann (1860) and Rankine and Hugoniot (1887) as normal compression shocks.

In oblique shocks (Prandtl-Meyer) only the velocity component normal to the shock front is modified.

In figure 2 the supersonic flow past the wall AE is deflected at E by an angle δ . A compression shock is produced and the shock front ES is inclined at an angle γ - the shock angle - toward the air flow direction.

With subscript 1 denoting the state before the shock and subscript 2 that after the shock it can be proved that (refs. 3 and 4)

$$\frac{p_2}{p_1} = \frac{2\kappa}{\kappa + 1} \left(M_1^2 \sin^2 \gamma - \frac{\kappa - 1}{2\kappa} \right) \quad (15)$$

$$\frac{p_2}{p_0} = \frac{\kappa - 1}{\kappa + 1} \left(\frac{p_1}{p_0} \right)^{\frac{1}{\kappa}} \left\{ \frac{4\kappa}{(\kappa + 1)^2} \sin^2 \gamma - \left(\frac{\kappa - 1}{\kappa + 1} \right)^2 \left[1 + \frac{4\kappa}{(\kappa - 1)^2} \sin^2 \gamma \right] \left(\frac{p_1}{p_{01}} \right)^{\frac{\kappa - 1}{\kappa}} \right\} \quad (16)$$

$$\frac{\rho_1}{\rho_2} = \frac{2}{\kappa + 1} \left(\frac{1}{M_1^2 \sin^2 \gamma} + \frac{\kappa - 1}{2} \right) \quad (17)$$

$$\cot \delta = \left(\frac{\kappa + 1}{2} \frac{M_1^2}{M_1^2 \sin^2 \gamma - 1} - 1 \right) \tan \gamma \quad (18)$$

$$\frac{u_2}{u_1} = \frac{\cos \gamma}{\cos(\gamma - \delta)} \quad (19)$$

$$\frac{\tan(\gamma - \delta)}{\tan \delta} = \frac{\rho_1}{\rho_2'} = \frac{1}{\frac{\kappa + 1}{2} \left[\frac{1}{M_2^2 \sin^2(\gamma - \delta)} + \frac{\kappa - 1}{2} \right]} \quad (20, 21)$$

A direct relation between the Mach numbers before and after the shock can be established

$$\frac{M_2'}{M_1} = \frac{\cos \gamma}{\cos(\gamma - \delta)} \sqrt{\frac{\rho_2'/\rho_1}{p_2'/p_1}} \quad (22)$$

The relation for the change of the static pressure by the shock is the same as for the normal shock when it is applied to the velocity component perpendicular to the shock front. Consequently

$$\frac{p_{02}'}{p_{01}} = \left(\frac{\frac{\kappa + 1}{2} M_1^2 \sin^2 \gamma}{1 + \frac{\kappa - 1}{2} M_1^2 \sin^2 \gamma} \right)^{\frac{\kappa}{\kappa - 1}} \left(\frac{2\kappa}{\kappa + 1} M_1^2 \sin^2 \gamma - \frac{\kappa - 1}{\kappa + 2} \right)^{\frac{1}{1 - \kappa}} \quad (23)$$

From these equations it follows that the shock angle γ is greater than the Mach angle, that is, the speed of propagation of a finite disturbance is greater than the sonic velocity. When the angle of deflection δ approaches zero, $\gamma = \mu$ and the shock changes to a Mach wave.

Also of interest is the shock angle at which the Mach number after the minimum shock becomes equal to unity. Denoting this angle by γ_s it can be proved (the weak stable compression shock is always allowed for) (ref. 3, p. 47) that

$$\left(1 - \sin^2 \gamma_s\right) \left(2 \sin^2 \gamma_s - \frac{1}{M_1^2}\right) = \left(\sin^2 \gamma_s - \frac{1}{M_1^2}\right) \left[1 - \frac{2}{\kappa + 1} \left(\sin^2 \gamma_s - \frac{1}{M_1^2}\right)\right] \quad (24)$$

This equation is used to determine the maximum shock angle which corresponds to a Mach number before the shock $M_1 = \infty$ and a Mach number $M_2' = 1$ after the shock. The result is

$$\sin^2 \gamma_s = \frac{\kappa + 1}{2\kappa} \quad (25)$$

hence

$$\gamma_s = 67.8^\circ$$

at $\kappa = 1.400$ (air).

By equation (18) the corresponding deflection angle δ_s is

$$\delta_s = 45.58^\circ$$

Table 1 and figure 3 represent the values of γ_s and δ_s ² at various Mach numbers M_1 .

4. Lift and Drag of an Infinitely Thin Plate (Exact Solution)

An infinitely thin plate ab in parallel flow at supersonic velocity U_1 is placed at the angle ψ . It is assumed that the width of the plate transverse to the flow direction is ∞ , so that the problem is two dimensional.

The streamlines above oa (fig. 4) experience a deflection which is associated with an expansion. So the state at the upper side of the plate can be defined by equations (10) to (14). But below the plate a compression shock ad occurs. The state of the flow on the lower side of the plate is accordingly determined from the formulas (16) to (21).

The force on the plate per unit area is

$$K = (p_2' - p_2) \quad (26)$$

²The weak stable shock is always taken into account. See Richter, ZAMM, 1948 and Thomas, Proc. N.A. Sc., Nov. 1948.

where p_2' and p_2 represent the pressure on the lower and upper side of the plate.

Obviously, the lift A and the drag W per unit width are

$$A = K \cos \psi L \quad (27)$$

$$W = K \sin \psi L \quad (28)$$

To compute a lift coefficient, a reference dynamic pressure of the inflow

$$q_1 = \frac{1}{2} \rho_1 u_1^2$$

or

$$q_1 = \frac{\kappa}{2} p_1 M_1^2 \quad (29)$$

is utilized.

As function of the Mach number M_1 , the ratio of dynamic to airstream pressure is

$$\frac{q_1}{p_1} = \frac{\kappa}{2} M_1^2$$

that of dynamic to stagnation pressure is

$$\frac{q_1}{p_0} = \frac{\kappa}{2} \frac{p_1}{p_0} M_1^2 = \frac{\kappa}{2} M_1^2 \left(\frac{\kappa - 1}{2} M_1^2 + 1 \right)^{\frac{\kappa}{1-\kappa}} \quad (30)$$

The results are represented in table 1 and figure 5.

Lift and drag coefficients are herewith

$$\left. \begin{aligned} c_a &= \frac{A}{q_1 l} = \frac{p_2' - p_2}{q_1} \cos \psi \\ c_w &= \frac{W}{q_1 l} = \left(\frac{p_2' - p_2}{q_1} \right) \sin \psi \end{aligned} \right\} \quad (31)$$

or, if all pressures are referred to stagnation pressure p_0 ,

$$c_a = \left[\frac{\left(\frac{p_2'}{p_0} - \frac{p_2}{p_0} \right)}{\frac{q_1}{p_0}} \right] \cos \psi \quad c_w = \left[\frac{\left(\frac{p_2'}{p_0} - \frac{p_2}{p_0} \right)}{\frac{q_1}{p_0}} \right] \sin \psi \quad (32)$$

The drag/lift ratio is

$$\epsilon = \frac{c_w}{c_a} = \tan \psi \quad (33)$$

Table 2 gives the values of c_a , c_w , and ϵ up to $M_1 = 10$ as computed by the formulas (32) and (33).

In the calculation of the Mach numbers up to $M_1 = 4$, the tables by Keenan and Kaye (ref. 6) as well as those by Ferri (ref. 3) were used to define p_2/p_0 and p_2'/p_1 ($\kappa = 1.400$).

For higher Mach numbers, the formulas of sections 2 and 3 were employed. At each Mach number, the angle of attack was varied up to $\psi_s (M_2' = 1)$.

Figures 6 and 7 show the variation of c_w and c_a over the angle of attack ψ ; figure 8 shows the polars c_a plotted against c_w .

The boundary curves show the maximum lift and drag coefficients that can be expected without getting in the transonic range.

Other values for the boundary curve are given in table 3. Since the pressure distribution on the upper and lower side is constant, the resultant force is applied at plate center and is normal to the plate. There is no suction force as in subsonic flow.

5. Lift and Drag at High Mach Numbers

At high Mach numbers the angle of attack of the plate can exceed the maximum expansion angle Θ_{\max} (section 2) corresponding to the Mach number of the airstream $\Theta_{\max} = \psi_s$ at $M_1 \cong 6.4$). Hence, when assuming continuous flow, an empty wedge-shaped zone between plate and flow appears. This zone is largest at constant angle of attack when $M_1 = \infty$. In that event, no deflection of flow is possible.

Owing to this vacuum space, the pressure at the upper side is zero. The resultant force K is obtained then from the pressure on the lower side, behind the compression shock. Hence, per unit area

$$K = p_2' \quad (34)$$

or, when referred to the dynamic pressure of the airstream,

$$\frac{K}{q_1} = \frac{p_2'}{q_1} = \frac{2}{\kappa M_1^2} \frac{p_2'}{p_1} \quad (35)$$

Introducing p_2'/p_1 from equation (15) gives

$$\frac{K}{q_1} = \frac{4}{\kappa + 1} \sin^2 \gamma - \frac{\kappa - 1}{\kappa + 1} \frac{2}{\kappa M_1^2}$$

where the term containing $1/M_1^2$ can be disregarded without great error.

$$\frac{K}{q_1} = \frac{4}{\kappa + 1} \sin^2 \gamma \quad (36)$$

So the lift and drag coefficient are

$$\left. \begin{aligned} c_a &= \frac{4}{\kappa + 1} \sin^2 \gamma \cos \psi \\ c_w &= \frac{4}{\kappa + 1} \sin^2 \gamma \sin \psi \end{aligned} \right\} \quad (37)$$

Both formulas are dependent on γ and ψ only. Between these there exist the relation given in equation (18), which can be written as follows ($\delta = \psi$):

$$\cot \psi = \left(\frac{\kappa + 1}{2} \frac{1}{\sin^2 \gamma - \frac{1}{M_1^2}} - 1 \right) \tan \gamma$$

where the term $\frac{1}{M_1^2}$ can be disregarded again. Then

$$\cot \psi = \left(\frac{\kappa + 1}{2 \sin^2 \gamma} - 1 \right) \tan \gamma \quad (38)$$

The values and curves designated with $M = \infty$ in table 2 and figures 6, 7 and 8 were defined by equations (37) and (38). For comparison the lift and drag was also computed by Newton's formula (the normal component)

$$\left. \begin{aligned} c_a &= 2 \sin^2 \psi \cos \psi \\ c_w &= 2 \sin^3 \psi \end{aligned} \right\} \quad (39)$$

The corresponding values and curves carry the subscript N.

6. Calculation of Lift and Drag by Linearized Theory

According to Ackert's linearized theory, the members of higher order in $\frac{\partial \phi}{\partial y}$ can be disregarded without great error in the potential equation

$$\frac{\partial^2 \phi}{\partial x^2} \left[1 - \frac{1}{a^2} \left(\frac{\partial \phi}{\partial x} \right)^2 \right] + \frac{\partial^2 \phi}{\partial y^2} \left[1 - \frac{1}{a^2} \left(\frac{\partial \phi}{\partial y} \right)^2 \right] - \frac{2}{a^2} \frac{\partial \phi}{\partial x} \frac{\partial \phi}{\partial y} \frac{\partial^2 \phi}{\partial x \partial y} = 0$$

for slender bodies at small angles of attack, because the interference flows are small compared to that of the airstream.

The equation reads accordingly

$$\frac{\partial^2 \phi}{\partial x^2} \left[1 - \frac{1}{a^2} \left(\frac{\partial \phi}{\partial x} \right)^2 \right] + \frac{\partial^2 \phi}{\partial y^2} = 0$$

Inserting

$$\frac{1}{a^2} \left(\frac{\partial \phi}{\partial x} \right)^2 = M^2$$

and observing that M is greater than unity, the equation reads

$$\frac{\partial^2 \phi}{\partial x^2} (M^2 - 1) - \frac{\partial^2 \phi}{\partial y^2} = 0 \quad (40)$$

The general solution of this equation is

$$\phi = f \left(x - y \sqrt{M^2 - 1} \right) \quad (41)$$

It indicates, as stated in section 2, that the lines of constant potential are the Mach lines of flow, and their slope has the Mach angle μ .

This solution shows further that the flow velocities

$$u = \frac{\partial \phi}{\partial x} \quad \text{and} \quad v = \frac{\partial \phi}{\partial y}$$

satisfy the condition

$$u = - \frac{v}{\sqrt{M^2 - 1}} \quad (42)$$

At the surface of a body in the stream

$$\frac{u}{U} = \frac{dy}{dx}$$

is applicable.

The pressure variation by the momentum equation reads

$$\frac{\Delta p}{\rho} = - U \Delta U = - U u \quad (43)$$

where U is flow velocity and u is interference flow in stream direction.

Accordingly

$$\frac{\Delta p}{\frac{1}{2} \rho U^2} = \frac{4}{\sqrt{M^2 - 1}} \frac{dy}{dx} \quad (44)$$

The pressure difference between both sides of a flat plate is

$$\frac{\Delta p}{q} = \frac{4}{\sqrt{M^2 - 1}} \frac{dy}{dx} \quad (45)$$

The lift and drag coefficients at the angles in question are

$$\left. \begin{aligned} c_a &= \frac{4\psi}{\sqrt{M^2 - 1}} \\ c_w &= \frac{4\psi^2}{\sqrt{M^2 - 1}} \end{aligned} \right\} \quad (46)$$

The drag/lift ratio according to this theory is

$$\epsilon = \frac{c_w}{c_a} = \psi \quad (47)$$

Instead of the expansion wave and the compression shock at the leading edge, it has simple Mach lines as interference lines (fig. 9), in contrast to the exact theory.

The values given in table 4 and plotted in figures 10 and 11 were computed by these formulas. The calculations were carried out at each Mach number up to angle of attack ψ_s - from the exact theory. The corresponding c_a and c_w values lie on the curve G' .

At sonic velocity on the lower side of the plate $p_2'/p_0 = 0.5283$. This value, introduced in the following directly obtainable relation

$$p_2' - p_1 = \frac{1}{2} \Delta p = \frac{2\psi q_1}{\sqrt{M_1^2 - 1}} \quad (48)$$

and

$$\frac{p_2'/p_0 - p_1/p_0}{q_1/p_0} = \frac{2\psi}{\sqrt{M_1^2 - 1}}$$

gives the angle of attack (ψ_{s1}) corresponding to $M_2' = 1$, which in general is greater than ψ_s .

7. Comparison of the Results of the Linearized Theory With

Those of the Exact Method

In table 5, the difference is ($c_G - c_L$), where c_G is the coefficient of the exact method and c_L is that of the linearized theory at Mach numbers $M_1 = 1.40$ and $M_1 = 5.00$.

It follows that the linearized theory is a very good approximation for small angles (up to about 10°). For greater angles the values of c_a and c_w are too small.

In figures 6 and 7, the c_a and c_w curves by linearized theory marked A' and A are included for comparison.

CHAPTER II. INTERSECTION, OVERTAKING AND REFLECTION OF COMPRESSION SHOCKS AND EXPANSION WAVES

1. Introduction

Overtaking of expansion waves and compression shocks in supersonic flows occurs when the marginal streamlines - or boundary walls - change their direction twice in the opposite sense (fig. 12(a)).

If expansion waves or compression shocks strike a fixed wall and their slope toward the wall does not exceed a given angle, they are reflected as expansion waves or compression shocks (fig. 12(c)). Crossings occur in flows through channels and free jets (fig. 12(b)). All these events can occur in cascade flows (fig. 12(d)).

2. Small Variations

(a) Suppose that a small expansion occurs at B in the supersonic flow M_1 , p_1 , a_1 , ρ_1 past the wall AB (fig. 13). The angle of expansion is $\Delta\theta$. If $\Delta\theta$ is sufficiently small, differential considerations are permissible.

Bernoulli's equation gives

$$\Delta p_1 = - \rho_1 U_1 \Delta U_1 \quad (49)$$

where U is the magnitude of the velocity and ΔU its variation; Δp is the pressure variation.

Since the vectorial velocity variation is normal to the interference line, the variation of U is

$$\Delta |U| = U_1 \tan \mu_1 \Delta\theta = \frac{U_1 \Delta\theta}{\sqrt{M_1^2 - 1}} \quad (50)$$

hence

$$\Delta p = - \frac{\rho_1 U_1^2 \Delta \theta}{\sqrt{M_1^2 - 1}} \quad (51)$$

But, as the dynamic pressure q is given by

$$q = \frac{1}{2} \rho_1 U_1^2 = \frac{1}{2} \kappa p_1 M_1^2$$

the pressure variation can be written as

$$\Delta p = - \frac{\kappa p_1 M_1^2 \Delta \theta}{\sqrt{M_1^2 - 1}} \quad (52)$$

The variation of the Mach number M follows at (ref. 3, p. 26)

$$\Delta M = \frac{M_1}{\sqrt{M_1^2 - 1}} \left(1 + \frac{\kappa - 1}{2} M_1^2 \right) \Delta \theta \quad (53)$$

The Mach line BE_1 forms with flow direction AB the Mach angle μ_1 , the Mach line BE_2 at the end of the expansion the Mach line μ_2 . Now it may be assumed that this small expansion takes place on the interference line BE' , whereby

$$\angle A'BE' = \frac{\mu_1 + \mu_2 - \Delta \theta}{2} \quad (54)$$

(b) A simple differentiation gives the change of the shock angle γ as well as the pressure change p_2' after the shock, due to a small variation of the angle of deflection δ , for the compression shock AB (fig. 14).

Between γ and δ the relation (eq. 18)

$$\cot \delta = \tan \gamma \left(\frac{\frac{\kappa + 1}{2} M_1^2}{M_1^2 \sin^2 \gamma - 1} - 1 \right)$$

exists, and therefore

$$\Delta \delta = - \sin^2 \delta \left[\sec \gamma \left(\frac{A}{B} - 1 \right) - M_1^2 \sin^2 \gamma \frac{2A}{B^2} \right] \Delta \gamma = C \Delta \gamma \quad (55)$$

where

$$A = \frac{\kappa + 1}{2} M_1^2$$

$$B = (M_1^2 \sin^2 \gamma - 1)$$

and

$$C = - \sin^2 \delta \left[\sec^2 \gamma \left(\frac{A}{B} - 1 \right) - M_1^2 \sin^2 \gamma \frac{2A}{B^2} \right]$$

The pressure p_2' after the shock is (eq. 15)

$$p_2' = p_1 \left(\frac{2\kappa}{\kappa + 1} M_1^2 \sin^2 \gamma - \frac{\kappa + 1}{\kappa - 1} \right) \quad (56)$$

and the result for a small variation of the shock intensity is

$$\Delta p_2' = p_1 M_1^2 \frac{2\kappa}{\kappa + 1} \sin 2\gamma \Delta \gamma \quad (57)$$

3. Overtaking of Compression Shock and Expansion Wave

(a) The supersonic flow M_1 , p_1 , ρ_1 past the wall AE (fig. 15(a)) undergoes a directional change δ at E. The compression shock EF and the flow direction form the shock angle γ_1 in zone (1). At C an expansion takes place about an angle Θ , and the expansion wave FCG overtakes the compression shock at F. To simplify the calculation, the continuous expansion is replaced by a given number of expansion waves of finite intensity, whereby a successive expansion through these waves is assured. If n is the number of waves, the expansion due to a wave is $\Theta/n = \Delta\Theta$. The number n must be so chosen that $\Delta\Theta$ is sufficiently small.

Now consider the intersecting of wave $CF_1(\Delta\Theta)$ and compression shock $EF_1(\delta)$, figure 15(b).

From F_1 the compression shock advances with weaker intensity in direction G_1 , that is, it deflects the flow less - say by δ' . F_1G_1 forms with the flow direction the angle γ' at (1). Indicating the various zones by (1), (2), (3), and (4), the streamline through F_1 splits the zone (4) into the portions (4_o) and (4_u) . The flow in (2) and (3) is fully known, because the angles δ and $\Delta\Theta$ are known.

To define the conditions in (4), the streamlines S_1 , S_2 , and S_3 are examined. The directional change of S_2 amounts to $(\delta - \Delta\Theta)$. But along S_3 the flow experiences the directional change δ' . To maintain equilibrium in (4), the pressure as well as the velocity direction above and below the streamline S_1 must be equal.

In general, the pressure change from (1) toward (3) is not the same as from (1) to (4), so that a reflected expansion wave - possibly a small compression too - must appear between (3) and (4), say along a line F_1H_1 .

Supposing that this reflected wave is an expansion wave of intensity $\Delta\Theta'$. By "intensity" of an expansion wave or a compression shock is meant the deflection, which the flow experiences in the process.

The pressure in (4_u) is, (according to section 2)

$$p_{4_u} = p_3 \left(1 - \frac{\kappa M_3^2}{\sqrt{M_3^2 - 1}} \Delta\Theta' \right) \quad (58)$$

The difference of the deflection angles amounts to $(\delta' - \delta) = \Delta\delta$. In general, this intensity decrease is small, because the compression shock is much stronger than the expansion wave. The corresponding change in shock angle γ is $\Delta\gamma$.

The pressure in (4_0) follows from the change in shock intensity. Hence we can say that

$$p_{4_0} = p_2' - \Delta p_2' \quad (59)$$

This is again the equation for small variations derived for shocks from equation (57). Accordingly

$$p_{4_0} = p_2' - p_1 M_1^2 \frac{2\kappa}{\kappa + 1} \sin 2\gamma \Delta\gamma \quad (60)$$

Posting $p_{4_0} = p_{4_u}$, gives

$$p_3 \left(1 - \frac{\kappa M_3^2}{\sqrt{M_3^2 - 1}} \Delta\theta' \right) = p_2' - p_1 M_1^2 \frac{2\kappa}{\kappa + 1} \sin 2\gamma \Delta\gamma \quad (61)$$

For the velocity direction in zone (4) to be unequivocal, it must

$$\Delta\theta = \Delta\delta + \Delta\theta' \quad (62)$$

The relation between shock intensity variation and angle of shock (eq. (55)) together with the two previous equations gives

$$\Delta\theta' = \frac{\Delta\theta \left(G - \frac{Q}{C} \right)}{\left(\Delta\theta FG - \frac{Q}{C} - F \right)} \quad (63)$$

$$\Delta\gamma = \frac{\Delta\delta}{C} = \frac{\Delta\theta - \Delta\theta'}{C} \quad (64)$$

with the constants

$$F = \frac{\kappa M_3^2}{\sqrt{M_3^2 - 1}} \quad G = \frac{\kappa M_2^2}{\sqrt{M_2^2 - 1}} \quad Q = \frac{M_1^2 \sin 2\gamma}{\left(M_1^2 \sin^2 \gamma - \frac{\kappa - 1}{2\kappa}\right)}$$

The condition for equality of static pressures is not identical with that for equality of velocity magnitude above and below the streamline S_1 . As the shock losses on either side of the intersection point F are unlike, the stagnation pressures in the wake above and below streamline S_1 are different, hence there is a small vortex layer along this streamline.

Figure 16 represents the graphical solution of the problem by means of the characteristics and the shock polars. The condition for equality through equality of velocity magnitude in the entire zone (4) is approximated.

(b) The reflected wave is disregarded:

In general, the angle of deflection $\Delta\theta'$ - intensity of the reflected wave - is very small (compare numerical example). Thus the pressure in (3) is not much unlike that in (4), so that this reflected wave F_1H_1 can be discounted.

In this event the flow directions in zones (3) and (4) are identical, or in other words

$$\Delta\theta = \Delta\delta \quad (65)$$

With equation (55) $\Delta\delta$ can be defined and from it the new direction γ' of the compression shock. The velocities in (3) and (4) have then obviously the same direction but not the same magnitude by reason of the small vortex layer developing between (3) and (4).

Numerical Example

Free stream:

$$p_1/p_0 = 0.12780$$

$$M_1 = 2.000$$

Before overtaking:

shock intensity

$$\delta = 6^\circ$$

shock angle

$$\gamma = 35.24^\circ$$

hence the state in zone (2)

$$p_2/p_0 = 0.1773$$

$$M_2 = 1.780$$

intensity of the expansion wave

$$\Delta\theta = 1^\circ$$

state in zone (3):

$$p_3/p_0 = 0.1693$$

$$M_3 = 1.818$$

Determination of constants:

$$C = 1.078$$

$$F = 3.04$$

$$G = 3.015$$

$$Q = 3.175$$

Inserted in equation (63) and (64) gives: intensity of the reflected wave

$$\Delta\gamma = 0.89^\circ$$

$$\Delta\theta' = 0.06^\circ$$

By equation (62)

$$\Delta\delta = \Delta\theta - \Delta\theta' = 0.94^\circ$$

Therefore the shock intensity after overtaking is

$$\delta = 5.04^\circ$$

The new shock angle is

$$\gamma' = \gamma - \Delta\gamma = 34.35^\circ$$

The reflected wave disregarded, leaves

$$\Delta\gamma = C \Delta\delta = C \Delta\theta = 1.078^\circ$$

shock intensity

$$\delta' = 5^\circ$$

angle of shock

$$\gamma' = 34.16^\circ$$

It is readily apparent that the reflected wave is very small, hence scarcely affects the pressure in zone (3).

4. Intersection of Compression Shock and Expansion Wave

Figure 18(a) represents an expansion wave $\Delta\theta$ of intensity θ proceeding from the corner A. At F this wave crosses a compression shock of intensity δ emanating from the corner B.

As before, the continued expansion is replaced again by n expansion waves between which the flow is straight. The deflection by each wave is

$$\Delta\theta = \frac{\theta}{n}$$

After crossing (fig. 18(b)) the compression shock has an intensity δ' and a shock angle γ' . Now the expansion wave has the intensity $\Delta\theta'$.

The zones produced this way are numbered (1), (2), (3), and (4). The streamline F_1S splits the zone (4) into (4_o) and (4_u).

Looked for now is the shock intensity δ' , shock angle γ' , and expansion angle $\Delta\theta'$ after crossing, and the state of flow in (4), when the state of flow in (1) δ , γ and $\Delta\theta$ are known.

According to chapter I the state of flow in (2) and (3) can be determined directly.

The pressure in (4_u) follows through a small expansion $\Delta\theta'$ according to the laws in chapter II at

$$p_{4u} = p_2 \left(1 - \frac{\kappa M_1^2}{\sqrt{M_1^2 - 1}} \Delta\theta' \right) \quad (66)$$

where $\Delta\theta$ is still unknown.

The method of solution consists in first making an assumption for the shock intensity after intersecting, which is

$$\delta_1 = (\delta - \Delta\theta) \quad (67)$$

The corresponding angle of shock would be γ_1 .

The state after this shock, indicated by $4_0'$, can again be defined according to chapter II. The pressure in $(4_0')$ is

$$p_{4_0'} = p_3 \left(\frac{2\kappa}{\kappa + 1} M_3^2 \sin^2 \gamma_1 - \frac{\kappa - 1}{\kappa + 1} \right) \quad (68)$$

Now the flows in (4_0) and (2) have identical directions, but the pressures and the magnitudes of the velocity are different.

To assure equilibrium within (4), the pressures and velocity directions in (4_0) and (4_u) must be equal. And to satisfy this condition the assumed shock must be intensified by $\Delta\delta_1$.

Obviously it shall

$$\Delta\delta_1 = \Delta\theta' \quad (69)$$

The new pressure in (4_0) is (according to section 2b)

$$p_{4_0} = p_{4_0'} + p_3 M_3^2 \frac{2\kappa}{\kappa + 1} \sin 2\gamma_1 \Delta\gamma_1 \quad (70)$$

where $\Delta\gamma_1$ is the change in shock angle γ_1 and is computed by equation (55)

$$\Delta\gamma_1 = \frac{\Delta\delta_1}{C} \quad (71)$$

(For the calculation of C see section 2b)

Posting $p_{4_0} = p_{4_u}$, equations (66), (68), (70), and (71) give

$$p_2 \left(1 - \frac{\kappa M_2^2}{\sqrt{M_2^2 - 1}} \Delta\theta' \right) = p_3 \left(\frac{2\kappa}{\kappa + 1} M_3^2 \sin^2 \gamma_1 - \frac{\kappa - 1}{\kappa + 1} \right) + p_3 M_3^2 \frac{2\kappa}{\kappa + 1} \sin 2\gamma \frac{\Delta\theta'}{C} \quad (72)$$

This equation is linear in $\Delta\theta'$.

Now the quantities δ' and γ' can be defined

$$\delta' = \delta_1 + \Delta\delta_1 = \delta_1 + \Delta\theta' \quad (73)$$

$$\gamma' = \gamma_1 + \Delta\gamma_1 = \gamma_1 + \frac{\Delta\theta'}{C} \quad (74)$$

The pressure in (4_0) can be obtained directly from equation (70). The Mach number M_{4_0} itself can be determined according to chapter I, if δ' and γ' are known. That in (4_u) is likewise directly obtainable from M_2 by the isentropic expansion $\Delta\theta'$.

The slight discrepancy between the values M_{4_0} and M_{4_u} is due, as stated in section 3, to the fact that the condition for pressure equality, owing to the change in static pressure after both shocks, does not require equal magnitude of velocity. So a small vortex layer along streamline F_1S is to be expected.

Before intersecting the expansion wave forms with the flow direction in zone (1) the angle (section 2)

$$X = \frac{\mu_1 + \mu_3 - \Delta\theta}{2}$$

After intersecting the angle with the stream direction in zone (2) is

$$Y = \frac{\mu_2 + \mu_4 - \Delta\theta'}{2}$$

But there is a difference δ between the flow directions in (1) and (2), so that the looked-for directional change is

$$\delta b = X + \delta - Y = \frac{\mu_1 + \mu_3 - \Delta\theta}{2} + \delta - \frac{\mu_2 + \mu_4 - \Delta\theta'}{2} \quad (75)$$

The directional change of the shock front is

$$\Delta c = \gamma - (\gamma' + \Delta\theta) \quad (76)$$

A negative angle b and a positive angle c indicates that the expansion wave or shock front after crossing is in more downstream direction.

For illustrative and comparative purposes, the graphical solution in figure 19 was made with the aid of the characteristics and shock polar. Here also the condition for pressure equality was replaced by velocity equality.

The described mode of calculation is used in the following numerical example for illustration.

Numerical Example

The flow in zone (1) is:

$p_1/p_0 = 0.22905$ $M_1 = 1.435$ $\mu_1 = 44.18^\circ$ (See cascade example of the following chapter III, zone (3)).

Data before crossing:

intensity of expansion wave	$\Delta\theta = 1^\circ$
intensity of compression shock	$\delta = 3.03^\circ$
shock angle of compression shock	$\gamma = 47.91^\circ$

With it the states in zone (3) become:

$p_3/p_{01} = 0.28478$ $M_3 = 1.469$ $\mu_3 = 42.89^\circ$

Therefore

$$p_2/p_1 = 1.157$$

$$p_2/p_{01} = 0.34560 \quad M_2 = 1.332 \quad \mu_2 = 47.75^\circ$$

Assumed shock intensity

$$\delta_1 = \delta - \Delta\theta = 3.03 - 1 = 2.03^\circ$$

corresponding angle of shock

$$\gamma_1 = 45.29^\circ$$

pressure after shock

$$p_{4_0}' / p_{0_1} = 0.3153$$

Determination of the constants

$$A = \frac{\kappa + 1}{2} M_3^2 = 2.592$$

$$B = (M_3^2 \sin^2 \gamma_1 - 1) = 0.092$$

$$C = -\sin^2 \delta_1 \left[\sec^2 \gamma_1 \left(\frac{A}{B} - 1 \right) - \sin^2 \gamma_1 M_1^2 \frac{2A}{B^2} \right] = 0.7504$$

Equality of pressure in (4₀) and (4_u) gives

$$p_{4_u} = p_2 \left(1 - \frac{\kappa M_2^2}{\sqrt{M_2^2 - 1}} \Delta \Theta' \right)$$

$$= p_{4_0} = p_{4_0}' + p_3 M_3^2 \frac{2\kappa}{\kappa + 1} \sin 2\gamma_1 \frac{\Delta \Theta'}{c}$$

which inserted gives

$$\Delta \Theta' = \Delta \delta_1 = 0.89^\circ$$

$$\Delta \gamma_1 = \frac{\Delta \delta_1}{c} = 1.19^\circ$$

After the crossing:

$$\text{shock intensity} \quad \delta' = \delta_1 + \Delta \delta_1 = 2.03 + 0.89 = 2.92^\circ$$

$$\text{shock angle} \quad \gamma' = \gamma_1 + \Delta \gamma_1 = 45.29 + 1.19 = 46.48^\circ$$

Hence

$$p_4/p_0 = 0.3303 \quad \mu_4 = 47.08^\circ$$

$$M_{4u} = 1.3643$$

$$M_{4o} = 1.3640$$

The comparison of the two Mach numbers indicates that the difference is quite small and lies within the calculation accuracy.

Directional changes:

$$\text{Expansion Wave} \quad \Delta b = 43.036 + 3.034 - 47.47 = -1.4^\circ$$

$$\text{Shock front} \quad \Delta c = 47.91 - 46.48 + 1 = +0.43^\circ$$

5. Crossing of Expansion Waves

Each expansion wave is again replaced by n small waves. In figure 20(a), two waves of intensity $\Delta\theta_1$ and $\Delta\theta_2$ cross each other in F. After crossing, the intensities are $\Delta\theta_1'$ and $\Delta\theta_2'$. In this case, only one stream direction is obtained in zone (4), when

$$\Delta\theta_1 + \Delta\theta_2 = \Delta\theta_1' + \Delta\theta_2' \quad (77)$$

Application of the relations of section 2 results in

$$p_4 = p_3 - \Delta p_3 = p_2 - \Delta p_2$$

that is

$$p_3 \left(1 - \frac{\kappa M_3^2}{\sqrt{M_3^2 - 1}} \Delta\theta_2' \right) = p_2 \left(1 - \frac{\kappa M_2^2}{\sqrt{M_2^2 - 1}} \Delta\theta_1' \right) \quad (78)$$

Since all other quantities are known, $\Delta\theta_2'$ and $\Delta\theta_1'$ can be computed from these two equations.

The directional change of the Mach lines is like that in the preceding section

$$\angle b = \frac{\mu_1 + \mu_3 - \Delta\theta_1}{2} + \Delta\theta_1 - \frac{\mu_2 + \mu_4 - \Delta\theta_1'}{2} \quad (79)$$

$$\angle c = \frac{\mu_1 + \mu_2 - \Delta\theta_2}{2} + \Delta\theta_2 - \frac{\mu_3 + \mu_4 - \Delta\theta_2'}{2} \quad (80)$$

Since all changes follow the same adiabatic curve, the condition for pressure equality yields equal velocity values at both sides of the streamline FS. Hence, no vortex layer will appear. Figure 20(b) represents the graphical solution.

Numerical Example

Airstream:

$$p_1/p_0 = 0.3295 \quad M_1 = 1.366 \quad \mu_1 = 47.05^\circ$$

The intensity of the first expansion wave is: $\Delta\theta_1 = 0.99^\circ$. Therefore

$$p_2/p_0 = 0.3134 \quad M_2 = 1.402 \quad \mu_2 = 45.50^\circ$$

The second expansion wave intensity is: $\Delta\theta_2 = 1.06^\circ$

The conditions in zone (3) are then

$$p_3/p_0 = 0.31245 \quad M_3 = 1.4041 \quad \mu_3 = 45.433^\circ$$

The two equations defining $\Delta\theta_1'$ and $\Delta\theta_2'$ are:

$$\Delta\theta_1 + \Delta\theta_2 = 0.03579 = \Delta\theta_1' + \Delta\theta_2'$$

$$p_4 = p_3 - \frac{\kappa p_3 M_3^2}{\sqrt{M_3^2 - 1}} \Delta\theta_1' = p_2 - \frac{\kappa p_2 M_2^2}{\sqrt{M_2^2 - 1}} \Delta\theta_2'$$

hence

$$\Delta\theta_1' = 0.0184 = 1.054^\circ$$

$$\Delta\theta_2' = 0.0174 = 0.997^\circ$$

after which the conditions in zone (4) become:

$$p_4/p_0 = 0.29722 \quad M_4 = 1.44 \quad \mu_4 = 44.01^\circ$$

By equation (79) and (80) the directional changes of the waves are

$$\Delta b = + 0.5^\circ \quad \text{and} \quad \Delta c = - 0.02^\circ$$

6. Reflection of Compression Shocks and Expansion Waves

No difficulties occur in the determination of the conditions existing behind the reflected compression shock FB (fig. 21). Those in zone (2) can be defined according to chapter I, if the state of the airstream and the intensity δ of shock AF are known. Obviously the reflected shock is of the same intensity as the impinging shock, so that the shock angle γ of the reflected shock and the conditions in zone (3) can be defined.

The same holds true for the reflection of expansion waves, when the intensity of the expansion waves and their slope with respect to the wall are known.

CHAPTER III. THE CASCADE PROBLEM

1. Problem

Visualize a cascade of infinitely many and infinitely thin flat plates, of which two adjacent plates AB and A'B' are represented in figure 22. The angle of stagger is $90 - \beta$, the spacing t and the blade chord L . This cascade is exposed at angle of attack ψ to a supersonic flow M_1 , p_1 , ρ_1 .

It is assumed that the flow is the same in all planes perpendicular to the plates and determines the force, that is, lift and drag as well as the pressure variation along the plate (blade).

2. Method of Calculation

To each plate there correspond interference lines (chapter I), that is, the expansion wave issuing from the leading edge and compression shock (fig. 22).

At wide spacing, the separate blades of the cascade will not affect each other and the problem reduces to the single plate.

Now if the spacing decreases for constant chord, the interference lines of one plate intersect those of the other, without, however, any force being exerted on the plates themselves for the time being. In this event, the force on each plate is the same as on the single plate, except that the wake flow is slightly disturbed.

The values of t/L , below which the interference line of a plate begins to exert an effect on the adjacent one, are called $(t/L)_{crit}$ "critical chord-spacing ratio."

At $t/L < (t/L)_{crit}$ the interference lines are reflected on the plates. After the crossings and reflections, new zones appear on both sides of the plate where the pressure as well as the velocities are unlike the uniform pressures and velocities to be found at either side of the plate. As a result, there is a change in the total force as well as the lift and drag on each plate.

The mode of calculation consists in defining each intersection and reflection with the laws of chapter II and from it determining the conditions in the several zones. Integration of the various pressures on both sides of the plate gives then the total force, that is, the lift and drag.

The resultant force still is perpendicular to the plate, but no longer through the plate center, hence produces a moment with respect to the center. The position of the force is defined by statistical methods.

This method is illustrated in the following example.

3. Example

The cascade ABA'B' (fig. 23) with 30° angle of stagger, that is, $\beta = 60^\circ$, and at angle of attack of $\psi = 3^\circ$ is placed in a stream with $M_1 = 1.4004$ (corresponding to $\nu = 9^\circ$).

The blade spacing was assumed at the beginning, while the plate chord was so chosen after completion of the calculation that the expansion wave was reflected exactly once on the bottom side of the upper plate. It was found that $t/L = 0.547$.

The flow experiences a compression shock starting at the leading edge A'. The shock angle $\gamma = 49.57^\circ$ is read from the shock tables and the shock front A'a can be plotted.

Proceeding from the leading edge A, an expansion wave spreads out between the Mach lines Ax and Ay. The first forms with the airstream direction the angle $\mu_1 = 45.56^\circ$. The characteristics tables give $M_7 = 1.503$, that is, the Mach number which is obtained at an expansion by 3° from the Mach number 1.4004. The corresponding Mach angle, that is, the angle which direction Ay forms with the plate, would be $\mu_7 = 41.70^\circ$. Instead of the continuous expansion, assume an expansion in three stages, each corresponding to a 1° deflection. The conditions in zones 1, 2, 3, and 4 are obtained from the characteristics tables, after which the directions Aa, Ab, and Ac can be defined.

By applying the methods of chapter II to the calculation of the crossings a, b, c, e, f, g, l, m, n, p, q, s and the reflections d, h, i, k, o, r, u, the static pressures, the Mach numbers (table 6), and the intensities of the expansion waves and compression shocks, as well as their directional changes (see table 7 and fig. 24) in the several zones, can be determined.

The static pressures were referred to the standard stagnation pressure p_{01} .

The stagnation pressure changes were disregarded in the determination of the Mach number. This change is rather small according to table 6,

so that no appreciable advantage was to be gained by including it. (For calculation of p_0/p_{01} , compare eq. (23).)

The pressure distribution past the plate is obtained immediately and represented in figure 25. There the passage of compression shocks and expansion waves is accompanied by a sudden pressure variation. Since the actual expansion is continuous, the serrated line is replaced by a smooth curve, such that the areas decisive for the force calculation are identical.

Note that the pressures on both sides of the plate cancel out over a large portion of the chord. The resultant force can be determined by integration of the various pressures; the various spacings l are read directly from figure 23.

The plate width was assumed at $b = 1$. The result is

$$\sum \left(\frac{p}{p_{01}} \frac{l}{L} \right): \begin{aligned} &= 0.2963 \text{ upper side} \\ &= 0.2896 \text{ lower side} \end{aligned}$$

Downward resultant force

$$\frac{K}{p_{01}L} = 0.0067$$

lift coefficient

$$c_a = \frac{K}{p_{01}L} \frac{p_{01}}{q} \cos \psi = 0.01532$$

drag coefficient

$$c_w = \frac{K}{p_{01}L} \frac{p_{01}}{q} \sin \psi = 0.00082$$

4. Calculation of Thrust, Tangential Force and Efficiency

(a) The resultant force on the blade is resolved into two components. One - the thrust S - is normal to the plane of the cascade, the other - the tangential force T - parallel to it (fig. 26).

If

K = resultant force per unit of area

$(90^\circ - \beta)$ = cascade stagger angle

then

$$\left. \begin{aligned} S &= K \cos \beta \\ T &= K \sin \beta \end{aligned} \right\} \quad (81)$$

As functions of lift and drag

$$S = A \cos(\beta - \psi) - W \sin(\beta - \psi)$$

$$T = A \sin(\beta - \psi) + W \cos(\beta - \psi)$$

Referring the force to the dynamic pressure q_1 of the airstream, gives the coefficients

$$\left. \begin{aligned} c_S &= \frac{K}{q_1} \cos \beta \\ c_T &= \frac{K}{q_1} \sin \beta \end{aligned} \right\} \quad (82)$$

similar to the lift and drag coefficients, which can be obtained directly from c_a and c_w .

At fixed blade chord and fixed angle of attack the resultant force reaches its maximum value when adjacent blades do not affect each other, that is, when $t/L > (t/L)_{crit}$. In this event

$$K = p_2' - p_2$$

where p_2' is pressure at lower side (behind compression shock) and p_2 is pressure at upper side (behind expansion wave).

For a given Mach number of flow and angle of attack the thrust and tangential force is maximum at $\beta = 0^\circ$ and $\beta = 90^\circ$, respectively.

At a given angle β and a given Mach number, T and S increase with increasing ψ . Owing to our assumptions ψ may not exceed ψ_s , in order to prevent subsonic flows on the bottom side of the plate.

(b) Definition of efficiency (no friction):

It is supposed that the air enters normal to the plane of the cascade at a speed v (fig. 26). The cascade moves with the tangential velocity u and finds itself accordingly in a relative flow with an angle of attack ψ , whereby $\tan(\beta - \psi) = v/u$. As a result of this flow, the two forces S and T normal and parallel to the plane of the cascade act on the plate; S and T are defined according to previous considerations. An efficiency is defined as on a propeller, by visualizing the blade being driven at speed u with respect to force T and so producing a force S in axial direction on the flowing air. Then the power input is $T \times u$, the power output $S \times v$ and the efficiency is

$$\eta = \frac{Sv}{Tu} \quad (83)$$

or

$$\eta = \frac{\tan(\beta - \psi)}{\tan \beta} = \frac{\left(1 - \frac{\tan \psi}{\tan \beta}\right)}{1 + \tan \psi \tan \beta}$$

The efficiency is seen to be dependent on ψ and β only. At constant β it decreases with increasing ψ . At $\psi = \text{constant}$, η has a maximum, if

$$\frac{\partial \eta}{\partial \beta} = 0 \quad (84)$$

that is, when

$$\tan \beta = \tan \psi + \sqrt{(\tan \psi)^2 + 1}$$

which approximately gives

$$\beta = 45^\circ + \frac{1}{2} \psi \quad (85)$$

The maximum efficiency is then

$$\eta_{\max} = \left(\frac{1 - \tan \frac{\psi}{2}}{1 + \tan \frac{\psi}{2}} \right)^2 \quad (86)$$

$\psi = \text{Constant}$

At small values of ψ , $\tan \psi = \psi$ and ψ^2 is negligibly small, hence
at $\beta = 45^\circ + \frac{1}{2} \psi$

$$\eta_{\max} = \frac{1 - \psi}{1 + \psi} \quad (87)$$

The efficiency for various β and ψ is represented in table 8 and figure 27.

CHAPTER IV. LINEARIZED CASCADE THEORY

1. Assumptions

The theory is based upon the following:

(a) All disturbances are small in the sense that all interference lines may be regarded as Mach lines. The expansions are simply concentrated in a Mach line and the compression shocks replaced by Mach compression waves.

(b) Intensity and direction of waves are not changed by intersection of expansion and compression waves. The justification of this assumption is indicated in the preceding numerical example, where it was shown that the directional changes of the wave fronts are small, as a rule.

On these premises, the interference lines AA' and AA'' parallel to BB' and BB'' start from the small disturbances A and B (fig. 28(a)). At the intersection in a the directions of the waves AA' and BB' as well as their intensities remain unchanged. The pressure and the velocities in the zones (2), (3), and (4) are defined by the laws of chapter II. In the hodograph these assumptions imply that the characteristics network in the applied zone is replaced by a parallelogram (fig. 28(b)).

2. Linearization of Cascade Problem

The application of these simplifications to the solution of the cascade problem produces parallel Mach lines within the cascade, which remain parallel after crossings or reflections (fig. 29(a)). (L = plate chord, t = spacing and ψ = angle of attack.) The Mach lines Aa and $A'a$ emanate from the leading edges A and A' ; the angles $aA'X'$ and aAX are Mach angles and both equal to μ_1 . On passing through $A'a$, the flow experiences a compression and a directional change ψ , along Aa an expansion with the same directional change.

The pressure in (2) and (3) can be defined by the laws of isentropic expansion and compression (chapter I); that of zone (4) is computed the same way from the pressure in (2) and is obviously equal to p_1 , as seen in the hodograph (fig. 29(b)). But the flow direction in (4) differs from that in (1) by an angle 2ψ .

The Mach line aC' intersects the plate at C' and is reflected along $C'E$, whereby $C'E$ is parallel to $A'a$. The pressure in zone (5) is again equal to that in (3) and the flow is obviously parallel again to the plate.

On passing through DE' the flow from (4) and (6) is compressed - the reflected wave DE' - so that in (7) the direction and the velocity of flow are the same as in (1); the same applies to the flows in (6) and (2).

Thus it is seen that the corresponding zones repeat themselves, hence that the further conditions are completely known without new calculations.

3. Calculation of Lift and Drag

The pressure variation on either side of the plate can be plotted (figs. 29(c) and 29(d)). The pressure remains constant over the lengths AC , CD , DE , EF and FB and over $A'C'$, $C'D'$, $D'E'$, $E'F'$ and $F'B'$ - where the interference lines strike the plate.

Along CD the pressures on both sides are equal and cancel out, whereas a downward pressure difference $p_3 - p_2$, obviously perpendicular to the plate, acts on AC and EF , and an identical upward pressure difference on DE .

The pressure pattern in figure 29(e) repeats itself in length direction of the plate over the period L_1 . If the plate chord is chosen exactly like L_1 or a multiple of it, there is no resultant force, that is, a plate of this length has neither lift nor wave resistance.

For the values of L , which satisfy the inequality

$$L_0 < (L - nL_1) < (L_1 - L_0)$$

whereby n can be $= 0, 1, 2, \dots$, the resultant force reaches its maximum value, and then

$$K = (p_3 - p_2)L_0 \quad (88)$$

Hence it serves no useful purpose to make the plate longer than L_0 , because there is no more lift increase anyhow. On the other hand, a moment occurs and, in the presence of friction, the drag would increase unnecessarily. The boundary $L_0 (= AC)$ is the plate length not touched by interference lines of the other plate and can be defined geometrically in terms of cascade spacing t and angles β , ψ , and μ .

$$L_0 = t \frac{\sin[\beta - (\mu_1 + \psi)]}{\sin(\mu_1 + \psi)} \quad L_1 = 2L_0 + t \frac{\sin[\beta + (\mu_1 + \psi)]}{\sin(\mu_1 - \psi)} \quad (89)$$

Accordingly the best ratio of spacing/chord is

$$\frac{t}{L} = \frac{t}{L_0} = \frac{\sin(\mu_1 + \psi)}{\sin[\beta - (\mu_1 + \psi)]} \quad (90)$$

Now c_a and c_w can be determined when

1. $L = nL_1$ then $c_a = c_w = 0$
2. $L_0 < (L - nL_1) < (L_1 - L_0)$, the boundary values are

$$\left. \begin{aligned} c_a &= \frac{K}{q_1 L} \cos \psi = \frac{p_3 - p_2}{q_1} F \cos \psi \\ c_w &= \frac{K}{q_1 L} \sin \psi = \frac{p_3 - p_2}{q_1} F \sin \psi \end{aligned} \right\} \quad (91)$$

where

$$F = \frac{t}{L} \frac{\sin[\beta - (\mu_1 + \psi)]}{\sin(\mu_1 + \psi)}$$

3. $L_0 > (L - nL_1)$

$$\left. \begin{aligned} c_a &= \frac{p_3 - p_2}{q_1 L} (L - nL_1) \cos \psi \\ c_w &= \frac{p_3 - p_2}{q_1 L} (L - nL_1) \sin \psi \end{aligned} \right\} \quad (92)$$

$$4. (L - nL_1) > (L_1 - L_0)$$

$$\left. \begin{aligned} c_a &= \frac{p_3 - p_2}{q_1 L} \left[(L - nL_1) - (L_1 - L_0) \right] \cos \psi \\ c_w &= \frac{p_3 - p_2}{q_1 L} \left[(L - nL_1) - (L_1 - L_0) \right] \sin \psi \end{aligned} \right\} \quad (93)$$

The linearization can be extended to the pressures p_2 and p_3 ; admittedly then only when the angle of attack is sufficiently small.³

The pressures can be defined by the laws of small variations (chapter II). Thus

$$p_{2(3)} = p_1 \left(1 \pm \frac{\kappa M_1^2 \psi}{\sqrt{M_1^2 - 1}} \right) \quad (94)$$

Inserting these values in the above formulas for c_a and c_w , while expressing the dynamic pressure with

$$q_1 = \frac{1}{2} \kappa p_1 M_1^2$$

and the values 1 and ψ for $\cos \psi$ and $\sin \psi$, gives as for the isolated plate,

³In the following table the pressures after expansion of $p_0 = 0.31404$ (corresponding to $M_1 = 1.4004$) are represented in terms of the expansion angle:

p_2 = pressure according to isentropic law of expansion

p_{2L} = pressure according to the laws of small variations (chapter II)

ψ°	1	2	3	4	6
p_2/p_0	0.29906	0.28478	0.27114	0.25809	0.23363
p_{2L}/p_0	0.29865	0.28335	0.26718	0.25266	0.22196
$(p_2 - p_{2L})/p_2$ percent	0.1	0.5	1.5	2.1	5.0

$$\left. \begin{aligned} c_a &= \frac{4\psi}{\sqrt{M^2 - 1}} F \\ c_w &= \frac{4\psi^2}{\sqrt{M^2 - 1}} F \end{aligned} \right\} \quad (95)$$

The factor F approaches 1 when $t/L = t/L_0$. The theory is now illustrated on the following numerical example.

4. Numerical Example

The cascade of the numerical example in chapter III is applied again with the same airstream as by linearized theory, figure 30.

It was

$$t/L = 0.547 \quad \beta = 60^\circ$$

$$M_1 = 1.4004 \quad \psi = 3^\circ$$

$$p_1/p_0 = 0.31404 \quad \mu_1 = 45.56^\circ$$

The Mach lines within the cascade can now be plotted. By equation (89)

$$L_0 = 0.144L$$

Geometrically defined are

$$(L_1 - L_0) = 0.778L$$

so that

$$(L - L_1) = 0.078L$$

The tables of characteristics give

$$p_2/p_{01} = 0.2711 \text{ (expansion by } 3^\circ \text{ starting from } p_1/p_{01})$$

$$p_3/p_{01} = 0.3640 \text{ (isentropic compression by } 3^\circ)$$

Assuming the plate width at one cm, gives:

$$\text{resultant force } \frac{K}{p_{01}} = (L - L_1) \frac{(p_3 - p_2)}{p_{01}} = 0.3436$$

$$\text{resultant force per unit length} = 0.0067$$

$$\text{lift coefficient } c_a = 0.0156$$

$$\text{drag coefficient } c_w = 0.0008$$

The pressure distribution on both sides and the resultant pressure are shown in figure 31.

5. Comparison With Exact Method

Instead of the lengthy calculations of all crossings and reflections, the linearized theory affords a quick and simple solution of the cascade problem. At small angles the results are reliable and the errors small, as seen from the comparison with the numerical examples in section 3, chapter III and the preceding section.

$$\frac{c_a(\text{exact}) - c_a(\text{linearized})}{c_a(\text{exact})} = -2 \text{ percent}$$

The interference lines of the linearized solution within the cascade - the Mach lines - are included in figure 23 for comparison. It is seen that the zones governing the resultant pressure are smaller by linearized theory.

The pressure distribution of the linearized example is also shown in figure 25.

CHAPTER V. SCHLIEREN PHOTOGRAPHS OF CASCADE FLOW

1. Cascade Geometry

A disturbance in supersonic flow is known to spread out only downstream of the source of disturbance. So the pressures and velocities on one of the sides of a profile, stipulated by the form of the surface, are not influenced by the other side.

This property is used to represent the flow through a cascade consisting of a number of infinitely thin plates. Two profiles with a flat surface on one side are so assembled that their flat sides face each other and are parallel. The flow between the parallel sides is exactly the same as that between two adjacent plates of the cascades.

The two profiles can be moved apart or shifted relative to one another, so that any desired ratio t/L and any stagger angle can be obtained.

The experimental cascade was patterned after the cascade in the numerical example of chapter III, which had the same angle of stagger of 30° . The Mach number of flow was - as in previous calculations - $M = 1.40$; the spacing ratio was $t/L = 0.517$. The angle of attack ψ ranged from 0° , 1.5° , 3° to 4.5° .

The maximum profile thickness was so chosen that no blocking of the tunnel (section 2) was produced at the selected Mach number and that the deflection of the profiles at maximum angle of attack is small.

Now at $M = 1.40$ the deflection due to compression shock, which exactly leads to sonic velocity, is $\delta_s = 9^\circ$. As there is to be no subsonic flow in the test section and since the angle of attack was assumed at 4.5° , the leading edge of the profile may at most form an angle of about 4° , which corresponds to the constructed profile.

The compression shock is not separated at the leading edge of an infinitely thin plate or an infinitely sharp wedge of sufficiently small included angle. Therefore the leading edge shall be as sharp as possible. It succeeded in attaining a thickness of $0.05 \div 0.07 \text{ mm}^4$ so that the distance of the separated shock from the edge is scarcely visible.

The profile chord L was 118 mm, so that the cascade lies within the tunnel window. Since the tunnel itself was 400 mm wide, the width of the profile was limited to 398 mm, figure 32.

⁴Hurit Co., Affoltern, Zurich.

2. Experimental Setup

The previously described profiles were mounted in the test section of the supersonic tunnel of the Institute⁵ on four supports (fig. 33).

The compression shock issuing from the leading edge of the top profile could not be reflected at the upper tunnel wall at maximum ψ , because the deflection to be made retrogressive at the wall was too great for the Mach number prevailing behind the shock. To avoid blocking in this region, a bend had to be made in the upper nozzle wall (fig. 34). The position of the bend was so chosen that the fan of expansions emanating from it hits the cascade downstream from the entering edge. This adjusts the wall to the flow direction after the shock to some extent as well as raises the Mach number between the upper plate and the nozzle wall.

The Mach number in the test section before the cascade was determined by pressure measurements at the upper, lateral, and lower walls. The investigation was carried out at a moisture content of air of about 0.5 g water/kg air.

3. Schlieren Photographs⁶

The schlieren photographs illustrating the flow through the plate cascade at $\psi = 0^\circ$, 1.5° and 3° are represented in figures 36, 37, and 38. Since a conical jet regime is involved, the photographs appear as shadows of the profiles. Figure 35 shows the position of the optical axis with respect to the cascade; it is seen that the shadows of the profiles are distorted on the mirror. At the top profile the perspective effect is more obvious, because the optical axis is closer to the bottom profile.

The equality of Mach's angle in figure 37 ($\psi = 0^\circ$) is indicative of an unchanged Mach number in the cascade. The visible disturbances within the cascade may be due to the fact that the plate surfaces do not exactly agree with the flow direction, or to thickening of the leading edges by a boundary layer.

In figure 38 ($\psi = 1.5^\circ$) the interference lines inside the cascade are almost parallel, as stipulated by the linearized theory.

⁵See Report No. 8 of the Institute for Aerodynamics, at the E.T.H., ref. 1.

⁶For description of schlieren apparatus see Report No. 8 of E.T.H. Institute.

At $\psi = 3^\circ$ (fig. 39) the deflection of the shock front at crossing of the expansion wave emanating from the top leading edge is plainly visible. Figure 40 represents an enlargement of the crossing to illustrate the numerical example in chapter III. The interference lines inside the cascade for this example are again shown in figure 41 at smaller scale (compare also fig. 23), whereby the perspective effect is indicated.

In the majority of photographs the retardation of the flow near the tunnel wall leads to separation of the head waves.

The flow in all photographs is from left to right.

CHAPTER VI. THE FLAT PLATE CASCADE AT SUDDEN

ANGLE-OF-ATTACK CHANGE

1. Problem

Visualize a cascade of flat plates in a flow with relative velocity W at an angle of attack ψ . A supersonic flow which may be regarded as two-dimensional prevails throughout the cascade. At a given moment the angle of attack of the airstream changes from ψ to ψ' within an infinitely short time interval. The transition to the new state, which is to last for a period, is analyzed.

Such a change in the angle of attack takes place when the cascade moves in an absolute flow which has not the same speed at every point, or when one of the velocity components of the flow, normal or parallel to the plane of the cascade, varies with respect to time.

Resolving the velocity W in two components V and U (fig. 42) normal and parallel to the plates, the change of the angle of attack, small in itself, can be regarded as a change of component V . This change in V is obtained by superposition of a velocity v_0 , which has the same direction as V and is obviously small compared to V and consequently smaller than sonic velocity. From the assumption of a small angle of attack, it follows that velocity component U remains greater than sonic velocity. Besides, an eventual variation of this component U is disregarded.

The problem therefore reduces to the study of the new forces on the cascade, resulting from a gust v_0 ⁷ which, together with the velocity U enters perpendicular to the plates.

Biot (ref. 5) solved the problem of an isolated plate by means of "unsteady sources." This method is applied to the cascade problem. But first the unsteady source is described in more detail. Since the plates are to be partly replaced by such sources, the pressures and velocities originating from a source distribution are analyzed. Then Biot's results for the isolated plate are correlated and extended to the cascade. The special case of straight cascade (nonstaggered) is examined.

⁷By "gust" is meant a continued, uniform vertical velocity distribution v_0 .

2. The Unsteady Source

According to linearized theory, the general potential equation (5) for two-dimensional unsteady flow can be simplified to

$$\frac{\partial^2 \phi}{\partial x^2} (1 - M^2) + \frac{\partial^2 \phi}{\partial y^2} - 2 \frac{M}{a} \frac{\partial^2 \phi}{\partial x \partial t} - \frac{1}{a^2} \frac{\partial^2 \phi}{\partial t^2} = 0 \quad (96)$$

ϕ = flow potential.

For a system of coordinates moving with velocity U ($U/a = M$), that is, air at rest at infinity, this equation gives the acoustic wave equation for two-dimensional motion

$$\frac{\partial^2 \phi}{\partial x^2} + \frac{\partial^2 \phi}{\partial y^2} - \frac{1}{a^2} \frac{\partial^2 \phi}{\partial t^2} = 0 \quad (97)$$

One solution for a linear sound source is

$$\phi = k \cosh^{-1} \frac{at}{r} \quad (98)$$

where $r = \sqrt{x^2 + y^2}$ and K = constant with dimensional length times velocity.

This solution is rewritten in the form

$$\left. \begin{aligned} \phi &= k \log_e \left(\frac{at}{r} + \sqrt{\frac{a^2 t^2}{r^2} - 1} \right) \\ &= k \log_e \left[\frac{1}{r} \left(at + \sqrt{a^2 t^2 - r^2} \right) \right] \\ &= -k \log_e \left(\frac{r}{at + \sqrt{a^2 t^2 - r^2}} \right) \end{aligned} \right\} \quad (99)$$

It represents a cylindrical wave varying in time rate. At $t = r/a$, $\phi = 0$, that is, if such a singularity appears in the zero point of the coordinate system, its effect is diffused inside a circle of radius $r = a \cdot t$.

If such a source appears at the point $(x, 0)$ - on the x-axis - at period t_1 , the potential in a point $P(x, y)$ of the surroundings of this source at a given period (fig. 43) is

$$\phi = k \log_e \left[\frac{r}{a(t - t_1) + \sqrt{a^2(t - t_1)^2 - r^2}} \right] \quad (100)$$

In this case

$$r = \sqrt{(x - x_1)^2 + y^2}$$

and the following velocity components are obtained by simple differentiation

$$v_r = \frac{\partial \phi}{\partial r} = k \frac{1}{r} \frac{a(t - t_1)}{\sqrt{a^2(t - t_1)^2 - r^2}} \quad (101a)$$

$$v_x = \frac{\partial \phi}{\partial x} = k \frac{(x - x_1)}{r^2} \frac{a(t - t_1)}{\sqrt{a^2(t - t_1)^2 - r^2}} \quad (101b)$$

$$v_y = \frac{\partial \phi}{\partial y} = k \frac{y}{r^2} \frac{a(t - t_1)}{\sqrt{a^2(t - t_1)^2 - r^2}} \quad (101c)$$

When y is small compared to $a(t - t_1)$ - near the source - the formula (101a) becomes

$$v_r = k/r$$

the same as that of a steady wave in incompressible flow, hence with Q denoting the strength of the source (dimensional length \times speed)

$$K = \frac{Q}{2\pi}$$

The pressure in the same point is computed by

$$\Delta p = -\rho \frac{\partial \phi}{\partial t} = \frac{\rho a Q}{2\pi} \frac{1}{\sqrt{a^2(t - t_1)^2 - r^2}} \quad (102)$$

It will be noted that v_y always equals zero for $y = 0$, except at $r = 0$ in the source itself. It means that such a source delivers at no other place on the x -axis a velocity component parallel to the y -axis.

3. Pressure and Velocity of a Periodically Arising Source Distribution

Consider a continuous distribution of infinitely small sources over the length OA (fig. 44) along the negative x -axis. The distance OA increases linearly with the time: $OA = Ut$, where U is a constant velocity and the sources on the x -axis appear momentarily at the point where A arrives at the moment. The strength of this source distribution per unit length of OA is assumed equal to q (dimension of a velocity) and remains constant in time.

(a) Pressure

At point $P(x, y)$ (fig. 44) the pressure p of the source distribution at time T is, by equation (102)

$$p = \frac{\rho a q}{2\pi} \int_{x_1 = -Ut}^{x_1 = 0} \frac{dx_1}{\sqrt{a^2(t - t_1)^2 - (x - x_1)^2 - y^2}} \quad (103)$$

t_1 the time of origin of the source in point x_1 .

With the following variable transformation

$$\left. \begin{aligned} \zeta &= \frac{x}{at} & \eta &= \frac{y}{at} \\ \zeta_1 &= \frac{x_1}{at_1} & \frac{a}{U} = \sin \mu = \frac{1}{M} \end{aligned} \right\} \quad (104)$$

we get

$$\frac{p}{\rho a q} = \frac{1}{2\pi} \int_{-1/\sin \mu}^0 \frac{d\zeta}{\sqrt{(1 + \zeta_1 \sin \mu)^2 - (\zeta - \zeta_1)^2 - \eta^2}} \quad (105)$$

The boundaries should be defined before the integral is evaluated. For the function in the denominator is real only in the zone affected by the source distribution; this is bound by the Mach line AM and the circle with center O and radius a.t. Hence the integration must be made between the zero places of the function where it is real.

Posting

$$(1 + \zeta_1 \sin \mu)^2 - (\zeta - \zeta_1)^2 - \eta^2 = 0 \quad (106)$$

the new boundaries are found at

$$\left. \begin{aligned} \zeta_1^{(1)} \\ \zeta_1^{(2)} \end{aligned} \right\} = \frac{-(\zeta + \sin \mu) \pm \sqrt{(1 + \sin \mu)^2 - \eta^2 \cos^2 \mu}}{-\cos^2 \mu} \quad (107)$$

To get an idea of the integrating process as function of the position of point P, $\zeta_1^{(1)}$ and $\zeta_1^{(2)}$ are plotted in terms of ζ . It results in two curves of the second degree, which cross in point Q(ζ, ζ_1) (fig. 45(a)) whereby

$$\zeta = -\left(\frac{1 - \eta \cos \mu}{\sin \mu}\right) \quad \zeta_1 = -\left(\frac{\eta - \cos \mu}{\sin \mu \cos \mu}\right) \quad (108)$$

The shaded area represents the range in which the integration should be made. At small ζ values up to $\zeta = \sqrt{1 - \eta^2}$, integrate between $\zeta_1^{(1)}$ and $\zeta_1^{(2)}$ and then between $\zeta_1^{(1)}$ and the ζ axis. In figure 45(b) the integral limits are shown plotted in the x, y -plane for explanation. The reason for not integrating over positive ζ_1 values is the absence of sources in the right-hand half plane.

Two integration cases are differentiated

$$\left. \begin{aligned} & -\left(\frac{1 - \eta \cos \mu}{\sin \mu}\right) < \zeta < -\sqrt{1 - \eta^2} \quad \text{and} \quad -\sqrt{1 - \eta^2} < \zeta < +\sqrt{1 - \eta^2} \\ & \text{that is} \\ & -\left(\frac{1 - \eta \cos \mu}{\sin \mu}\right) a t < x < -\sqrt{a^2 t^2 - y^2} \\ & \text{and} \\ & -\sqrt{a^2 t^2 - y^2} < x < +\sqrt{a^2 t^2 - y^2} \end{aligned} \right\} (109)$$

In the first instance the pressure integral is

$$\frac{p}{\rho a q} = \frac{1}{2\pi} \int_{\zeta_1^{(1)}}^{\zeta_1^{(2)}} \frac{d\zeta_1}{\sqrt{(1 + \zeta_1 \sin \mu)^2 - (\zeta - \zeta_1)^2 - \eta^2}} \quad (110)$$

But as $\xi_1^{(1)}$ and $\xi_1^{(2)}$ are the solutions of the expression below the root, it can be rewritten as

$$\frac{p}{\rho a q} = \frac{1}{2\pi} \int_{\xi_1^{(1)}}^{\xi_1^{(2)}} \frac{d\xi_1}{\sqrt{(\xi_1^{(1)} - \xi_1)(\xi_1^{(2)} - \xi_1)}} \quad (111)$$

With the substitution

$$\xi_1 = \xi_1^{(1)} + (\xi_1^{(2)} - \xi_1^{(1)}) \sin^2 \theta \quad (112)$$

this integral⁸ gives

$$\frac{p_c}{\rho a q} = \frac{1}{2 \cos \mu} \quad (113)$$

a formula that is independent of $\eta = y/at$.

In the second case, if point P is so situated that

$$-\sqrt{1 - \eta^2} < \xi < +\sqrt{1 - \eta^2}$$

it results in

$$\frac{p}{\rho a q} = \frac{1}{2\pi} \int_{\xi_1^{(1)}}^0 \frac{d\xi}{\sqrt{(1 + \xi_1 \sin \mu)^2 - (\xi - \xi_1)^2 - \eta^2}} \quad (114)$$

⁸As long as the function in the denominator can be brought, with the aid of the integral limits, into the form of equation (111), the integral gives the same value.

which after evaluation gives

$$\frac{p_y}{\rho a q} = \frac{1}{\pi \cos \mu} \cos^{-1} \left[\frac{(\xi + \sin \mu)}{\sqrt{(1 + \xi \sin \mu)^2 - \eta^2 \cos^2 \mu}} \right] \quad (115)$$

The ensuing pressure pattern along a line $y = \text{Constant}$ is represented in figure 46. For each y the pattern consists of two pieces. In the first piece the pressure is constant and equal to p_c , that is, along the length EF between the points where the Mach line emanating from A and the circle with center O and radius $a \cdot t$ intersects the line $y = \text{Constant}$. The second piece is composed of length

$FO' = -\sqrt{a^2 t^2 - y^2}$ and $O'G = +\sqrt{a^2 t^2 - y^2}$, where the pressure is variable; at G the pressure is zero. At $y = y_c$ the constant portion disappears and wherever $y = at$, the pressure becomes zero.

At $y = 0$ it represents Biot's case with the integral limits

$$\left. \begin{array}{ll} -\frac{1}{\sin \mu} < \xi < 1 & \text{and} \quad -1 < \xi < +1 \\ -\frac{at}{\sin \mu} < x < -at & \text{and} \quad -at < x < +at \end{array} \right\} \quad (116)$$

that is

The pressure p_c has the same value as before

$$\frac{p_c}{\rho a q} = \frac{1}{2 \cos \mu} \quad (117)^9$$

but the second piece of the pressure distribution becomes

$$\frac{p_{y=0}}{\rho a q} = \frac{1}{2\pi \cos \mu} \cos^{-1} \left(\frac{\frac{x}{at} + \sin \mu}{1 + \frac{x}{at} \sin \mu} \right) \quad (118)$$

⁹_q corresponds to Biot's $2v_0$.

It should be noted that a pressure effect appears also outside the area in which the sources are distributed, because the source in 0 affects the area inside the circle $a \cdot t$ as mentioned before.

(b) Velocity Calculation

In general, the velocity component is defined by the integration of the portions stemming from a single source (eq. (101)). In our problem the velocity v_y is of particular interest.

It becomes

$$v_y = \frac{q}{2\pi} \int_{x_1=-Ut}^{x_1=0} \frac{a(t - t_1)y \, dx_1}{[(x - x_1)^2 + y^2] \sqrt{a^2(t - t_1)^2 - [(x - x_1)^2 + y^2]}}$$

If $r = \sqrt{(x - x_1)^2 + y^2}$ is small compared to $a(t - t_1)$, that is, for the places close to the x-axis, this equation simplifies to

$$v_y = \frac{q}{2\pi} \int_{x_1=-Ut}^{x_1=0} \frac{y \, dx_1}{[(x - x_1)^2 + y^2]} = \frac{q}{2\pi} \left[\tan^{-1} \left(\frac{Ut + x}{y} \right) - \tan^{-1} \frac{x}{y} \right] \quad (119)$$

Letting y approach 0, positive y , the results for negative values of x are

$$v_y = \frac{q}{2} \quad (120)$$

which may be designated by v_0 (as in Biot's report).

For positive x values, $v_y = 0$.

It indicates that such a source distribution gives a uniform vertical velocity v_0 over the distance of the x-axis where the sources are. (For negative y , inverse velocities result.)

Biot mentioned this fact in his report and used it to calculate the pressure distribution over a plate in a vertical gust (compare next section).

The same variable change as in the pressure calculation gives

$$v_y = \frac{v_0}{\pi} \int_{\xi_1^{(1)}}^{\xi_1^{(2)}} \frac{\eta(1 + \xi_1 \sin \mu) d\xi_1}{[(\xi - \xi_1)^2 + \eta^2] \sqrt{(1 + \xi_1 \sin \mu)^2 - [(\xi - \xi_1)^2 + \eta^2]}} \quad (121)$$

The arguments for the integral limit are the same as for the pressure integral and $\xi_1^{(1)}$; $\xi_1^{(2)}$ is given by equation (107). Integrating between $\xi_1^{(1)}$ and $\xi_1^{(2)}$, that is, when

$$-\left(\frac{1 - \eta \cos \mu}{\sin \mu}\right) < \xi < \sqrt{1 - \eta^2}$$

it is seen that the integral gives the value $\frac{\pi}{\eta}$, so that v_y has the constant v_0 for this range of ξ .

For the second case $\left(-\sqrt{1 - \eta^2} < \xi < +\sqrt{1 - \eta^2}\right)$ the integration between $\xi_1^{(1)}$ and 0 indicates that¹⁰

$$v_y = \frac{v_0}{\pi} \left\{ \pi - \tan^{-1} \left[\frac{\eta \sqrt{1 - (\xi^2 + \eta^2)}}{\sin \mu (\xi^2 + \eta^2) - \xi} \right] \right\} \quad (122)$$

This identifies the velocity distribution on the lines $y = \text{Constant}$ (fig. 47).

¹⁰See note on p. 66.

From the calculation of the pressure and velocity distribution over the lines $y = \text{Constant}$, it is apparent that the flow outside the circle of radius $a \cdot t$ is steady. This is true from the physical standpoint too, since the gust front does not affect this area.

4. Single Flat Plate in a Vertical Gust

(Biot 1945)

The flat plate AB of length l at supersonic velocity U enters a gust with the transverse velocity v_0 (fig. 48(a)). Since the transverse velocity on the plate must be zero (no flow through plate) an equal and opposite velocity is superposed on the gust velocity v_0 in place of the plate. This velocity can be visualized as reflection of the gust on the plate (fig. 48(b)).

Since velocity U is greater than the sonic velocity, the sides of the plates are not affected by one another, so that one side of the plate can be analyzed separately. The pressure acting on one side is exactly the same as on the other, except with inverse prefix. As the interference velocity v_0 is much smaller than velocity U , the linearized potential equation can be applied to the stream potential. Selecting a system of coordinates that moves with the velocity U , (eq. (97)) according to which the disturbances are diffused with sonic velocity, can be applied to the flow potential.

Biot's method replaces the part AO of the plate struck by the gust, by unsteady sources. This source distribution, which increases in time, yields a uniform velocity v_0 normal to the plate, hence satisfies the boundary condition on the bottom side of the plate.

If the plate enters the gust at time $t = 0$, the distance at time t is $AO = -Ut$, the origin of the coordinate system being located in the gust front.

The results of section 3 can be applied directly, and the pressure variation along the plate defined (fig. 49(a)). As it is dependent solely on x/at the patterns are like those for the different Mach numbers. The total force on the plate - the lift - is obtained by integration of the pressure pattern. Three phases are involved here (fig. 49):

$$I \quad (U + a)t \leq l$$

that is, the trailing edge is outside the effective range of the gust front;

$$\text{II } (U + a)t > l > (U - a)t$$

that is, the trailing edge is inside the effective range of the gust front;

$$\text{III } (U - a)t \geq l$$

that is, the entire plate is outside the effective range of the gust front, hence is no longer exposed to any unsteady effect.

The integration gives the following lift values of the three phases:¹¹

$$\frac{A_I}{2\rho a v_0 l} = \frac{U t}{l} = \frac{a}{\sin \mu} t \quad (123)$$

$$\frac{A_{II}}{2\rho a v_0 l} = \frac{1}{\pi \cos \mu} \cos^{-1} \left[\frac{1}{\sin \mu} \left(1 - \frac{U t}{l} \cos^2 \mu \right) \right] + \frac{U t}{\pi l} \sin^{-1} \left[\frac{1}{\sin \mu} \left(\frac{l}{U t} - 1 \right) + \frac{\pi}{2} \right] \quad (124)$$

¹¹The integral

$$I = \int \frac{\xi d\xi}{(\xi + A) \sqrt{1 - \xi^2}}$$

appears in the calculation of A_I and A_{II} . With no boundary, the solution is

$$I = \sin^{-1} \xi - \frac{A}{\sqrt{A^2 - 1}} \sin^{-1} \left(\frac{1 + A\xi}{A + \xi} \right)$$

which gives

$$I = \pi \left(- \frac{A}{\sqrt{A^2 - 1}} \right)$$

between the limits -1 and $+1$.

(The \sin^{-1} to be taken between $-\frac{1}{2}\pi$ and $+\frac{1}{2}\pi$.)

$$\frac{A_{III}}{2\rho a v_0 l} = \frac{1}{\cos \mu} \quad (125)$$

In phase I and II the lift increases continuously with the time and reaches a maximum in phase III, where it becomes independent of the time. In the last phase the lift is the same as on a plate at angle v_0/U in steady flow.

5. The Straight Cascade

The cascade problem is unlike that of the plate to the extent that the plates mutually interfere. The sources replacing the portion of the plate struck by the gust create a pressure on the adjacent plates. They also produce a velocity v_u , which in order to satisfy the boundary condition of no through flow of the plate, makes a change in that source distribution necessary.

Since the disturbances are small the solution of the single plate can be superposed in the sense of the linearized theory of the adjacent plate effect.

As shown in sections 2 and 3, the unsteady source - and the source distribution - which lies on the x-axis, produces no vertical velocity component along this axis, outside the distance, where it is.

This characteristic enables the velocity component v_y to be replaced by an additive source distribution along the particular parts of the plate, which gives the velocity at each point. The new sources create a further pressure on the plate itself - and in general react on the adjacent plates.

The total force - the lift - on each plate consists then of the lift of the undisturbed plate (A_u), the lift from the pressure p_y of the sources of the adjacent plates (A_d) and the lift (A_v) of the new source distribution due to velocity v_y .

Suppose that h is the plate spacing and L the plate chord of the straight cascade (fig. 50). The lines $AM \dots$ represent the

Mach lines emanating from the leading edge, where angle MAB is the Mach angle $\mu = \sin^{-1} U/a$.

Then the following approximation is made: the relative flow and the plate form in reality the angle $\psi = \tan^{-1}(v_0/U)$. But as v_0 is small compared to U , this ψ is negligibly small with respect to μ , and it can be assumed that the Mach line itself rather than the relative flow direction forms the angle μ . In this event, the Mach lines form the same angle with both sides of the plate. The Mach lines emerging from the leading edge strike both sides of the plate at the same distance AE from the leading edge. At $(h/l) > \tan \mu$ the points are not located on the plates, and the plates do not influence each other. Consequently the cases where $(h/l) < \tan \mu$ are examined.

At time $t = 0$ the cascade is directly in front of the gust; the origin of the coordinates is placed in the gust front. In the first time intervals of the phenomenon the disturbances have not spread out enough to be able to influence the adjacent plates. As in figure 51, the distance is $a \cdot t < h$, so that the circles with center O and radius $a \cdot t$ do not touch the plates. Lift and pressure distribution are the same as on the single plate.

As soon as $t > h/a$, the plate AB comes within the effective range of its adjacent plates. On EFG (fig. 52) the source distributions $A'O'$ and $A''O''$ create an additional pressure which can be computed according to section 3. The points F and G are then the points of intersection of both circles with center O' and O'' and radius $a \cdot t$ with plate AB . It is readily apparent that the additive pressure on EF is constant and, according to equation (113), has the value

$$\frac{p_c}{\rho a v_0} = \frac{1}{\cos \mu} \quad (126)$$

If $\eta = h/at$ is inserted ($y = h$) in equation (115), the pressure on FG follows at

$$\frac{p_h}{\rho a v_0} = \frac{1}{\pi \cos \mu} \cos^{-1} \left[\frac{\left(\frac{x}{at} + \sin \mu \right)}{\sqrt{\left(1 + \frac{x}{at} \sin \mu \right)^2 - \frac{h^2}{a^2 t^2} \cos^2 \mu}} \right] \quad (127)$$

The ensuing additive pressure is represented in figure 52.

In addition, the following condition must be satisfied: The normal velocities $v_y = h$ created by the source distribution $A'O'$ and $A''O''$ are reflected on EO, so that at that point the gust is partly compensated. The source distribution to be applied is to compensate the velocity $(v_0 - v_y)$. The velocity v_y is computed as in section 3, and the pressure p_v - along the particular plate - is obtained by integration of the pressure contribution of each source. Assuming the local velocity v_y on a small distance dx_1 to be constant, the yield of the source distribution per unit length on this small distance is then $q = 2v_y$. Along this area of the plate the source distribution produces the pressure (compare section 2)

$$\Delta p_{y=0} = \frac{\rho a v_y}{\pi} \frac{dx_1}{\sqrt{a^2(t - t_1)^2 - r^2}} \quad (128)$$

hence

$$p_{v_{y=0}} = \int_{x_1(1)}^{x_1(2)} \frac{\rho a}{\pi} \frac{v_y dx_1}{\sqrt{a^2(t - t_1)^2 - r^2}} \quad (129)$$

with v_y periodically and locally variable. It is best to solve the integral graphically for each particular case. The arguments for the integral limit are the same as before. The lift contribution A_v at any instant is obtained by integration of the ensuing pressure plot.

To obtain the resultant pressure, this pressure is superimposed on the two previous pressure distributions.

In the following, the pressure contribution due to the additive pressure p_h is calculated. Three phases, depending on time and ratio h/l , are involved:

I. When $z \geq \left(Ut + \sqrt{a^2 t^2 - h^2} \right)$ (fig. 52), the lift is

$$A_{yI} = 2 \int_{\left(-Ut + \frac{y}{\tan \mu} \right)}^{-\sqrt{a^2 t^2 - h^2}} p_c \, dx + 2 \int_{-\sqrt{a^2 t^2 - h^2}}^{+\sqrt{a^2 t^2 - h^2}} p_h \, dx$$

with the previously employed variable change and with $y = h$

$$\begin{aligned} A_{yI} &= 2at \int_{-\frac{Ut+y/\tan \mu}{at}}^{-\sqrt{1-\eta^2}} p_c \, d\zeta + 2at \int_{-\sqrt{1-\eta^2}}^{+\sqrt{1-\eta^2}} p \, d\zeta \\ &= 2at p_c(\zeta) \Big|_{-\frac{Ut+y/\tan \mu}{at}}^{-\sqrt{1-\eta^2}} + 2at(p\zeta) \Big|_{-\sqrt{1-\eta^2}}^{+\sqrt{1-\eta^2}} - at \int_{-\sqrt{1-\eta^2}}^{+\sqrt{1-\eta^2}} \zeta \left(\frac{dp_h}{d\zeta} \right) d\zeta \end{aligned} \quad (130)$$

By equation (127)

$$\frac{dp_h}{d\zeta} = \frac{\rho a v_0}{\pi} \frac{(1 + \zeta \sin \mu) - \eta^2}{\left[(1 + \zeta \sin \mu)^2 - \eta^2 \cos^2 \mu \right] \sqrt{1 - \zeta^2 - \eta^2}} \quad (131)$$

hence the integral

$$\begin{aligned} I &= \int_{-\sqrt{1-\eta^2}}^{+\sqrt{1-\eta^2}} \zeta \frac{dp_h}{d\zeta} \, d\zeta \\ &= \int_{-\sqrt{1-\eta^2}}^{+\sqrt{1-\eta^2}} \frac{(1 + \zeta \sin \mu - \eta^2) \zeta}{\sqrt{1 - \zeta^2 - \eta^2} \left[(1 + \zeta \sin \mu)^2 - \eta^2 \cos^2 \mu \right]} \, d\zeta \end{aligned}$$

Its evaluation gives

$$I = - \frac{\pi}{\sin \mu \cos \mu} (\cos \mu - 1) \left[1 + \frac{\eta (\cos \mu + 1)}{\eta + \cos \mu} \right] \quad (132)$$

consequently

$$\frac{A_{yI}}{2\rho a^2 u_0} = \frac{t}{\sin \mu \cos \mu} \left\{ (1 - \eta \cos \mu) + (\cos \mu - 1) \left[1 + \frac{\eta (\cos \mu + 1)}{(\cos \mu + \eta)} \right] \right\} \quad (133)$$

II. But if (fig. 53)

$$\left(Ut + \sqrt{a^2 t^2 + y^2} \right) > z > \left(Ut - \sqrt{a^2 t^2 - y^2} \right)$$

the evaluation of the integral gives the formula

$$\begin{aligned} A_{yII} = & 2\rho e \left(\frac{z - Ut}{at} \right) + \frac{2\rho a v_0}{\cos \mu} \sqrt{1 - \eta^2} - \\ & \frac{2\rho a v_0}{\pi \sin \mu \cos \mu} \left\{ \eta \left[\sin^{-1} S - \frac{A}{\sqrt{A^2 - 1}} \sin^{-1} \frac{1 + AS}{A + S} + \frac{\pi}{2} \left(1 - \frac{A}{\sqrt{A^2 - 1}} \right) \right] - \right. \\ & \left. (\eta - \cos \mu) \left[\sin^{-1} S - \frac{B}{\sqrt{B^2 - 1}} \sin^{-1} \frac{1 + BS}{B + S} + \frac{\pi}{2} \left(1 - \frac{B}{\sqrt{B^2 - 1}} \right) \right] \right\} \quad (134) \end{aligned}$$

where

$$S = \frac{l - Ut}{\sqrt{a^2 t^2 - y^2}}$$

$$A = \frac{1 + \eta \cos \mu}{\sin \mu \sqrt{1 - \eta^2}} \quad \text{and} \quad B = \frac{1 - \eta \cos \mu}{\sin \mu \sqrt{1 - \eta^2}}$$

The pressure p_e is obtained from equation (127), when $x = (l - Ut)$ is inserted, at

$$\frac{p_e}{\rho a v_0} = \frac{1}{\pi \cos \mu} \cos^{-1} \left[\frac{\left(\frac{l - Ut}{at} + \sin \mu \right)}{\sqrt{\left(1 + \frac{l - Ut}{at} \sin \mu \right)^2 - \frac{h^2}{a^2 t^2} \cos^2 \mu}} \right] \quad (135)$$

III. If $l \geq (U - at)$, $p_y = p_c$ along the entire distance EB, so that the additive lift

$$\frac{A_{yIII}}{2\rho a v_0} = \frac{1}{\cos \mu} \left(l - \frac{h}{\tan \mu} \right) \quad (136)$$

reaches a value that is independent of the time.

Note on the Velocity Integral

By a simple transformation the integral can be rewritten in the following form:

$$I = \int_{\xi_1(1)}^{\xi_1(2)} \frac{(A + B\xi_1)d\xi_1}{(\xi_1^2 + a)\sqrt{\alpha\xi_1^2 + B\xi_1 + \gamma}}$$

This integral can be solved by means of tables (Integral table, Part I, by Gröbner and Hofreiter, Springer Co., Wien). Although the general solution is quite complicated, the result is found to be independent of ξ_1 , once the limits have been inserted.

Bearing in mind that the integration limits are the solutions of the function below the root, the integral is rewritten as function of the limits

$$I = \int_{\xi_1^{(1)}}^{\xi_1^{(2)}} \frac{(1 - \xi_1 \sin \mu) d\xi_1}{\left[(1 - \xi_1 \sin \mu)^2 - \cos^2 \mu (\xi_1 - \xi_1^{(1)}) (\xi_1^{(2)} - \xi_1) \right] \sqrt{(\xi_1 - \xi_1^{(1)}) (\xi_1^{(2)} - \xi_1) \cos \mu}}$$

The following substitutions are made consecutively:

$$1. X = 1 - \xi_1 \sin \mu$$

The limits are thus X_1 and X_2 ($X_2 > X_1$)

$$2. Y = \frac{1}{X} \frac{2X_1 X_2}{X_1 + X_2} - 1$$

$$3. Z = Y(X_2 + X_1) / (X_2 - X_1)$$

$$4. t = Z^2$$

$$5. s = \frac{1}{A' + t} \quad A' = \frac{4X_1 X_2 - \cos^2 \mu (X_1 + X_2)^2}{\cos^2 \mu (X_1 - X_2)^2}$$

6. Numerical Example

Dimensions of cascade

$$h/l = 0.55$$

Mach number of flow

$$M = 1.414 (= \sqrt{2}) \text{ corresponding to a}$$

Mach angle

$$\mu = 45^\circ$$

The period t_e up to the end of the phenomenon is determined by

$$(U - a)t_e = l$$

whence

$$t_e = \frac{l}{0.414a}$$

All time intervals are referred to y/a in order to obtain a dimensionless ratio ($= l/\eta$). Then

$$\frac{t_e}{y/a} = 4.38 \quad (y = h)$$

The three pressure contributions p_u , p_h , and p_v are defined by the formulas of the preceding section at various time intervals indicated by the digits 0, 1, 2, 3, . . . 10.¹² The time intervals were chosen as follows: The time interval denoted by 3 represents the end of the first phase of the undisturbed plate (compare section 4). At $\eta = 1$ (period: 4) the influence of the adjacent plates begins and ends at $\eta = 0.244$ (period: 9). At $\eta = 0.707$ (period: 6), the Mach line emerging from the leading edge of the plate strikes the adjacent plate.

Figure 54 represents the position of the gust front and the area disturbed by it at the different time intervals.

Figure 55 illustrates the pressure of the undisturbed plate p_u .

Figure 56 illustrates the pressure contribution p_h .

The pressure contribution p_v is computed graphically, the velocity distributions v_y/v_0 required for it are obtained by equation (122) for the time intervals 5, 6, 7, 8 and reproduced in figure 57.

¹²The corresponding curves in figures 55, 56, 57, 60, and 61 are denoted by the same digits.

Since the integrand

$$f = \frac{v_y/v_0}{\sqrt{\left(1 - \frac{t_1}{t}\right)^2 - (\xi - \xi_1)^2}}$$

becomes infinite at the two limits $\xi_1^{(1)}$ and $\xi_2^{(2)}$ which are, as known, the solution of the function below the root, the graphical solution is continued to $(\xi_1^{(1)} - \epsilon)$ and $(\xi_1^{(2)} - \epsilon')$ where ϵ , ϵ' are small real values in comparison to ξ_1 .

Figure 58 represents several of the functions f for different time intervals.

The integration over ϵ and ϵ' is made analytically, by putting $v_y/v_0 = \text{constant mean value}$.

The relation for t_1/t at $\eta < 0.707$, that is, when the additional source distribution is bound by a Mach line, is

$$t_1/t = \eta \cos \mu + \xi_1 \sin \mu$$

If the source distribution is limited by the circle of radius $R = at$, a similar relation

$$t_1/t = \eta \cos \beta + \xi_1 \sin \beta$$

is applicable (fig. 59).

Figure 60 represents the pressure contribution p_v , figure 61 the resultant pressure distributions.

The lift of the plate (fig. 62) is obtained by graphical integration over the resultant pressures. At the appearance of the adjacent plate effect the lift decreases with the time interval; A' represents the steady lift of the undisturbed plate.

Figure 63 shows the moment distribution M plotted against plate center; M_{st} represents its steady value. Here the moment increases with the time because of the built-up negative pressure from $t = h/a$.

CHAPTER VII. EFFICIENCY OF A SUPERSONIC PROPELLER

1. Introduction

The cascade efficiency defined from thrust and tangential force is suitable also for the propeller. But in the preceding arguments the flow was assumed parallel and the blades as infinitely thin plates, which now must be modified. The friction at the plates must be allowed for and the infinitely thin plates replaced by profiles of finite thickness. Then the results are used to calculate the efficiency of a real propeller in order to obtain an approximate picture of the efficiency to be expected.

2. Effect of Friction on Cascade Efficiency

When the friction at the plate surfaces is taken into account, the resultant force K without friction defined in chapters III and IV, is supplemented by an additional resistance F , so that K' is the total force acting on the plate (fig. 64).

The frictional force is parallel to the plate. But since its component normal to the airstream direction is small at the angles of attack in question, the total frictional force can be assumed to be in the flow direction.

The drag coefficient is expressed by

$$c_w' = \frac{4\psi^2}{\sqrt{M^2 - 1}} + 2c_f \quad (137)$$

$c_f = \frac{F}{2q_1}$ is coefficient of friction of one side of the plate and q_1 is dynamic pressure of inflow.

The lift coefficient remains

$$c_a = \frac{4\psi}{\sqrt{M^2 - 1}} \quad (138)$$

as for parallel flow.

According to the definition introduced in chapter III, the cascade efficiency is

$$\eta = \frac{S'v}{T'u} \quad (139)$$

where S' and T' are the thrust and tangential force corresponding to the new force K' .

In terms of angles β , ψ and α (fig. 64) the efficiency is

$$\eta = \tan \alpha \tan(\beta - \psi)$$

where

$$\alpha = \tan^{-1} \frac{S'}{T'} \quad (140)$$

Introducing the drag/lift ratio

$$\epsilon' = \frac{W + F}{A} = \frac{c_w'}{c_a} = \left(\psi + \frac{c_f \sqrt{M^2 - 1}}{2\psi} \right) \quad (141)$$

the efficiency η becomes

$$\eta = \frac{1 - \epsilon' \tan(\beta - \psi)}{1 + \epsilon' / \tan(\beta - \psi)} \quad (142)$$

Hence it is apparent that, contrary to the earlier results, the efficiency is now dependent on the Mach number.

With the assumption of a turbulent boundary layer

$$c_f = \frac{0.455}{\log_{10} Re^{2.58}} \quad (143)$$

according to Schlichting, where Re is the Reynolds number based upon chord l and relative velocity w .

The values plotted in table 9 and figure 65 as functions of the angle of stagger were calculated with the Mach numbers $M = 1.40$ and $M = 2.50$, then at an angle $\psi = 3^\circ$ and the optimum angles¹³ $\psi = 2.65^\circ$ ($M = 1.40$) and $\psi = 4.11^\circ$ ($M = 2.50$). The Reynolds number assumed at $Re = 10^6$ corresponds to $c_f = 0.0045$.

The effect of friction is illustrated in figure 65, along with the efficiency curve for $\psi = 3^\circ$ with friction discounted.

3. Effect of Thickness

To assure minimum wave resistance the contour of a supersonic profile must consist of straight lines and its maximum thickness lie in the center, hence a double-wedge profile is recommended (fig. 66).

By linearized airfoil theory (ref. 1) the thickness causes a drag which increases quadratically with the thickness ratio d/l , and which can be directly superposed on the lift coefficient and the frictional drag of the plate.

Hence the drag coefficient of a profile of finite thickness ratio with friction is

$$c_w'' = \frac{4}{\sqrt{M^2 - 1}} \left[\psi^2 + \left(\frac{d}{l} \right)^2 + c_f \frac{\sqrt{M^2 - 1}}{2} \right] \quad (144)$$

But the lift coefficient remains unchanged

$$c_a = \frac{4\psi}{\sqrt{M^2 - 1}}$$

¹³

As stated in the introduction, $\psi_{opt} = \sqrt{(d/l)^2 + c_f \frac{\sqrt{M^2 - 1}}{2}}$, for the plate, obviously $d/l = 0$.

and the drag/lift ratio to be inserted in equation (141) in place of ϵ' is

$$\epsilon'' = \frac{c_w''}{c_a} = \psi + \frac{1}{\psi} \left[\left(\frac{d}{l} \right)^2 + c_f \frac{\sqrt{M^2 - 1}}{2} \right] \quad (145)$$

Table 10 shows the efficiencies of two cascades of double-wedge profiles and the relative maximum thickness ratio

$d/l = 0.05$ and 0.10 - with friction

at $M = 1.40$

$\psi = 3^\circ$

$c_f = 0.0045$

These values are also shown in figure 67 together with those for $d/l = 0$ (the plate) for comparison.

The angle of stagger β - with friction and finite thickness - for maximum efficiency at fixed angle of attack and fixed Mach number is found by simple differentiation at

$$\begin{aligned} \beta_{\eta_{\max}} &= \tan^{-1} \left(-\epsilon \pm \sqrt{\epsilon^2 + 1} \right) \\ &= 45^\circ + \left(\psi - \frac{1}{2} \tan^{-1} \epsilon \right) \end{aligned} \quad (146)$$

4. Appraisal of the Efficiency of a Supersonic Propeller

On a supersonic propeller the blades are struck at a relative speed which at every point of the blade is greater than the sonic velocity. Two types of propellers are differentiated. The one moves forward at supersonic speed, so that supersonic speed occurs at every rpm and every β . On the other the supersonic speed is reached without it having to move forward with supersonic speed. The efficiency of the first type propeller is calculated.

The propeller has a forward speed v of about 406 m/sec ($M = 1.20$ - sonic velocity $a = 338$ m/sec); it has four blades of 2m outside diameter and 1m inside diameter and 0.5 hub ratio. The cross section of the blade is a double-wedge profile, with maximum thickness ratio of $d/l = 0.07$ at the hub, and tapering to $d/l = 0.05$ at the tip.

The maximum efficiency of a profile is reached with $\beta = 45^\circ$, according to chapter III. At the blade tip where the thrust is highest, this condition gives a tip speed of 400 m/sec; that corresponds to 3,820 rpm. For reasons of strength the blade chord tapers from $L_N = 40$ cm at the hub to $L_g = 30$ cm at the tip.

In each coaxial cylindrical section - with respect to the propeller axis - the angle between the relative flow direction and the profile axis - the angle of attack - was assumed at ψ_{opt} (compare introduction). To satisfy this condition, the angle of stagger in each section, that is, the angle between profile axis and direction of peripheral speed U must be varied. The relation

$$\tan(\beta - \psi) = v/u$$

must be satisfied.

With reference to a system of coordinates fixed in space, each point of the propeller moves on a helical line. Disturbances issue from each point which at the assumed pressure conditions and angles of attack can be regarded only as sound disturbances. The zone disturbed by each blade is then limited by the enveloping curve of all spheres whose centers lie on the various helical lines and whose radii at the same time are equal to sonic velocity \times time. Figure 68 represents the disturbed zone of an edge OA , which, for example, moves at a forward speed of $1.2 \times a$ and whose maximum tip speed equals the sonic velocity; $O'A'$ represents the position of the same edge after a time interval Δt , which corresponds to a fourth of a revolution.

Considering that the blades are twisted, that the disturbances of different sections can influence one another and be reflected on propeller hub, it is readily apparent that an exact calculation of the forces on each blade represents a difficult problem. When each blade is outside the zone of disturbance of the other blade, the blade can be examined separately. Assuming homogeneous flow and coaxial cylindrical areas, that is, radial equilibrium, the blade forces can be determined from a two-dimensional consideration of the developed blade (fig. 69), by computing the lift and drag and from it the thrust and tangential force in each cross section by linearized theory.

At the velocities selected the boundary effect is confined to a moderately large zone compared to blade area, so that its effect within the framework of the intended appraisal on the total forces can be disregarded.

The thrust of the whole blade is then

$$S_{\text{blade}} = \int_{\text{hub}}^{\text{tip}} \frac{dS}{dr} dr \quad (147)$$

The integration is made by graphical method (fig. 71(a)) with

$$\frac{dS}{dr} = \frac{4\psi}{\sqrt{M^2 - 1}} \frac{\rho w^2}{2} \cdot \frac{\cos[(\beta - \psi) + \gamma]}{\cos \gamma} \quad (148)$$

computed for five sections (fig. 69).

The corresponding Reynolds number for all sections was assumed at $c_f = 0.004$ (turbulent boundary layer).

The torque D of a blade is defined the same way as the thrust by integration (fig. 71(b)). The following relation applies:

$$D_{\text{blade}} = \int_{\text{hub}}^{\text{tip}} \frac{dT}{dr} r dr = \int \frac{4\psi}{\sqrt{M^2 - 1}} \frac{\rho w^2}{2} \cdot \frac{\sin[(\beta - \psi) + \gamma]}{\cos \gamma} r dr \quad (149)$$

The characteristics for the five sections are correlated in table 2. The integration gives

$$S_{\text{blade}} = 425 \text{ kg}$$

$$D_{\text{blade}} = 600 \text{ kg/m}$$

hence for the propeller

$$S = 1700 \text{ kg}$$

$$D = 2400 \text{ kgm}$$

The efficiency of the propeller is given by

$$\eta = \frac{Sv}{2\pi nD} \quad (150)$$

with the values inserted gives

$$\eta = 71.8 \text{ percent}$$

A quick and close estimate of the efficiency is obtainable directly from the calculation of $\left(\frac{dS}{dr}\right)_M$ and $\left(\frac{dD}{dr}\right)_M$, where these values are applicable to the whole blade.

SUMMARY

1. Lift and drag coefficients for the flat plate at various Mach numbers, ranging from 1.20 to 10, and for different angles of incidence are calculated, account being taken of the exact flow over both sides of the plate. These values are tabulated and also given in the form of charts. The same coefficients are also calculated under the assumptions of linearized flow over the plate, according to the Ackeret theory. A comparison of both methods shows reasonable agreement between the linearized theory and the exact method within the usual range of angles of incidence (max 10°) and for the usual Mach numbers. Special formulas for calculating the lift and drag coefficients for very high Mach numbers are derived.

2. An analytical solution of the problem of the interaction between shock waves and expansion waves has been established.

3. A method for calculating the lift and drag coefficients for a cascade of flat plates is described and applied to an example, with the aid of the formulas derived in the foregoing item. A definition for the

efficiency of the cascade - without friction - is introduced and the efficiency is evaluated for two Mach numbers and different angles of blading.

4. A linearized theory for supersonic flow through a cascade of flat plates is established and applied to the example already treated. Comparison of the lift coefficients shows reasonable agreement.

5. For demonstration purposes, schlieren photographs were made showing the flow between two flat surfaces. They serve to confirm the established linearized theory for small angles of incidence and show clearly the interaction between shock and expansion waves.

6. Under the assumption that the flow through the cascade of flat plates undergoes a small sudden change of direction, that is, a small change in the angle of incidence, the nonstationary flow in the cascade is discussed to show the kind of forces which act on the plates during the transition period. An example has been calculated in detail.

7. The definition of the efficiency mentioned in 3, is especially suitable for application to a supersonic propeller. The effect of friction and blade thickness on that efficiency is shown. A rough estimation of the efficiency of a supersonic propeller is then made.

Translated by J. Vanier
National Advisory Committee
for Aeronautics

REFERENCES

1. Ackeret, J.: Gasdynamik, Handbuch der Physik, Bd. 8, S: 289-342, 1925. Gasdynamik, Vorlesungen an der E.T.H., u.a. Mitteilung Nr. 8 des Institutes für Aerodynamik.
2. Sauer: Einführung in die technische Gasdynamik. Springer-Verlag, Berlin, 1943.
3. Ferri: Elements of Aerodynamics of Supersonic Flows. The Macmillan Company, New York, 1949.
4. Schubert: Zur Theorie der stationären Verdichtungsstöße. Z.A.M.M., Heft 3, Juni, 1943.
5. Biot: Loads on a Supersonic Wing Striking a Sharp-Edged Gust. Journal of Aeronautical Sciences, May, 1949.
6. Keenan and Kaye: Gas Tables. John Wiley & Sons, New York, 1945.

TABLE 1

M_1	δ_s°	γ_s°	p_1/p_0	q/p_0	q/p_1
1.00	0	90	0.52830	0.36981	0.700
1.10	1.40	73.68	.46835	.39704	.847
1.20	3.70	68.08	.41238	.41567	1.008
1.30	6.32	65.12	.36092	.42689	1.183
1.40	9.03	63.33	.31424	.43114	1.372
1.50	11.67	62.25	.27240	.43050	1.575
1.60	14.24	61.65	.23527	.42182	1.792
1.70	16.63	61.37	.20259	.40995	2.023
1.80	18.84	61.28	.17404	.39472	2.268
1.90	20.87	61.35	.14924	.37714	2.527
2.00	22.71	61.48	.12780	.35750	2.800
2.20	25.90	61.90	.09352	.31684	3.388
2.50	29.67	62.40	.05853	.25610	4.375
3.00	34.01	63.77	.02722	.17143	6.300
4.00	38.75	65.25	.00658	.07375	11.20
5.00	41.11	66.20	.00189	.03306	17.50
6.00	42.44	66.75	.00063	.01588	25.20
8.00	43.79	67.00	.00010	.00448	44.80
10.00	44.43	67.12	.00002	.00165	70.00
∞	45.58	67.70	0	0	∞

TABLE 2
LIFT AND DRAG COEFFICIENTS

M_1	ψ°	P_2/P_0	γ_0	P_2'/P_1	P_2'/P_0	C_a	C_w	ϵ
1.20	1	0.39145	58.75	1.056	0.43527	0.1054	0.0018	0.0175
	2	.37210	61.10	1.120	.46187	.2158	.0075	.0349
	3	.35403	64.37	1.199	.49444	.3373	.0177	.0524
	3.7	.35952	68.08	1.277	.52681	.4011	.0259	.0641
1.40	1	.29910	46.87	1.051	.33027	.0723	.0013	.0175
	2	.28480	48.19	1.104	.34692	.1440	.0050	.0349
	3	.27114	49.57	1.159	.36420	.2156	.0113	.0524
	4	.25824	51.15	1.219	.38306	.2888	.0202	.0699
	6	.23376	54.62	1.353	.42517	.4415	.0464	.1052
	8	.21130	59.36	1.527	.47984	.6168	.0867	.1406
	9.03	.20050	63.17	1.655	.52007	.7321	.1159	.1584
1.60	1	.22374	39.67	1.060	.24939	.0608	.0011	.0175
	2	.21269	40.73	1.104	.25978	.1116	.0039	.0349
	3	.20207	41.82	1.161	.27300	.1679	.0088	.0524
	4	.19191	42.93	1.219	.28679	.2244	.0157	.0699
	6	.17280	45.36	1.345	.31637	.3385	.0356	.1051
	8	.15525	48.04	1.484	.34938	.4557	.0641	.1406
	10	.13914	51.14	1.644	.38685	.5783	.1019	.1762
	12	.12438	54.89	1.832	.43101	.7110	.1511	.2125
	14.24	.11022	61.65	2.143	.50418	.9052	.2532	.2532
1.80	1	.16503	34.64	1.054	.18352	.0468	.0008	.0175
	2	.15640	35.53	1.110	.19318	.0931	.0033	.0349
	3	.14813	36.48	1.170	.20363	.1404	.0074	.0524
	4	.14019	37.44	1.230	.21407	.1867	.0131	.0699
	6	.12534	39.49	1.362	.23704	.2814	.0296	.1051
	8	.11175	41.69	1.505	.26193	.3768	.0530	.1406
	10	.09935	44.06	1.661	.28908	.4734	.0834	.1763
	12	.08806	46.70	1.835	.31936	.5732	.1218	.2126
	15	.07303	51.35	2.139	.37227	.7323	.1962	.2679
	18	.06011	58.00	2.551	.44398	.9249	.3005	.3249
	18.84	.05788	61.28	2.740	.47687	1.0045	.3427	.3412
2.00	1	.12076	30.82	1.058	.13521	.0404	.0007	.0175
	2	.11401	31.65	1.118	.14288	.0807	.0028	.0349
	3	.10757	32.58	1.181	1.15093	.1211	.063	.0523
	4	.10141	33.40	1.247	.15937	.1618	.0113	.0699
	6	.08994	35.24	1.377	.17726	.2429	.0255	.1051
	8	.07949	37.22	1.539	.19668	.3246	.0456	.1406
	10	.07005	39.32	1.707	.21815	.408	.0719	.1763
	12	.06149	41.59	1.889	.24141	.4923	.1046	.2125
	15	.05024	45.34	2.195	.28052	.6222	.1667	.2679
	18	.04070	49.78	2.555	.32653	.7604	.2471	.3249
	21	.03265	55.67	3.014	.38519	.9207	.3534	.3838
	22.71	.02886	61.48	3.460	.44219	1.0659	.4462	.4187

TABLE 2.- Concluded

LIFT AND DRAG COEFFICIENTS

M_1	ψ°	P_2/P_0	γ_0	P_2'/P_1	P_2'/P_0	c_a	c_w	ϵ
2.50	1	0.05296	24.35	1.068	0.06251	0.0373	0.0006	0.0175
	2	.05113	25.05	1.141	.06678	.0611	.0021	.0349
	3	.04772	25.82	1.216	.07117	.0914	.0048	.0524
	4	.04450	26.62	1.296	.07585	.1221	.0085	.0699
	6	.03857	28.27	1.452	.08498	.1826	.0189	.1051
	8	.03455	30.00	1.658	.09704	.2416	.0340	.1406
	10	.02859	31.86	1.865	.10916	.3098	.0536	.1763
	12	.02445	33.81	2.091	.12232	.3738	.0795	.2126
	15	.01917	36.95	2.467	.14439	.4723	.1266	.2679
	18	.01484	40.40	2.895	.16949	.5742	.1865	.3249
	22	.01035	45.62	2.557	.20816	.7162	.2893	.4040
	28	.00575	56.35	4.885	.28592	.9659	.5136	.5317
	29.67	.00482	62.65	5.602	.44220	1.0960	.6240	.5695
5.00	3.60	.00118	14	1.541	.00291	.0523	.0033	.0627
	6.17	.00084	16	2.051	.00388	.0914	.0098	.1076
	10.68	.00043	20	3.247	.00614	.1698	.0319	.1879
	16.60	.00018	26	5.436	.01027	.2926	.0869	.2972
	20.21	.00009	30	7.129	.01347	.3800	.1393	.3666
	26.78	.00002	38	10.893	.02059	.5557	.2792	.5024
	31.21	.000009	44	13.913	.02629	.6805	.4088	.6000
	36.29	.000003	52	17.953	.03392	.8284	.6048	.7301
	41.11	.000001	66	24.206	.04575	1.0427	.9098	.8726
10.00	3.21		8	2.091		.0228	.0013	.0560
	7.65		12	4.877		.0614	.0082	.1340
	13.31		18	10.981		.1549	.0365	.2356
	18.53		24	19.135		.2613	.0877	.3351
	23.47		30	29.018		.3828	.1662	.4341
	28.17		36	40.164		.5079	.2726	.5366
	32.59		42	52.080		.6288	.4017	.6393
	36.64		48	64.263		.7488	.5565	.7437
	40.18		54	76.213		.8641	.7292	.8441
	42.90		60	87.361		.9529	.8862	.9293
	44.43		67.12	98.713		1.0125	.9925	.9803
∞	8.37		10			.0497	.0073	.1471
	16.57		20			.1873	.0558	.2973
	24.50		30			.3795	.1731	.4557
	28.31		35			.4741	.2559	.5386
	32.05		40			.5843	.3662	.6261
	35.55		45			.6812	.4846	.7146
	38.81		50			.7840	.6121	.8042
	41.6		55			.8735	.7754	.8876
	43.9		60			.9452	.9123	.9623
	45.58		67.8			1.0001	1.0204	1.0200
N	5					.0152	.0013	.0875
	10					.0594	.0105	.1763
	15					.1294	.0347	.2679
	20					.2198	.0801	.3640
	25					.3238	.1509	.4663
	30					.4330	.2500	.5774
	35					.5388	.3772	.7002
	40					.6331	.5311	.8391
	45					.7068	.7068	1.0000
	50					.7547	.8992	1.1918

TABLE 3

LIFT AND DRAG COEFFICIENTS OF THE BOUNDARY CURVE

M_1	ψ_s°	p_2/p_0	γ_s °	p_2'/p_1	p_2'/p_0	c_a	c_w	ϵ
1.10	1.4	0.43110	73 14	1.130	0.52924	0.2471	0.0104	0.0248
1.20	3.70	.35952	68 5	1.277	.52681	.4011	.0259	.0641
1.30	6.32	.26668	65 7	1.457	.52586	.6035	.0668	.1107
1.40	9.03	.20050	63 10	1.656	.52009	.7321	.1159	.1584
1.50	11.67	.14392	62 15	1.894	.51593	.8339	.1724	.2068
1.60	14.24	.11022	61 39	2.143	.50418	.9052	.2297	.2532
1.70	16.63	.07918	61 22	2.439	.49412	.9697	.2897	.2988
1.80	18.84	.05788	61 17	2.741	.47687	1.0045	.3427	.3412
1.90	20.87	.04047	61 21	3.097	.46220	1.0449	.3983	.3812
2.00	22.71	.02886	61 29	3.460	.44219	1.0665	.4465	.4187
2.20	25.90	.01417	61 54	4.250	.38746	1.0883	.5284	.4855
2.50	29.67	.00482	62 39	5.602	.44221	1.0960	.6242	.5695
3.00	34.01	.00073	63 46	8.385	.22824	1.0735	.7243	.6747
4.00	38.75	.000014	65 15	15.25	.10060	1.0650	.8551	.8025
5.00	41.11	.000001	66 12	24.40	.04612	1.0515	.9107	.8652
6.00	42.44	0	66 45	35.25	.02231	1.0362	.9432	.9136
8.00	43.79	0	67 0	63.11	.00630	1.0171	.9692	.9601
10.00	44.43	0	67 7	98.90	.00233	1.0121	.9895	.9803
∞	45.58	0	67 41			1.0050	1.0185	1.0200

TABLE 4

LIFT AND DRAG COEFFICIENTS ACCORDING TO THE LINEARIZED THEORY

M_1	α°	c_a	c_w	c
1.20	1	0.10553	0.00018	0.0175
	2	.21046	.00734	.0349
	3	.31600	.01655	.0524
	3.7	.38957	.02516	.0646
1.40	1	.07144	.00125	.0175
	2	.14248	.00497	.0349
	3	.21392	.01121	.0524
	4	.28496	.01989	.0698
	6	.42744	.04480	.1047
	8	.56992	.07950	.1396
	9.03	.64259	.10112	.1574
1.60	1	.05604	.00089	.0175
	2	.11177	.00390	.0349
	3	.16781	.00879	.0524
	4	.22353	.01560	.0698
	6	.33530	.03458	.1047
	8	.44707	.06240	.1396
	10	.55884	.09732	.1745
	12	.67060	.14040	.2094
	14.24	.79582	.19772	.2485
1.80	1	.04676	.00082	.0175
	2	.09325	.00326	.0349
	3	.14001	.00734	.0524
	4	.18650	.01302	.0698
	6	.27976	.02932	.1047
	8	.37301	.05205	.1396
	10	.46626	.08135	.1745
	12	.55952	.11714	.2094
	15	.69953	.18314	.2618
	18.84	.87855	.28884	.3288
2.00	1	.04042	.00070	.0175
	2	.08060	.00281	.0349
	3	.12102	.00634	.0524
	4	.16120	.01125	.0698
	6	.24180	.02532	.1047
	8	.32240	.04995	.1396
	10	.40301	.07030	.1745
	12	.48361	.10125	.2094
	15	.60463	.15829	.2618
	18	.72564	.22802	.3142
	21	.84643	.31040	.3665
	22.71	.91502	.36259	.3962
2.50	1	.03054	.00053	.0175
	2	.06091	.00213	.0349
	3	.09145	.00479	.0524
	4	.12181	.00851	.0698
	6	.18272	.01915	.1047
	8	.24363	.03400	.1396
	10	.30454	.05318	.1745
	12	.36544	.07650	.2094
	15	.45689	.11962	.2618
	18	.54834	.17230	.3142
	22	.67016	.25742	.3840
	28	.85288	.41675	.4887
	29.67	.90366	.46789	.5178
3.00	4	.05699	.00398	.0698
	6	.08549	.00896	.1047
	12	.17097	.03579	.2094
	18	.25654	.08061	.3142
	24	.34203	.14321	.4189
	30	.42752	.22385	.4712
	36	.47030	.32232	.5760
	41.11	.58584	.42033	.7175
10.00	4	.02806	.00196	.0698
	6	.04209	.00441	.1047
	12	.08418	.01762	.2094
	18	.12631	.03969	.3142
	24	.16840	.07051	.4189
	30	.21049	.11022	.4712
	36	.25258	.15800	.5760
	42	.29467	.21600	.7330
	44.43	.31172	.24177	.7755

TABLE 5

M_1	ψ°	$(c_{aG} - c_{aL})$	c_{aG}	$(c_{wG} - c_{wL})$	c_{wG}
1.40	1	0.00084	0.07228	0	0.0013
	2	.00151	.14399	0	.0050
	3	.00163	.21555	.0001	.0113
	4	.00385	.28881	.0002	.0202
	6	.01408	.44152	.0010	.0464
	8	.04690	.61682	.0072	.0867
	9.03	.08950	.73209	.0148	.1159
5.00	4	.0005	.0523	.0009	.0033
	6	.0030	.0914	.0010	.0098
	12	.0255	.1698	.0063	.0319
	18	.0696	.2996	.0246	.0869
	24	.1391	.3800	.0341	.1393
	30	.1846	.5557	.1453	.2792
	36	.3972	.6805	.2698	.4088
	41.11	.4669	.8284	.4895	.6048

TABLE 6

Region	P/P_{01}	M	μ^0	P_0/P_{01}
1	0.31404	1.4004	45.5	1
2	.3645	1.293	50.6	.9996
3	.2991	1.435	44.2	1
4	.3455	1.332	48.8	.9997
5	.2848	1.469	42.9	1
6	.3304	1.364	47.1	.9997
7	.2711	1.503	41.7	1
8	.3139	1.401	45.7	.9998
9	.3285	1.368	47.0	.9997
10	.3139	1.401	45.6	.9997
11	.2985	1.436	44.1	.9997
12	.2999	1.433	44.2	.9997
13	.2850	1.468	42.9	.9997
14	.2708	1.504	41.7	.9997
15	.3624	1.154	50.1	.9982
16	.3445	1.334	48.6	.9997
17	.3295	1.366	47.0	.9997
18	.3124	1.404	45.4	.9997
19	.3276	1.370	46.9	.9998
20	.3134	1.402	45.5	.9997
21	.2972	1.439	44.0	.9997
22	.2996	1.434	44.8	.9997
23	.2842	1.483	42.8	.9997
24	.2696	1.507	41.6	.9997
25	.3610			

TABLE 7

(a) Angle of deflection and shock angle of the shocks between the zones

Regions	Angle of deflection δ°	Shock angle γ°
1-2	3.00	49.57
3-4	3.03	47.91
5-6	2.93	46.48
7-8	2.93	45.13
8-15	2.93	49.43
11-16	2.92	47.78
13-17	2.90	46.40
14-18	2.93	45.03
18-25	2.93	49.30

(b) Intensity of expansion waves between the zones

Regions	Intensity $\Delta\theta^\circ$	Regions	Intensity $\Delta\theta^\circ$
1-3	1.00	13-14	1.02
2-4	1.03	15-16	1.00
3-5	1.00	16-17	.88
4-6	.89	16-19	1.00
4-9	1.03	17-18	1.06
5-7	1.00	17-20	.99
6-8	1.00	18-21	1.00
8-11	1.01	19-20	.89
9-10	.92	20-21	1.05
10-11	1.00	21-23	.89
10-12	.92	22-23	1.05
11-13	.91	23-24	1.05
12-13	1.02		

TABLE 8

CASCADE EFFICIENCY η PERCENT = $f(\beta, \psi)$ (NO FRICTION)

$\psi^\circ \backslash \beta^\circ$	1	3	5	7	10
10	89.8	69.6	49.6	29.72	
20	94.7	83.9	73.6	63.4	48.4
30	96.0	88.3	80.8	73.5	63.1
40	96.5	89.8	83.4	77.3	68.8
50	96.6	90.00	83.8	78.2	70.4
60	96.0	88.8	82.4	76.5	68.8
70	94.8	85.7	78.2	71.4	63.1
80	90.6	76.4	65.8	57.65	48.4
β° for max. η	45.5	46.5	47.5	48.5	50.0
η_{\max} , percent	96.3	90.2	83.7	78.2	70.4

TABLE 9

CASCADE EFFICIENCY WITH FRICTION ALLOWED FOR

β°	M = 1.40		M = 2.50	
	$\psi = 3^\circ$	$\psi = 2.65$	$\psi = 3^\circ$	$\psi = 4.11$
10	55.8	57.0	44.1	41.1
20	74.2	74.6	63.9	63.7
30	80.3	80.4	71.2	71.8
40	82.5	82.8	73.9	74.8
50	82.6	82.7	73.5	74.7
60	80.5	80.6	69.9	71.8
70	74.7	74.6	60.6	63.8
80	57.8	57.2	33.5	41.4

TABLE 10

CASCADE EFFICIENCY WITH DOUBLE-WEDGE PROFILE AND FRICTION

 $M = 1.40 \quad \psi = 30^\circ$

β°	$d/l = 0.05$	$d/l = 0.10$
10	45.53	29.04
20	65.28	47.22
30	72.52	74.78
40	75.11	56.93
50	74.83	54.82
60	71.50	47.31
70	62.71	29.25
80	37.18	

TABLE 11

Section	1 hub N	2	3 center M	4	5 tip S
Radius, r_m	0.500	0.625	0.750	0.875	1.000
Profile chord, m	0.450	0.425	0.400	0.375	0.350
Thickness ratio, d/l	0.070	0.065	0.06	0.055	0.050
Max. thickness, dm	0.0315	0.0282	0.024	0.0206	0.0175
Tip speed, um/sec	200	250	300	350	400
Relative velocity, wm/sec	452.7	476.8	504.6	536.0	570.0
Relative Mach number, M	1.339	1.411	1.493	1.586	1.687
Angle of attack, ψ_{opt} $\begin{cases} \star \\ 0 \end{cases}$	0.0818 4.67	0.0787 4.52	0.0761 4.38	0.0742 4.25	0.0721 4.13
Lift coefficient, c_a	0.3672	0.3164	0.2745	0.2407	0.2120
Drag/lift ratio, ϵ	0.1637	0.1572	0.1523	0.1484	0.1442
Gliding angle, γ°	9.30	8.95	8.66	8.43	8.21
Stagger, β°	68.8	62.9	57.9	53.5	49.58
dS/dr , kg/m	612	748	825	878	904
dD/dr , kg	1026	1118	1173	1212	1224

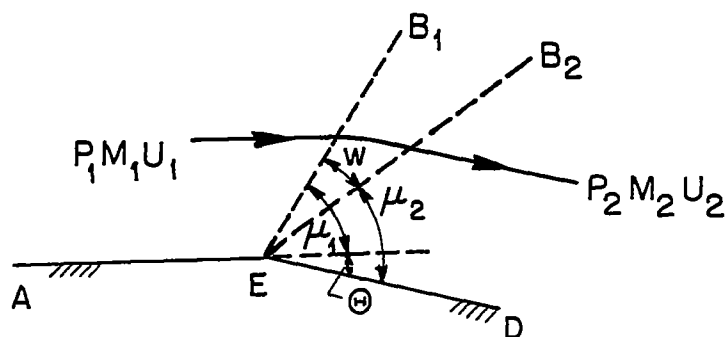


Figure 1.- Expansion around a corner.

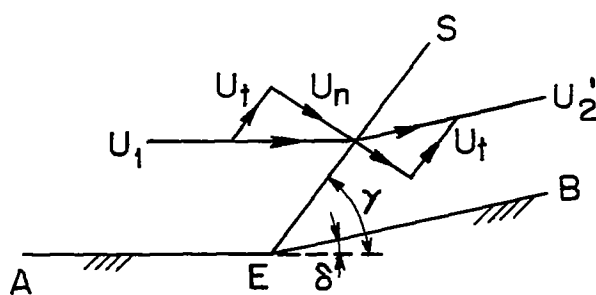


Figure 2.- Oblique compression shock.

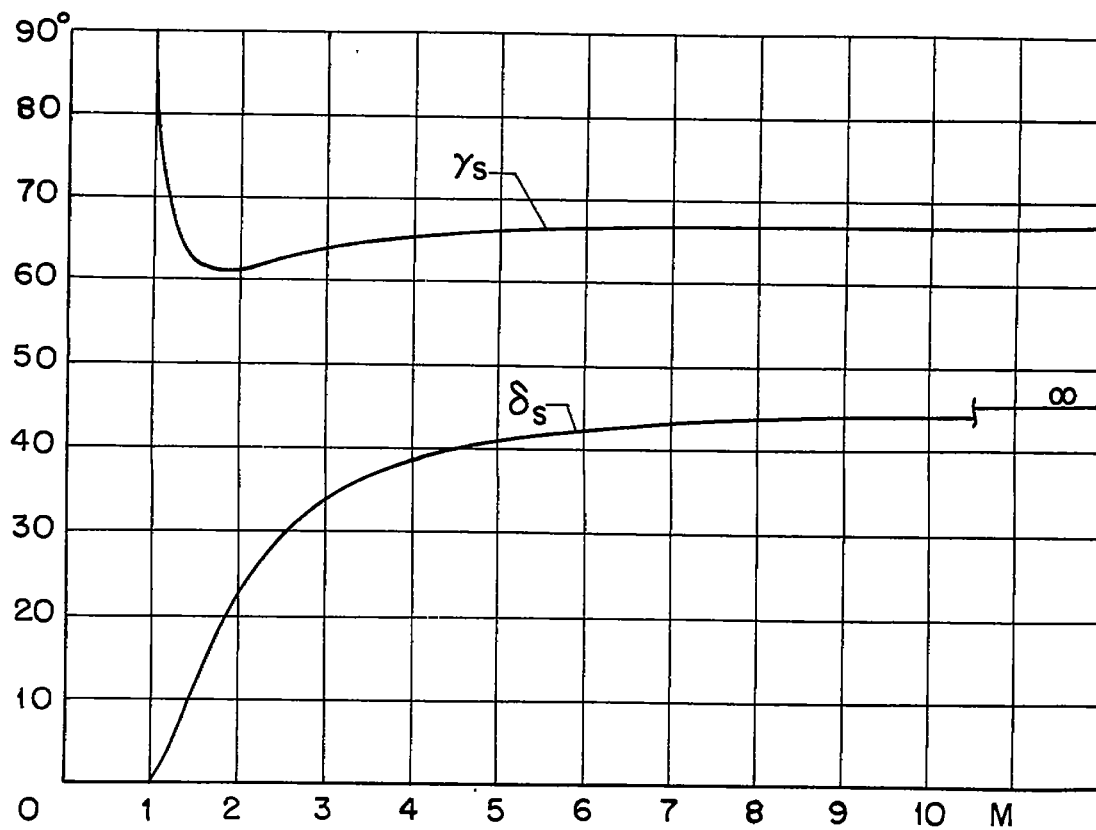


Figure 3.- Shock and flow deflection angles for $M_2 = 1$.

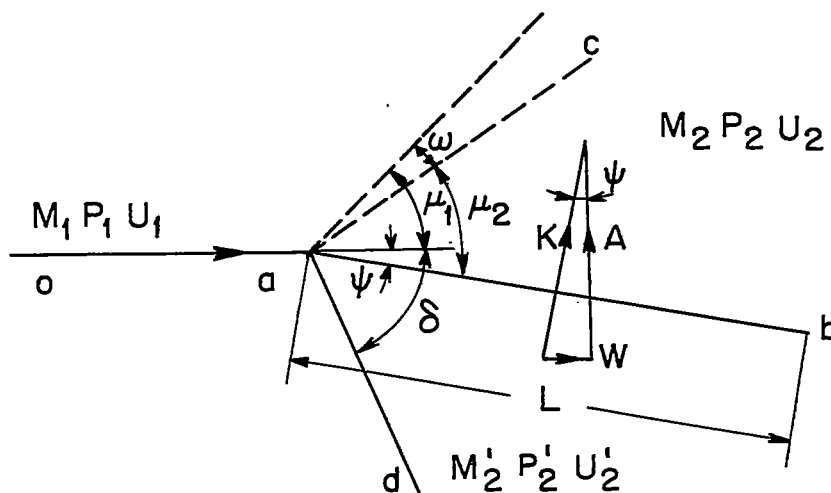


Figure 4.- Flat plate in supersonic flow.

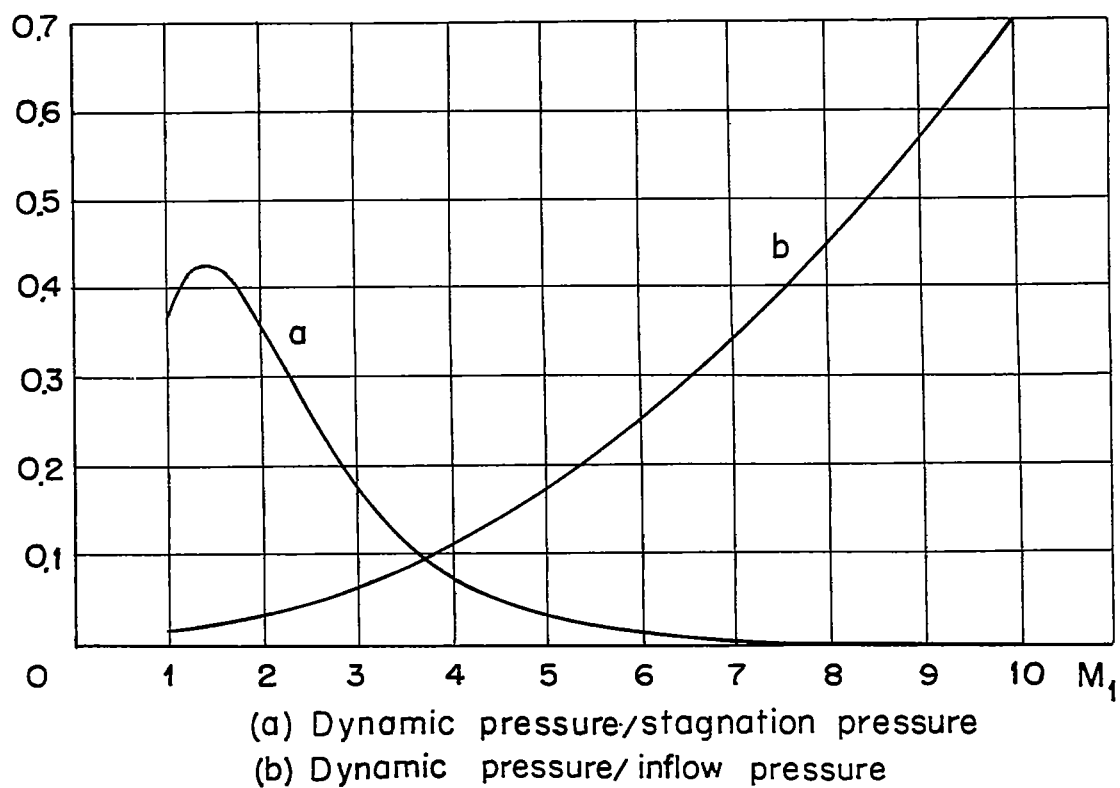


Figure 5.

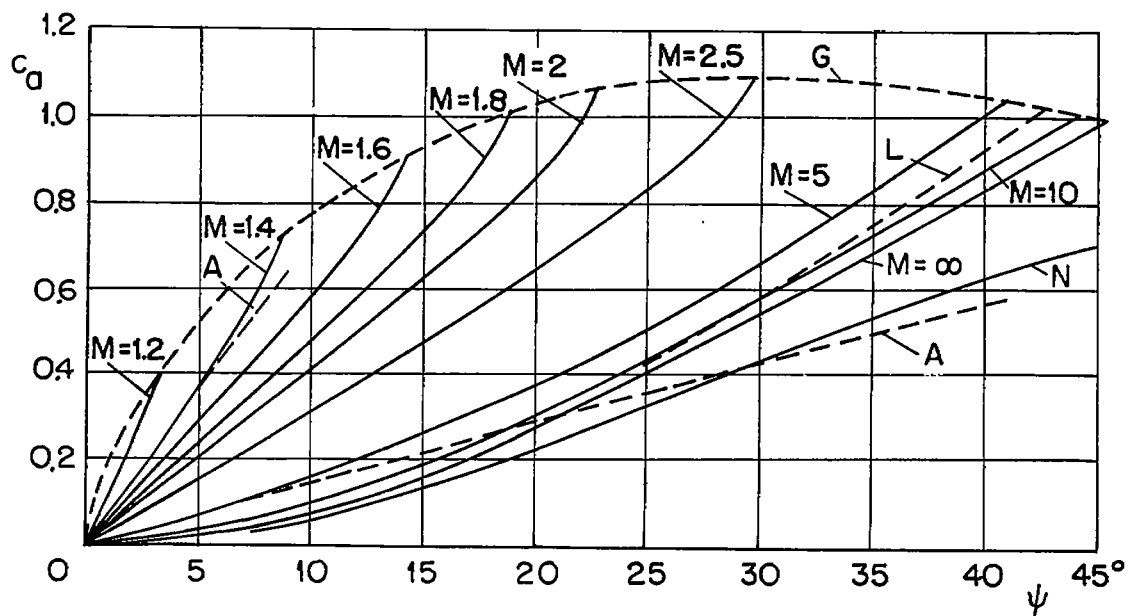


Figure 6.- Lift of the flat plate.

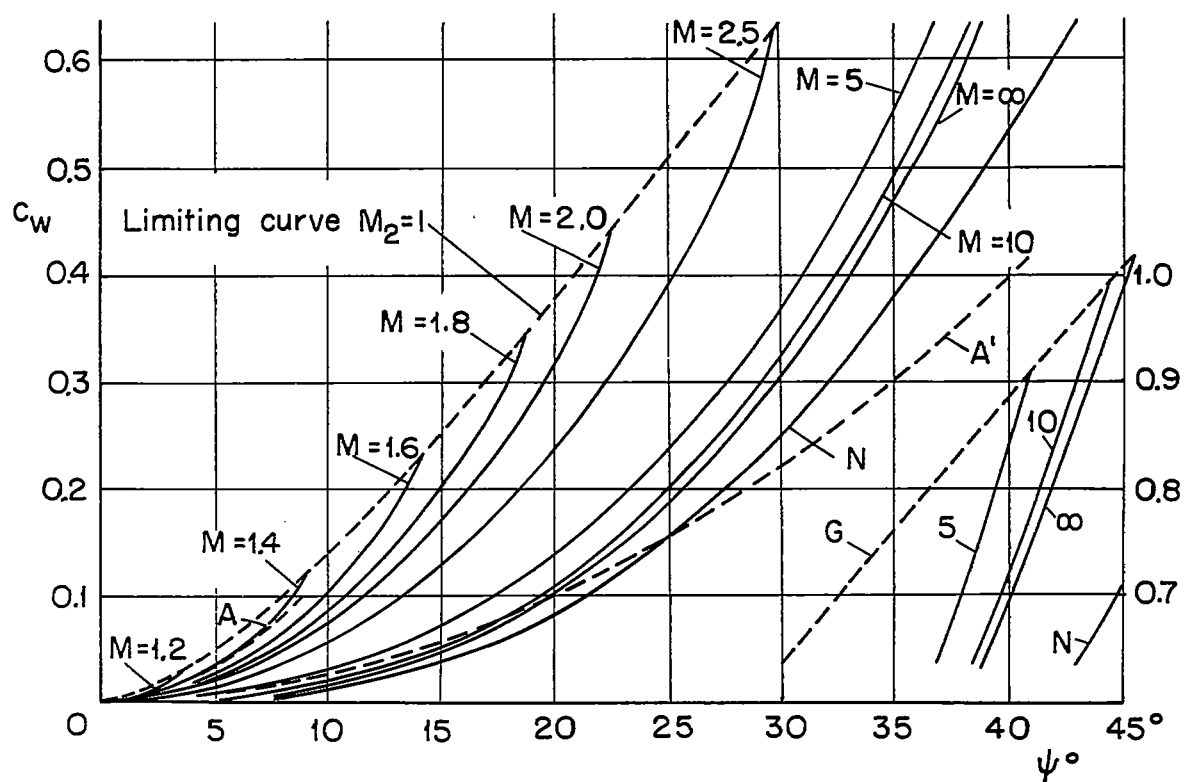


Figure 7.- Drag of flat plate.

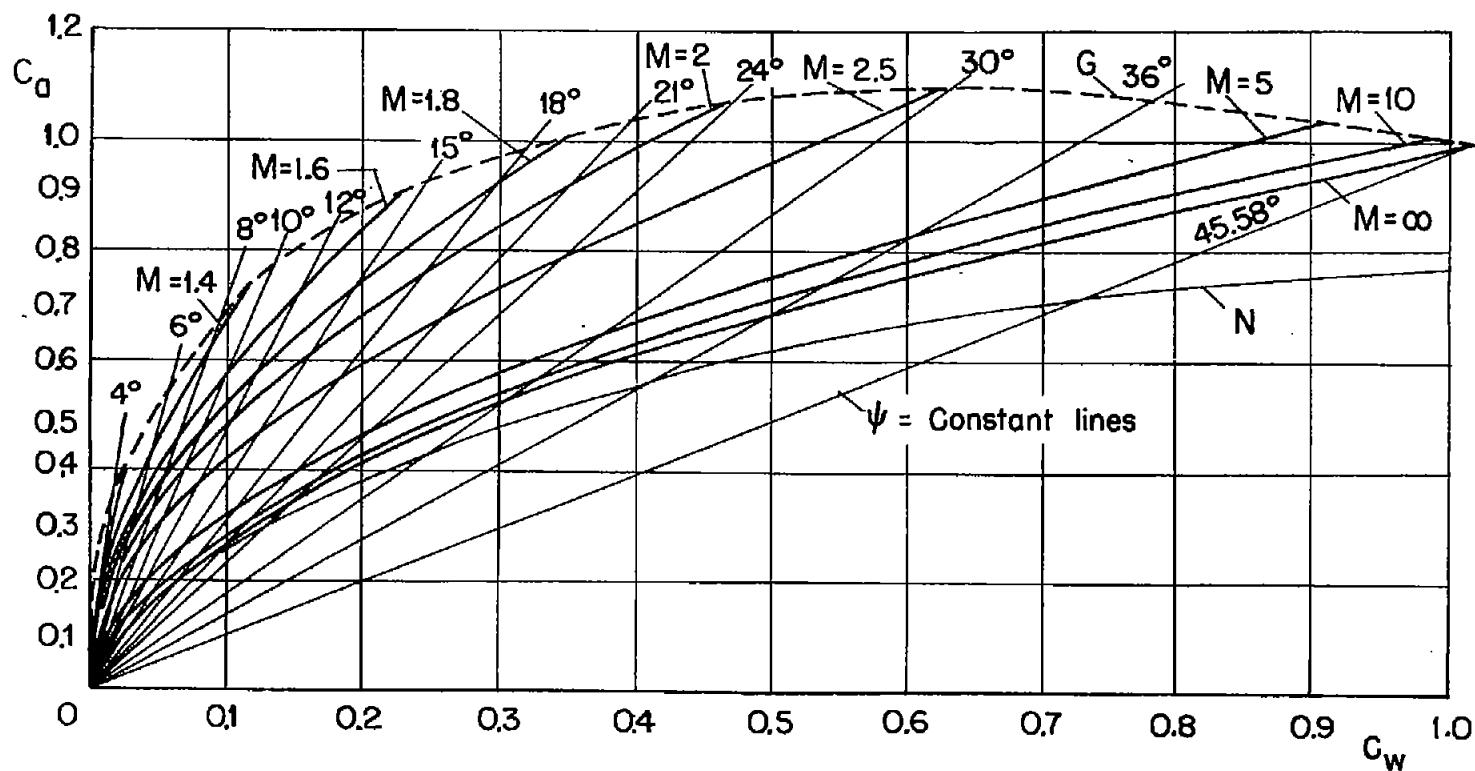


Figure 8.- Polars of flat plate.

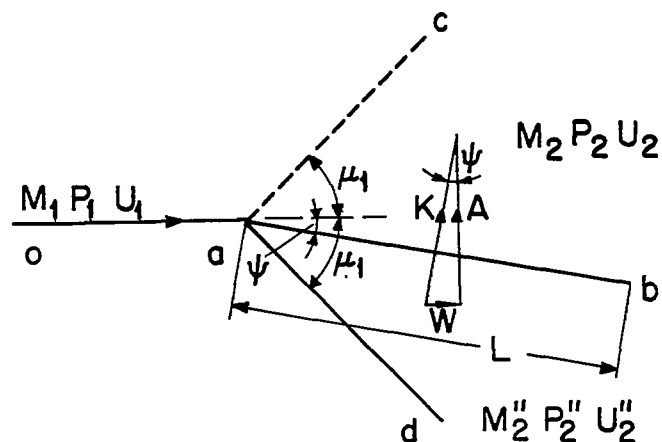


Figure 9.- Flat plate in linearized flow.

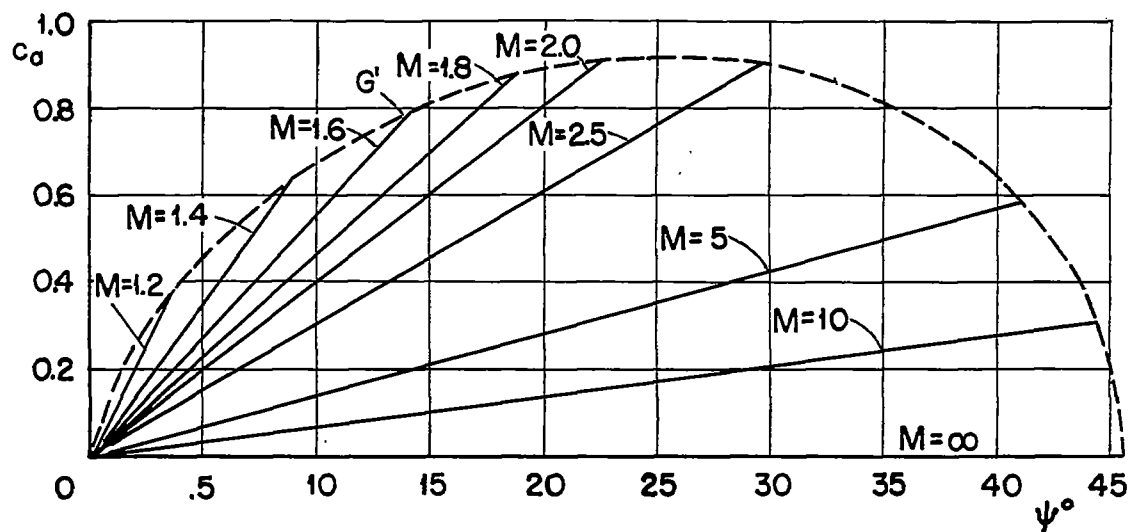


Figure 10.- Lift by linearized theory.

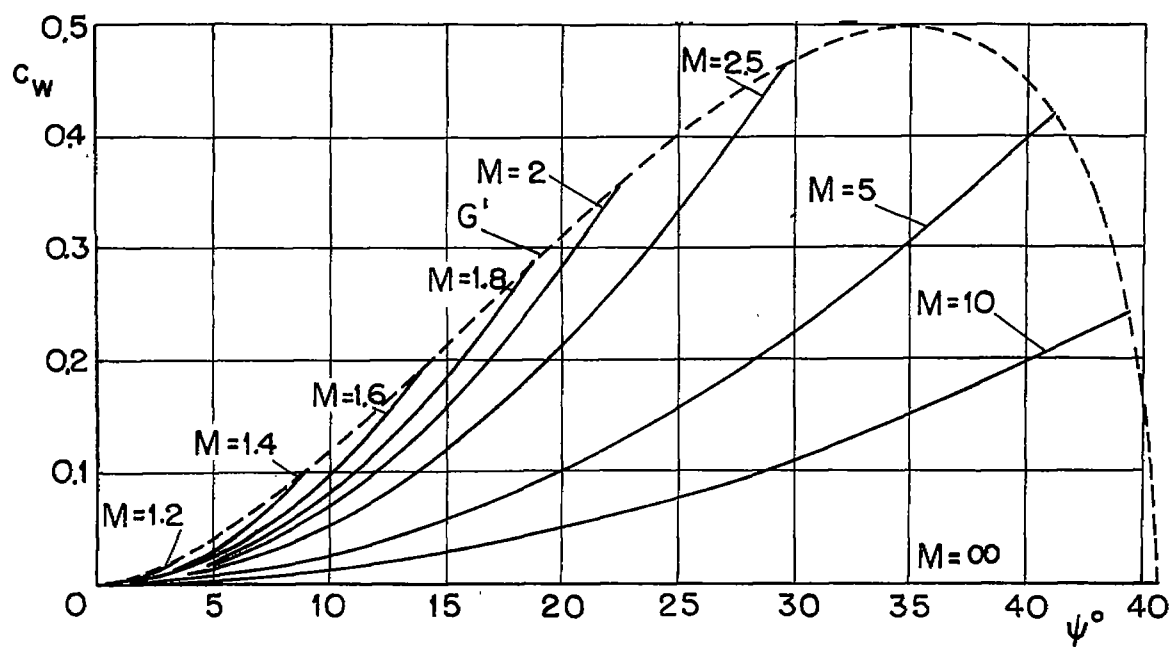


Figure 11.- Drag by linearized theory.

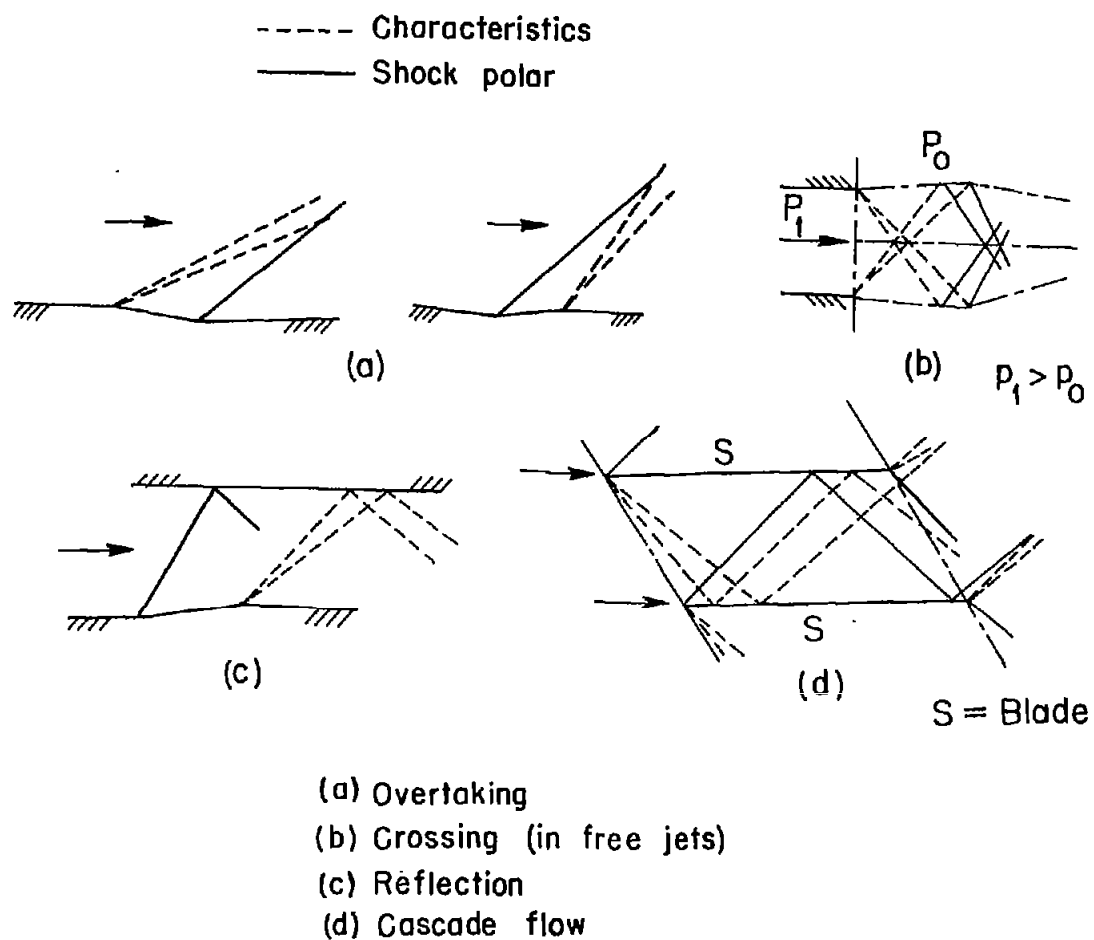


Figure 12.- Interaction between expansion waves and compression shocks.

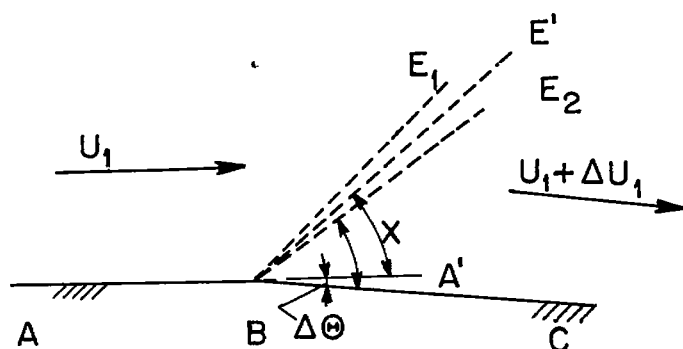


Figure 13.- Small expansion.

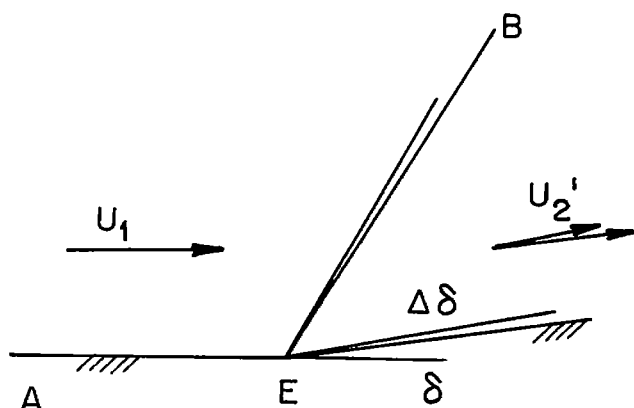


Figure 14.- Small variation for one compression shock.

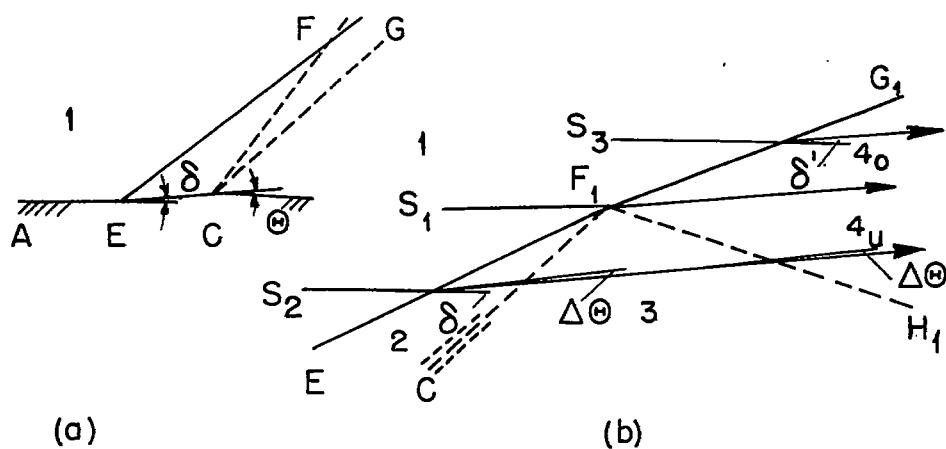


Figure 15.- Compression shock overtaken by expansion wave.

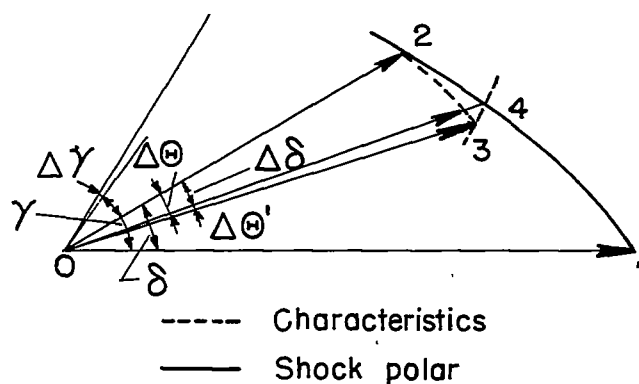


Figure 16.- Schematic representation of the graphical solution.

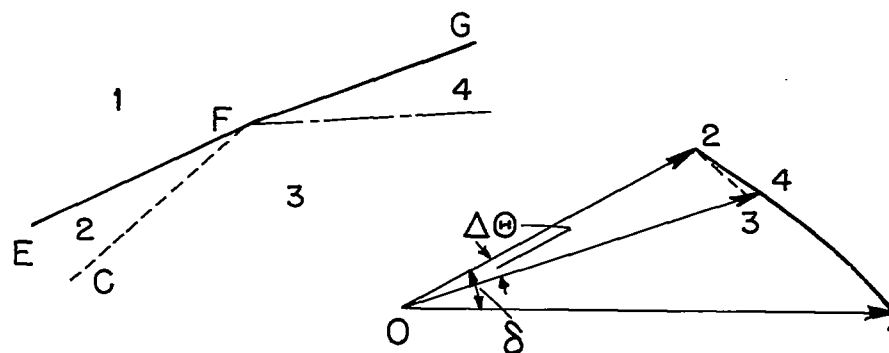


Figure 17.- Reflected wave disregarded.

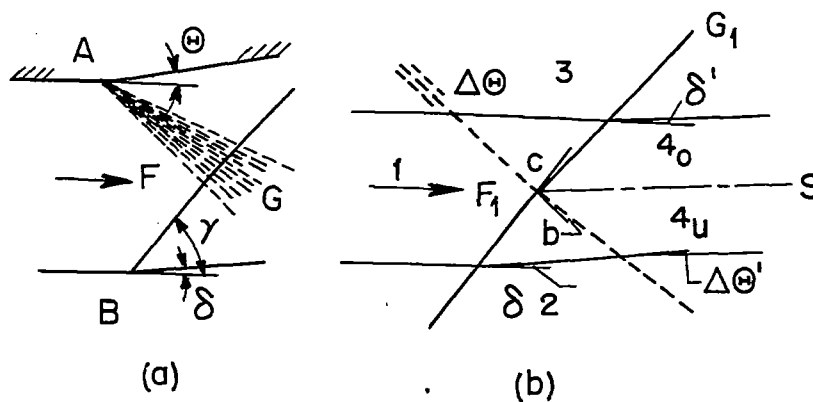


Figure 18.- Expansion wave crosses compression shock.

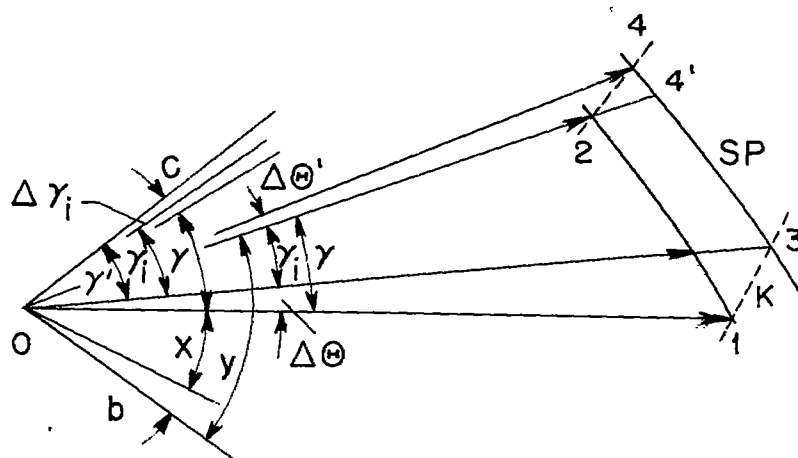


Figure 19.- Schematic representation of graphical solution.

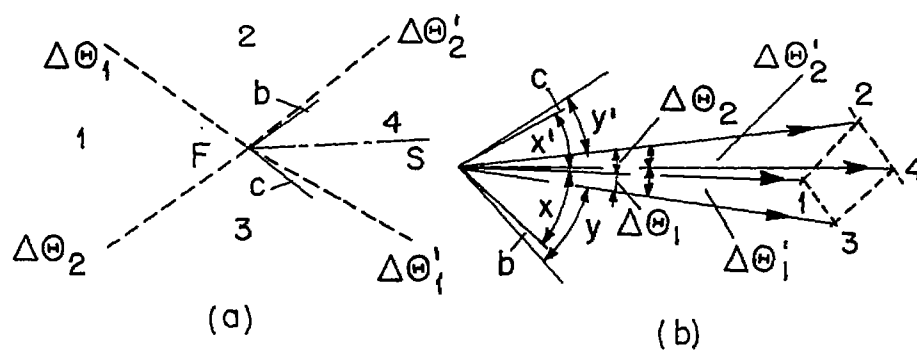


Figure 20.- Crossing of expansion waves.

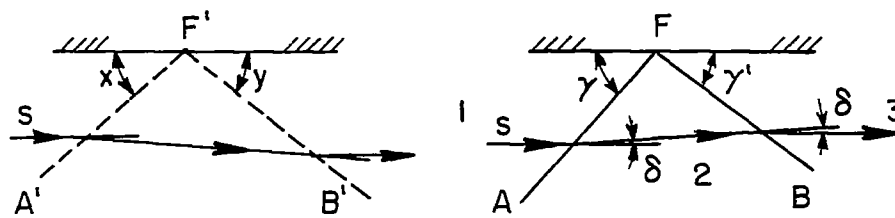


Figure 21.- Reflection of expansion waves and compression shocks.

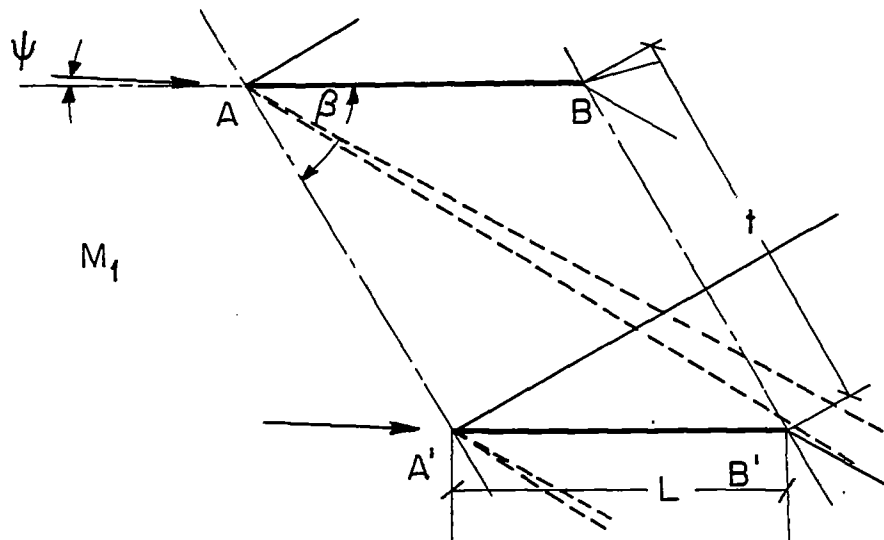


Figure 22.- The cascade problem.

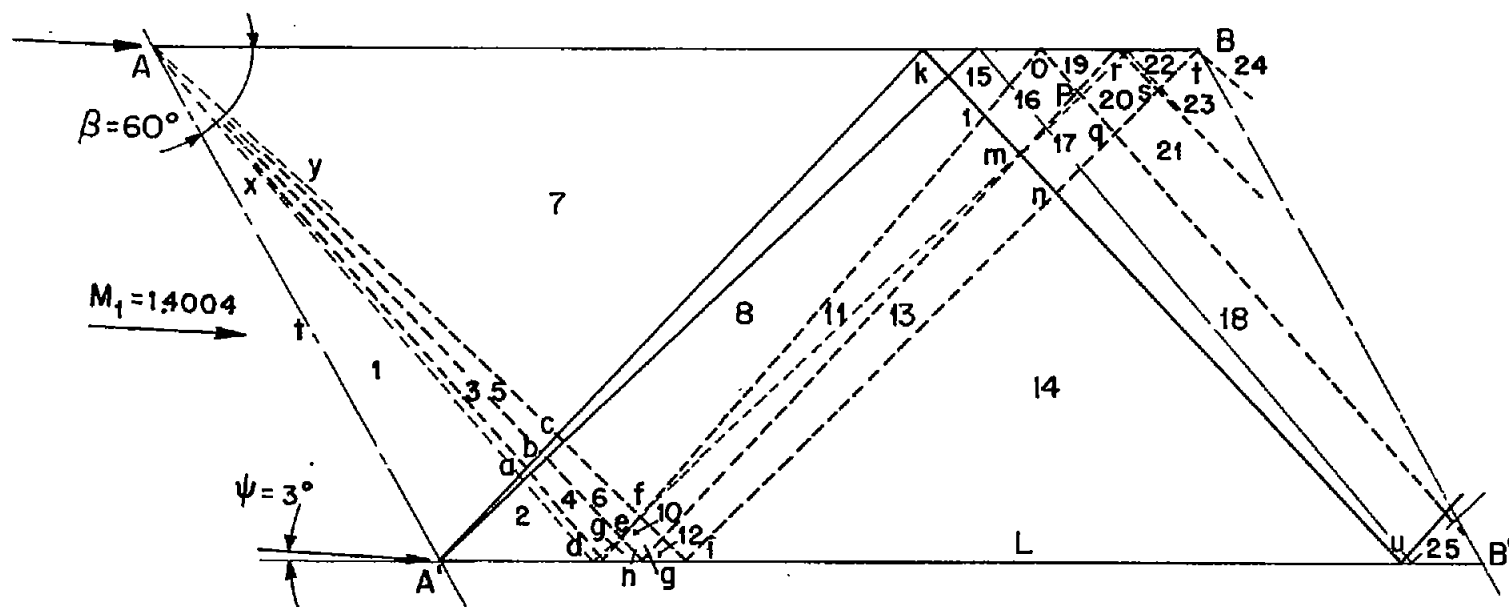


Figure 23.- Cascade example.

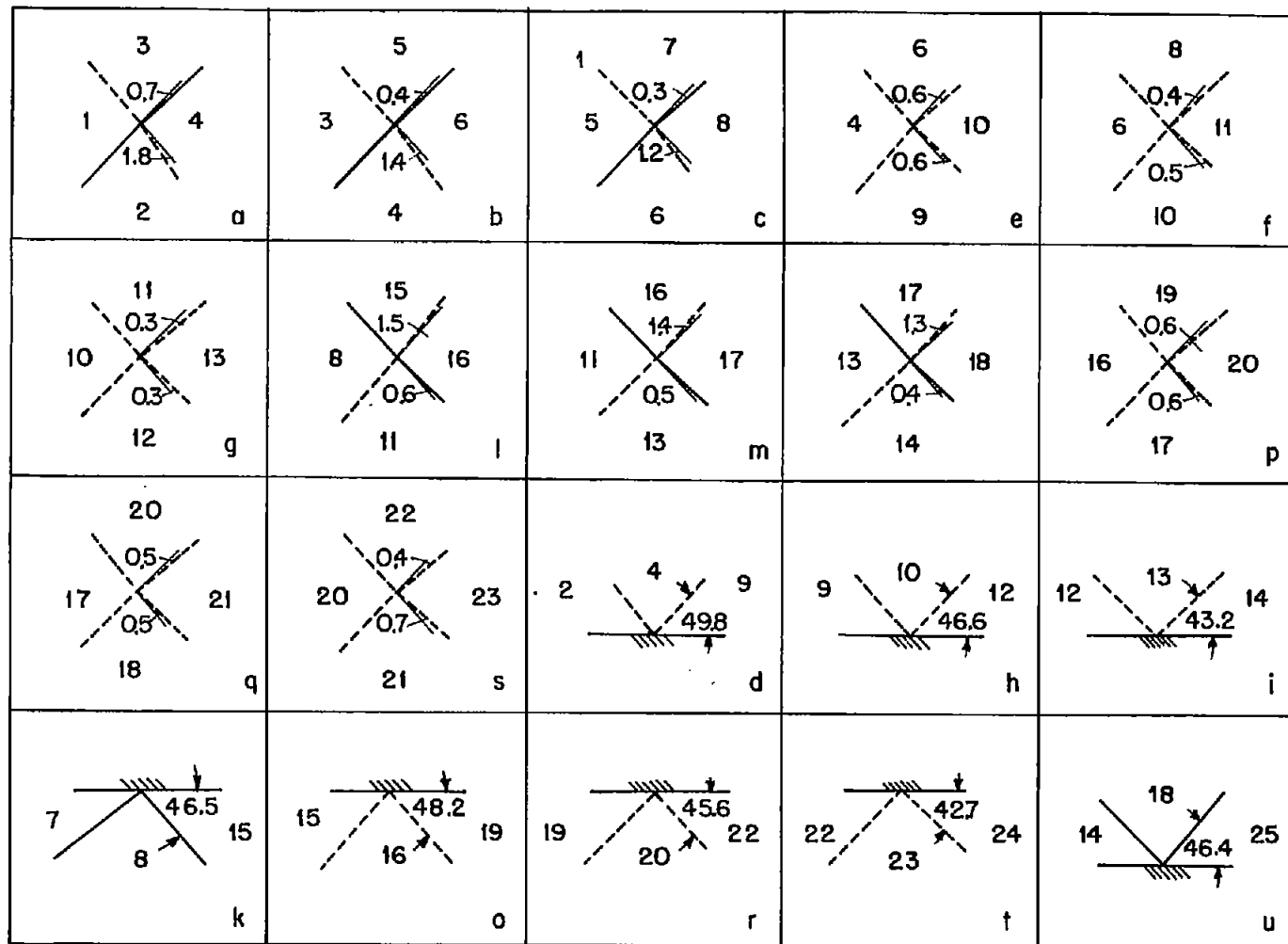


Figure 24.- Directional changes of interference lines of the cascade example. Large digits denote zones; small digits denote directional changes at crossing of expansion waves and compression shocks. At reflections they indicate the direction of the reflected waves; flow always from left to right.

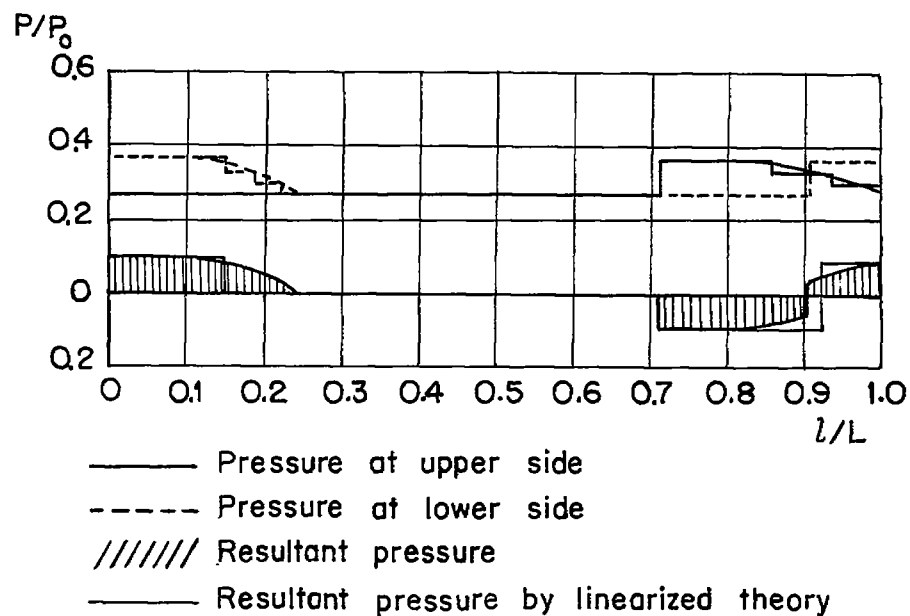


Figure 25.- Pressure variation along the plate (exact method).

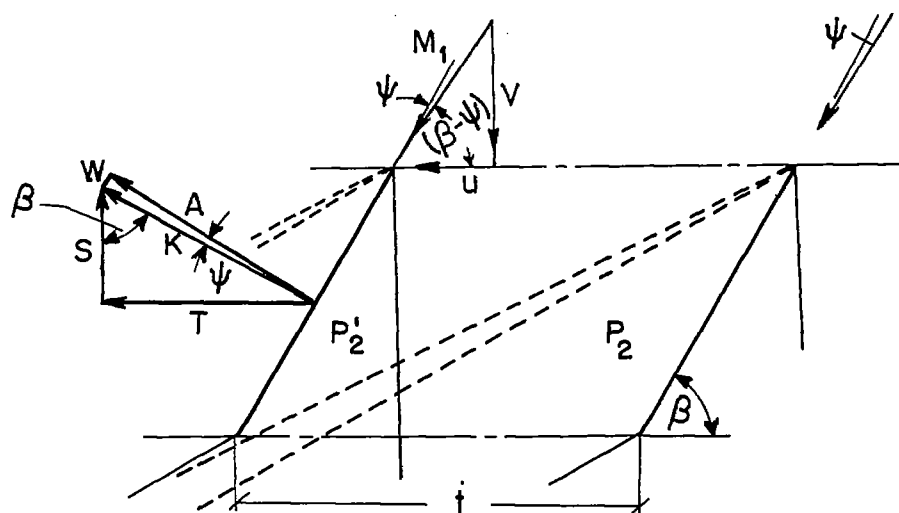


Figure 26.- Definition of thrust and tangential force.

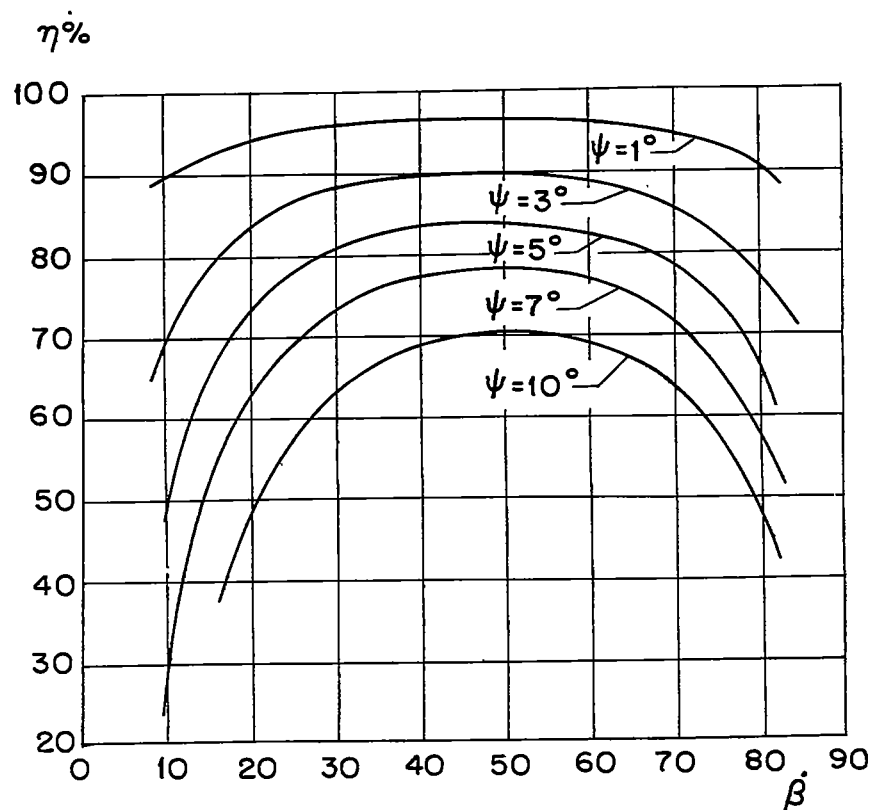


Figure 27.- Cascade efficiency (no friction).

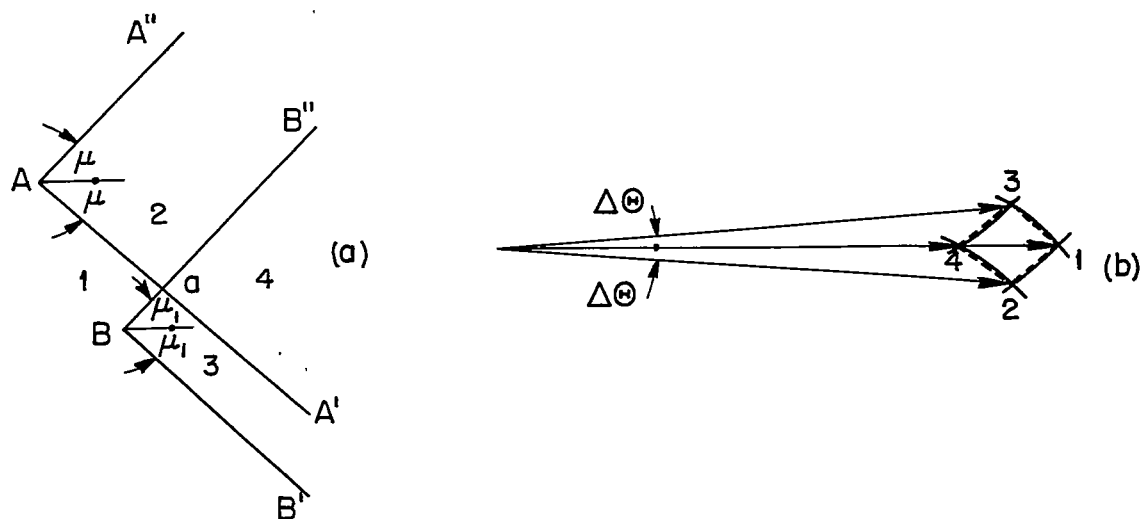


Figure 28.- Linearization of crossing.

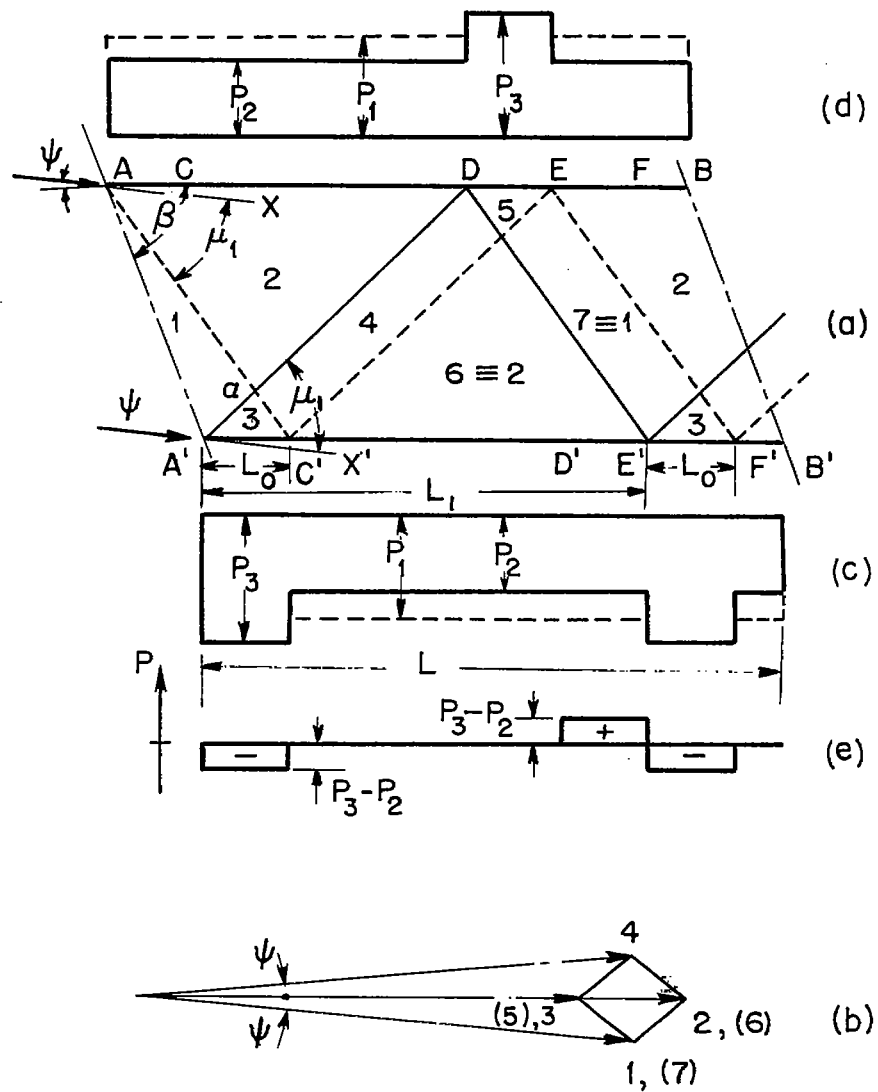


Figure 29.- Linearized cascade theory.

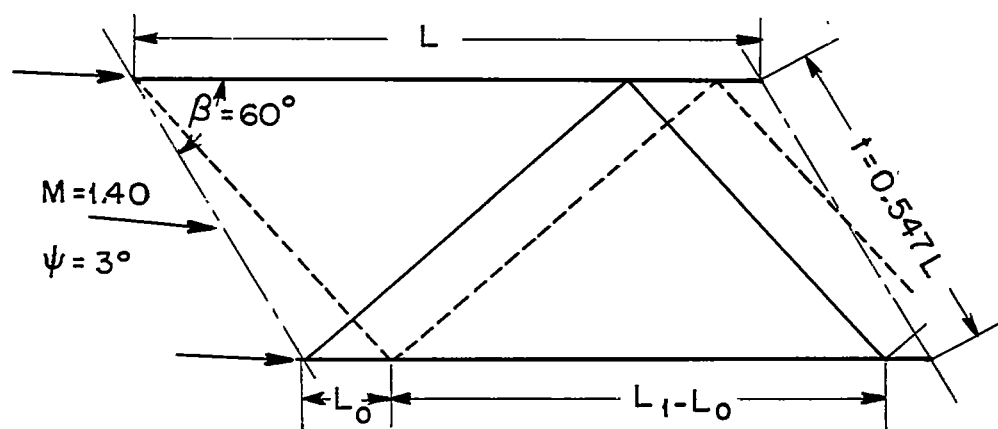


Figure 30.- Numerical example of linearized cascade theory.

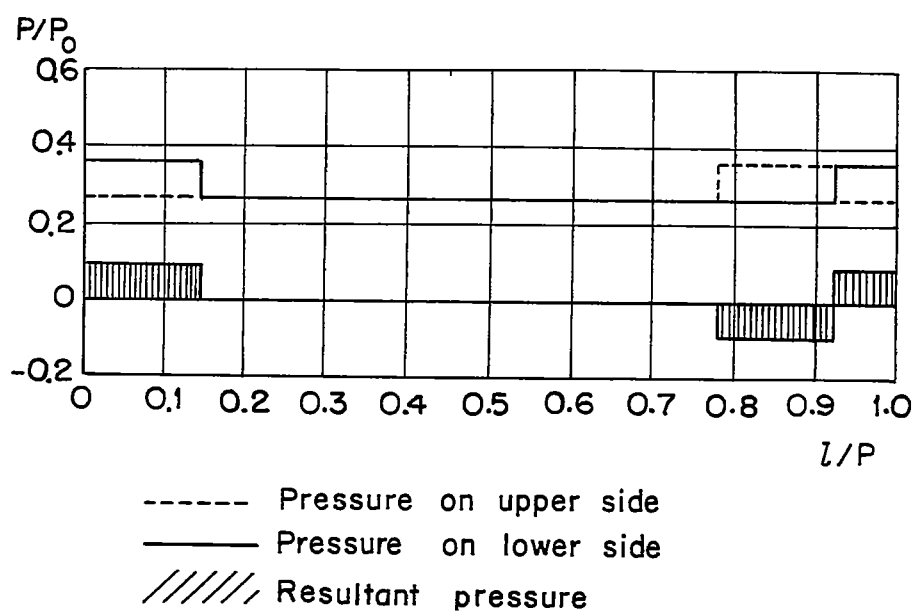


Figure 31.- Pressure distribution over plate by linearized cascade theory.

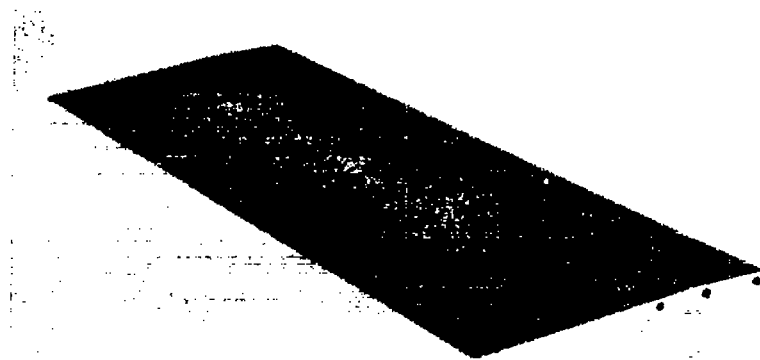


Figure 32.- The profile.

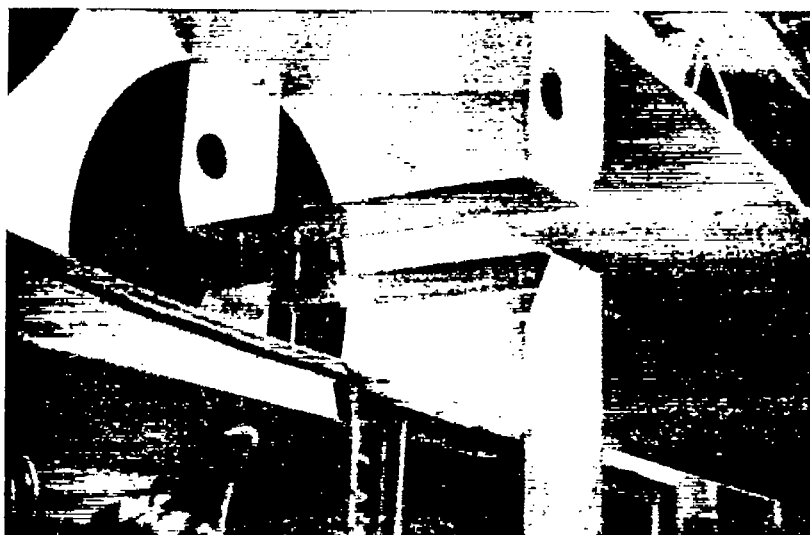
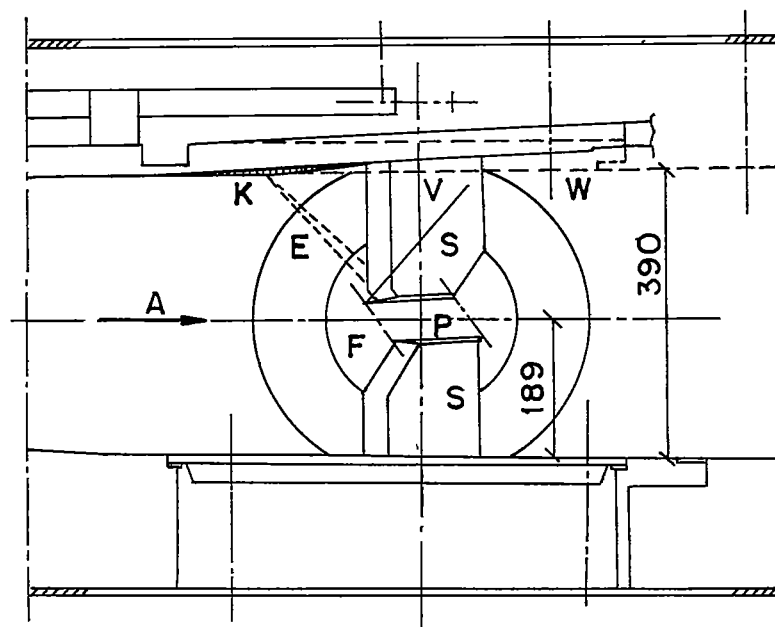


Figure 33.- Profile in test section of tunnel.



- | | | | |
|---|-------------|---|-------------------------------------|
| A | Tunnel axis | S | Supports |
| W | Tunnel wall | V | Compression shock |
| F | Window | K | Bend |
| P | Profiles | E | Expansion branch released from bend |

Figure 34.- Schematic representation of the bend in the upper tunnel wall.

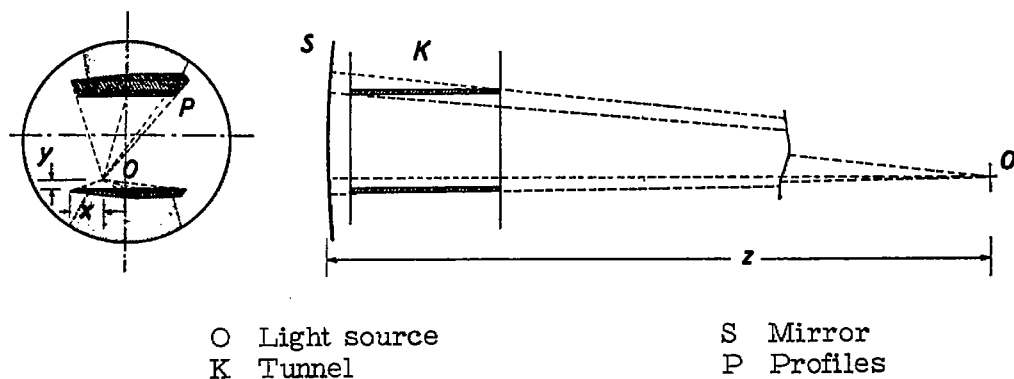


Figure 35.- Position of optical axis and shadow formation. $x = 8$ cm;
 $y = 4.5$ cm; $Z = 300$ cm.

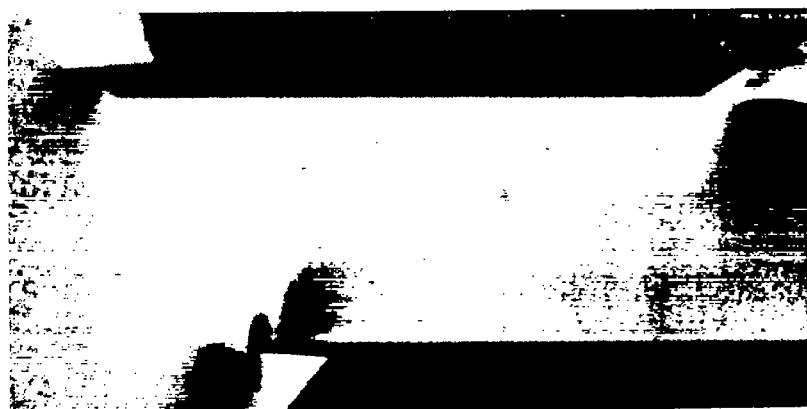


Figure 36.- Profile at starting.

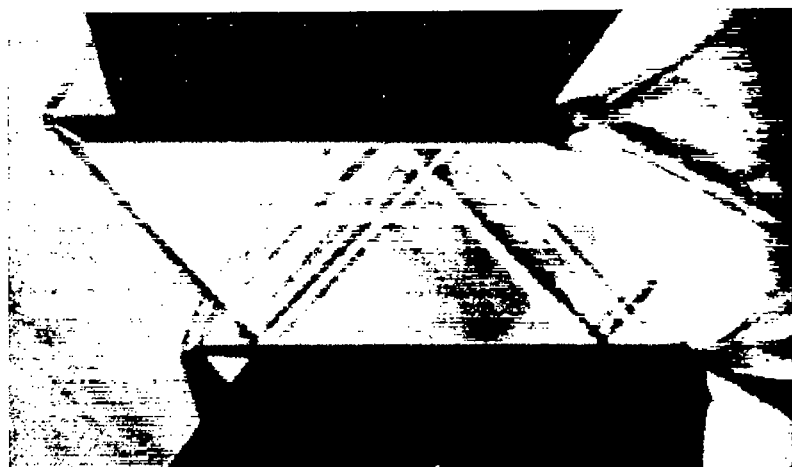


Figure 37.- Schlieren diaphragm vertical. $\psi = 0^\circ$.

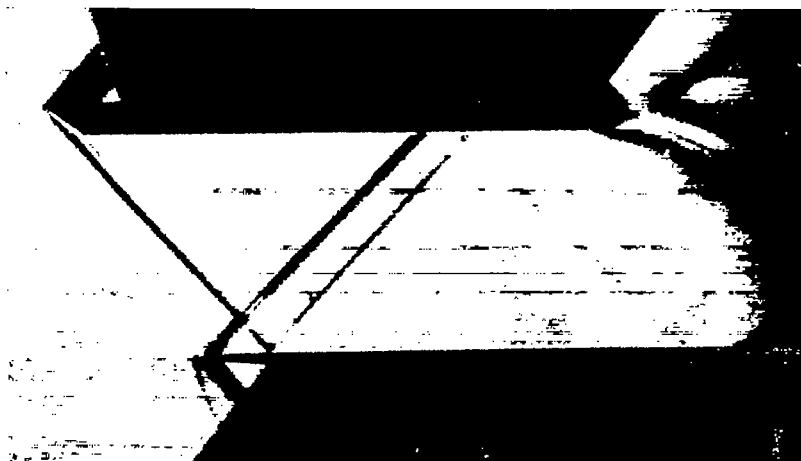


Figure 38.- Schlieren diaphragm vertical. $\psi = 1.5^\circ$.

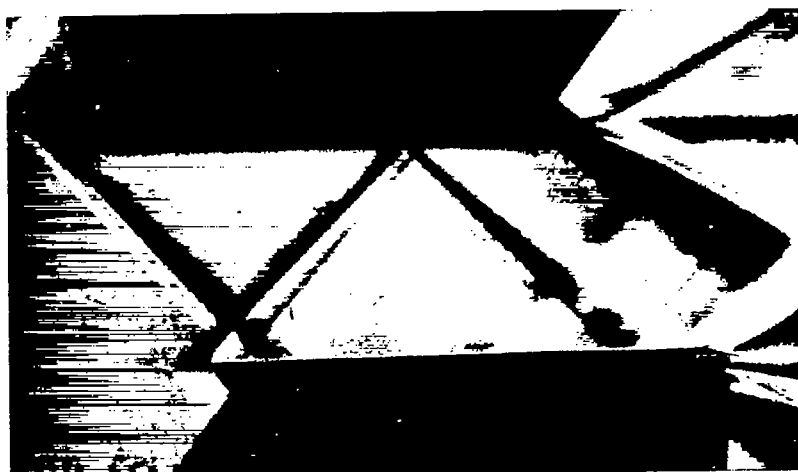


Figure 39.- Schlieren diaphragm horizontal. $\psi = 3.0^\circ$.

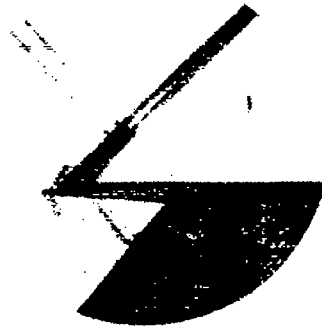


Figure 40.- Photograph of crossing.

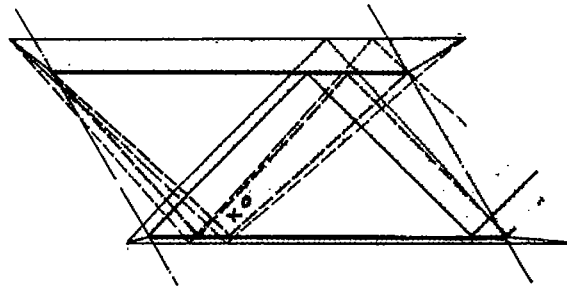


Figure 41.- Perspective distortion of figure 23. For comparison with schlieren photograph in figure 39. (O represents the position of the light source; the finer lines represent the shadow boundaries of the plate and interference lines.)

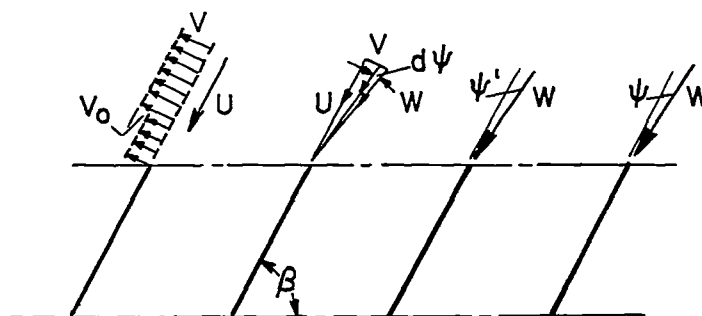


Figure 42.- Sudden change in angle of attack.

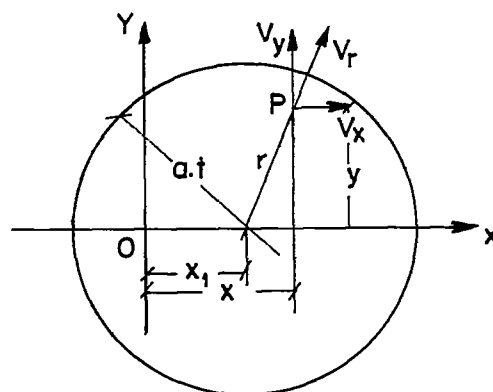


Figure 43.- The unsteady source.

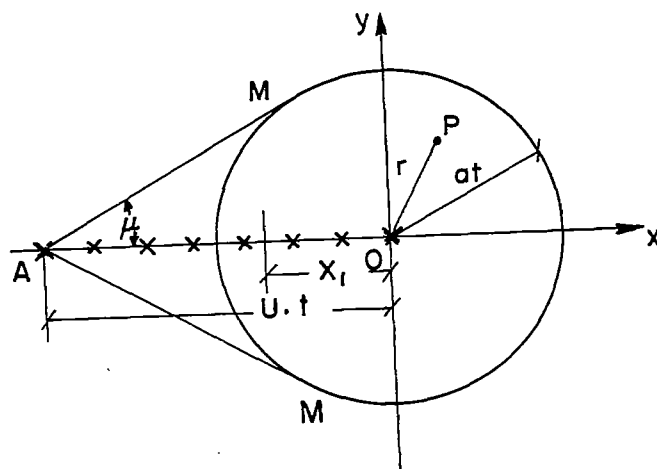


Figure 44.- The periodically created source distribution.

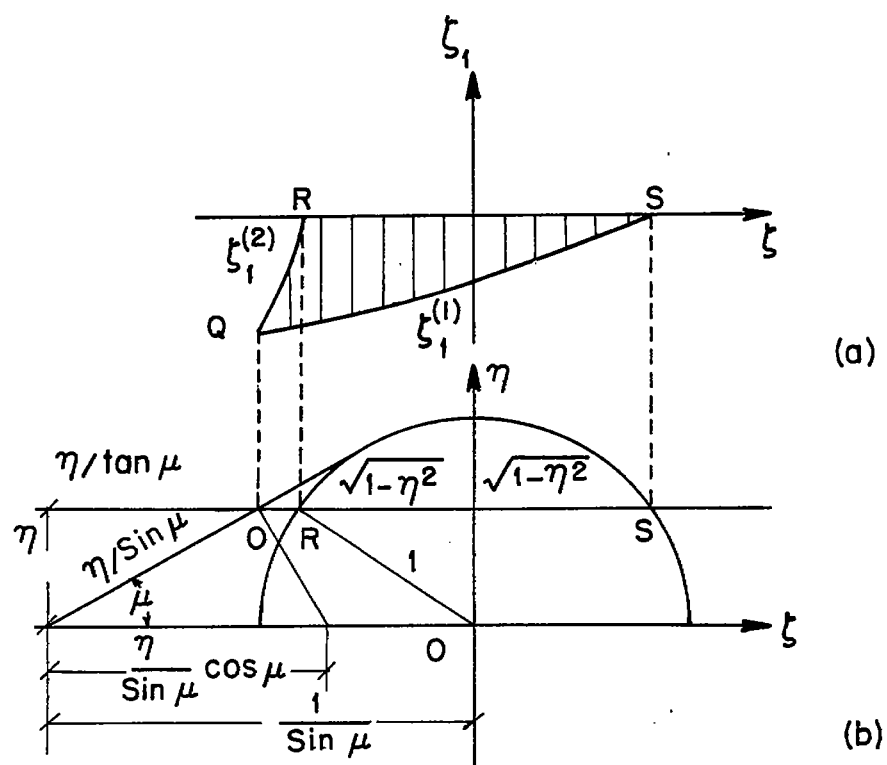
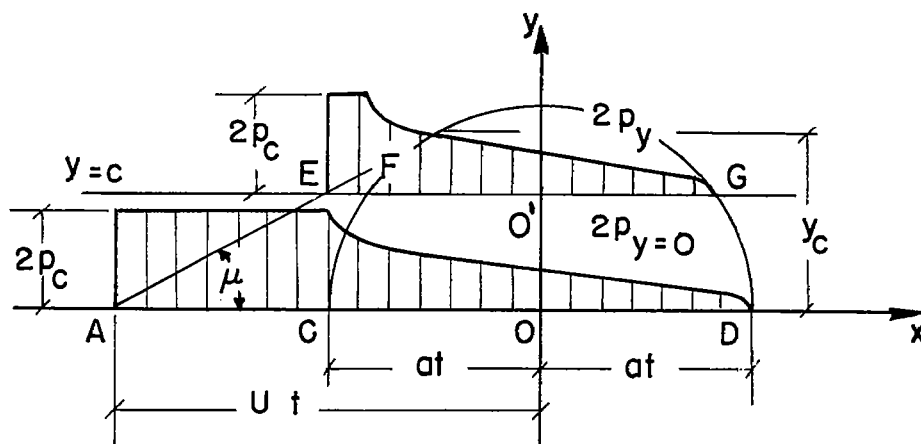


Figure 45.- The integration limit.

Figure 46.- Pressure distribution at $y = \text{constant}$ lines.

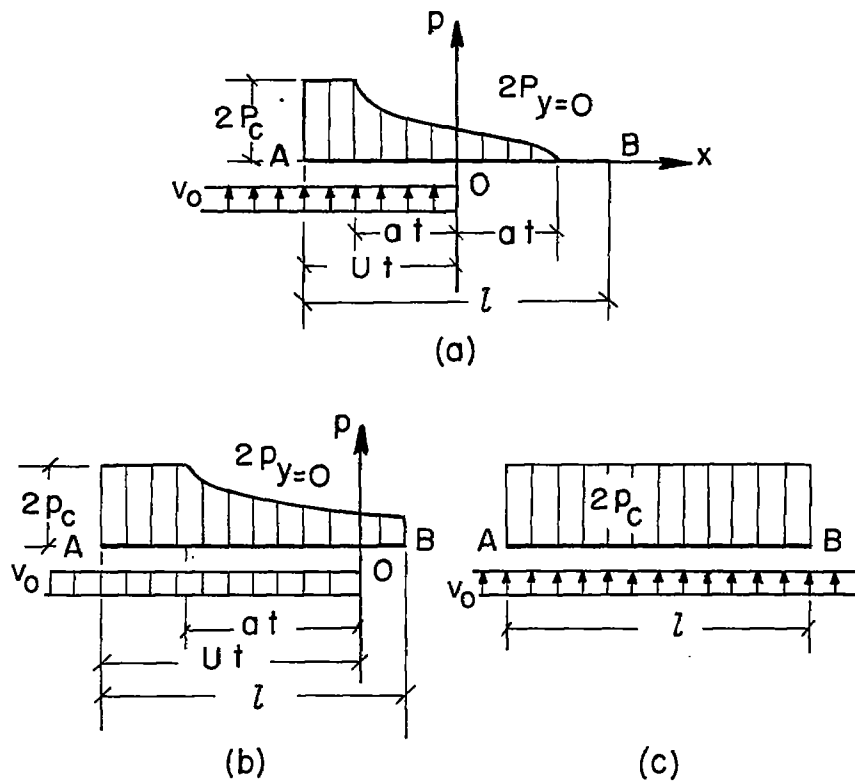


Figure 49.- Pressure distribution along the plate.

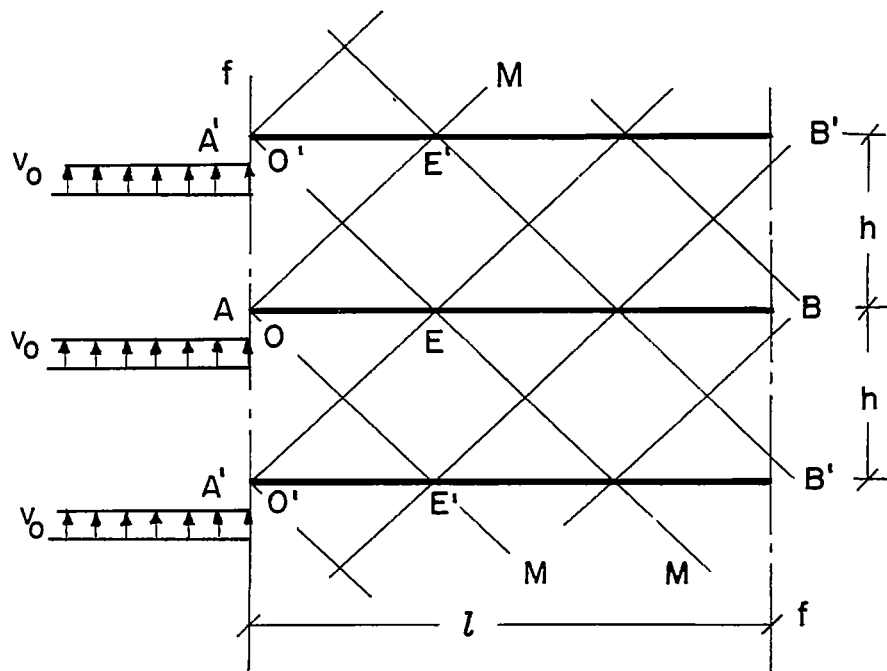


Figure 50.- The straight cascade in vertical gust.

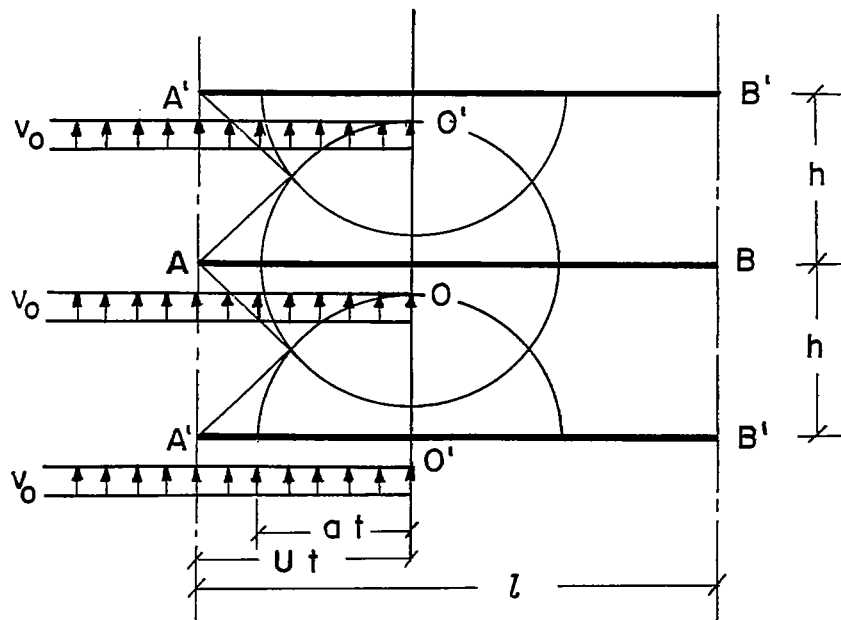


Figure 51.- Start of process.

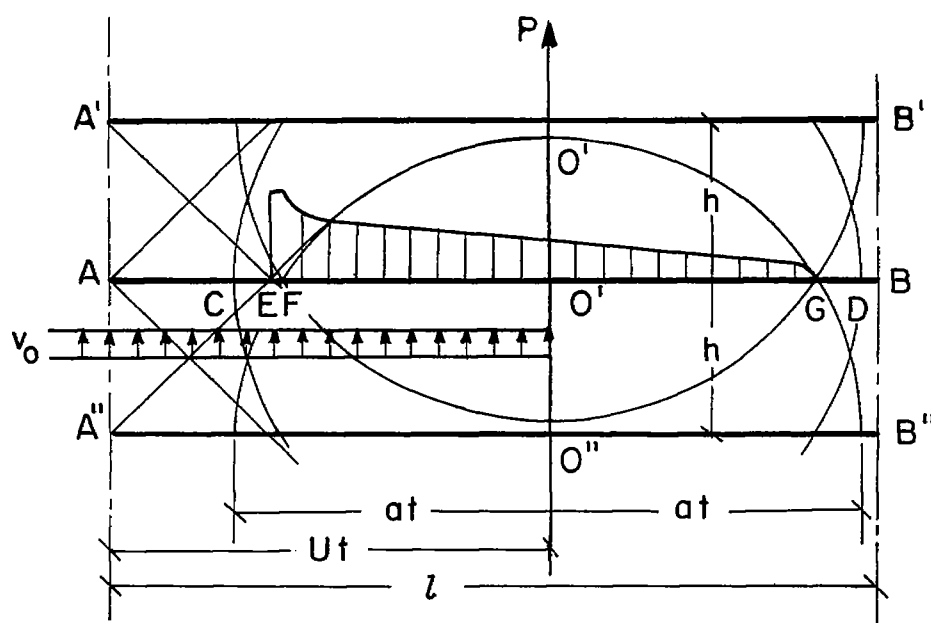
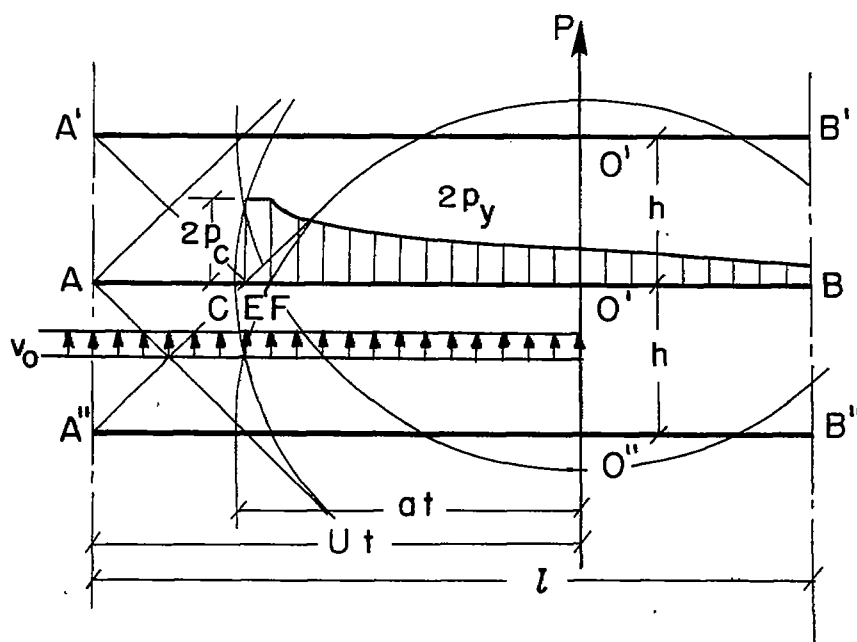
Figure 52.- $t > h/a$.

Figure 53.- Second phase of additional pressure.

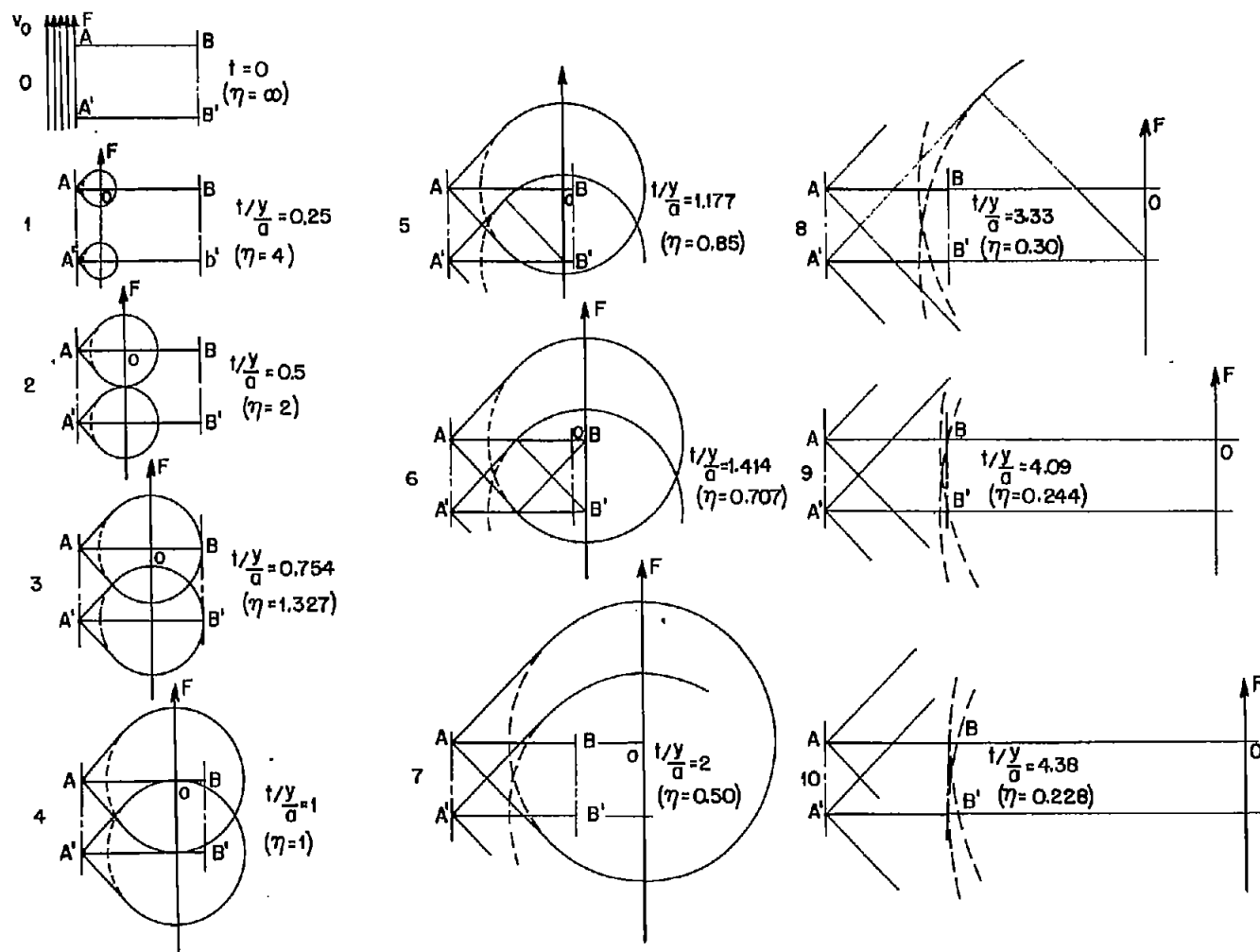
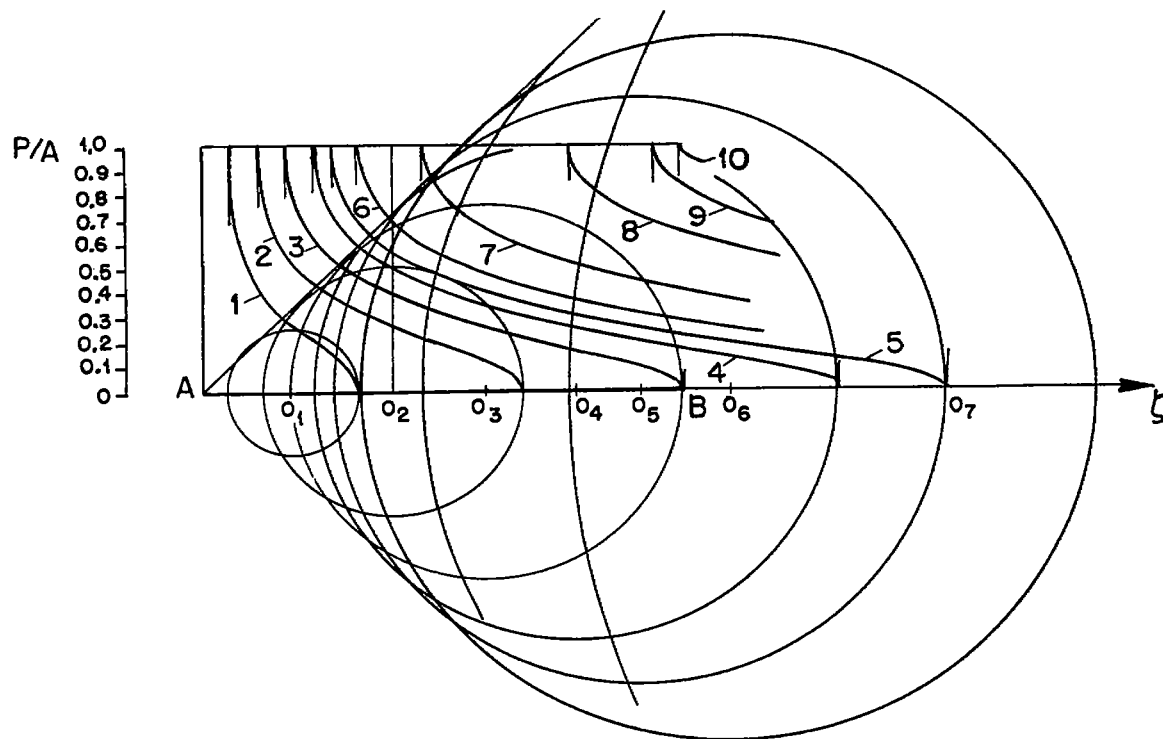
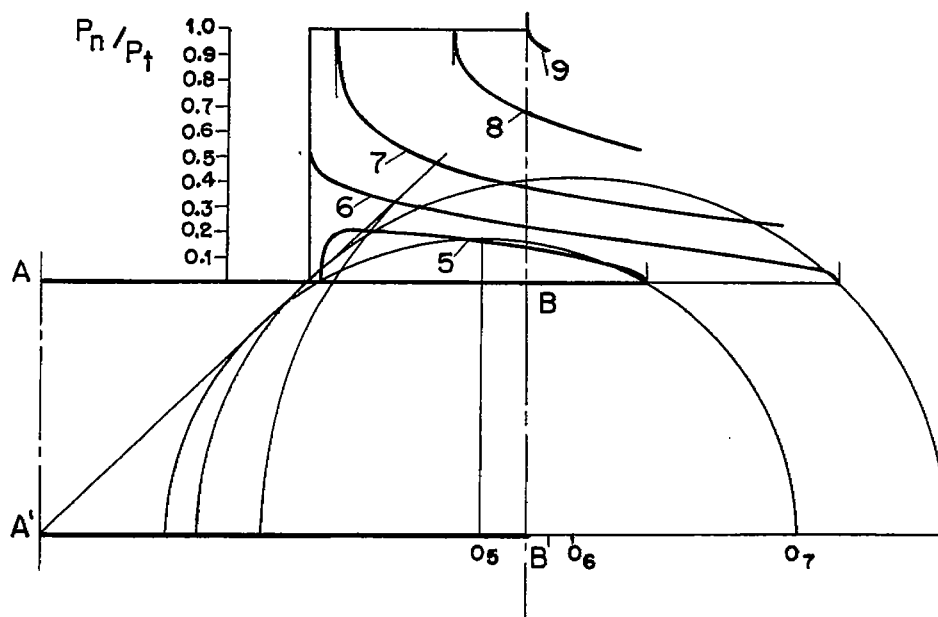


Figure 54.- Location of gust front and disturbed areas at various time intervals.

Figure 55.- Pressure of undisturbed plate p_u .Figure 56.- Pressure contribution p_h .

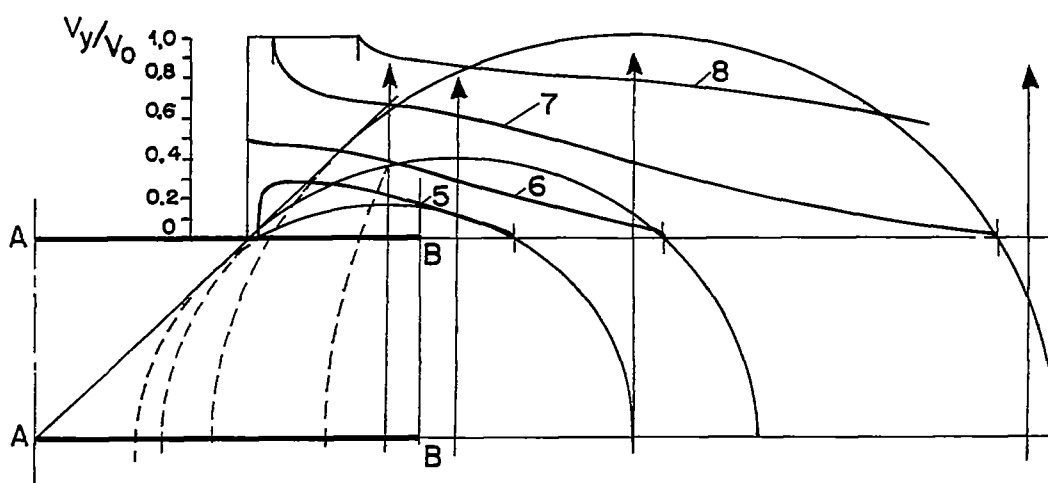


Figure 57.- Velocity distributions v_y/v_0 at times 5, 6, 7, and 8.

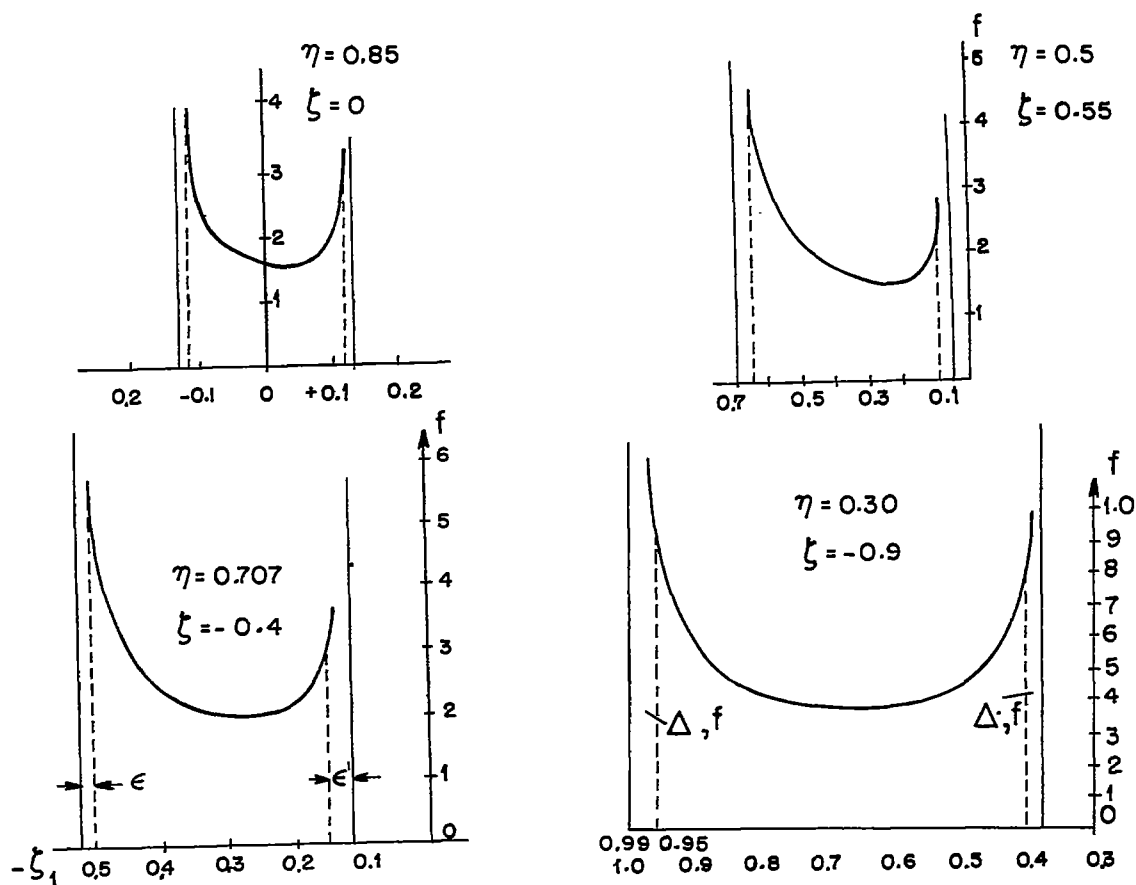


Figure 58.- Functions f for various time intervals.

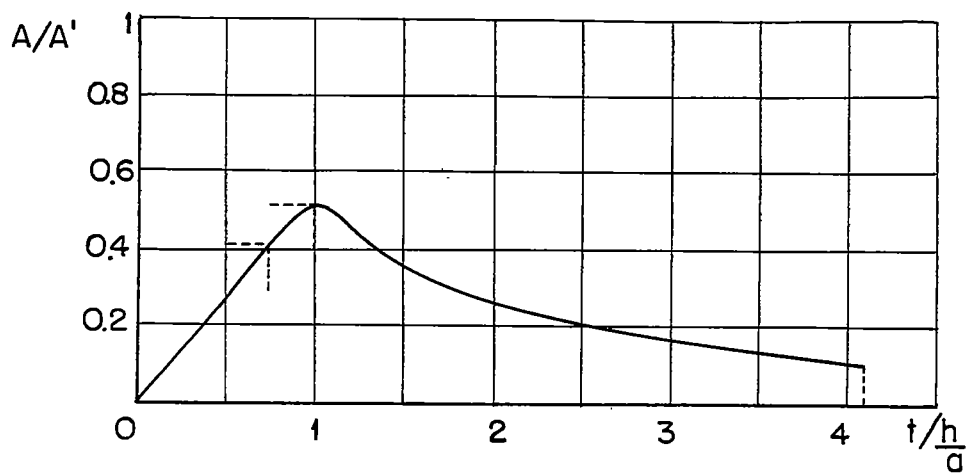
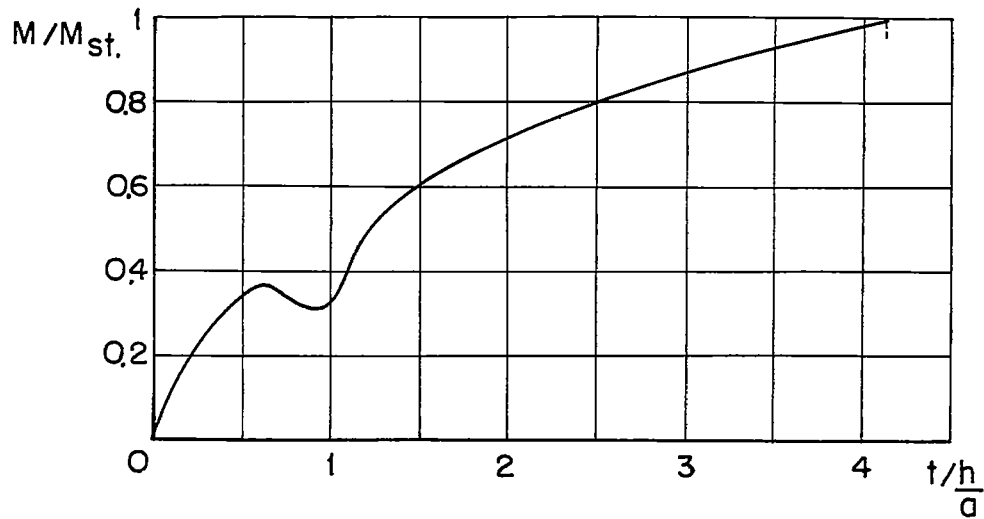


Figure 62.- Lift of plate.

Figure 63.- Moment distribution M referred to plate center.

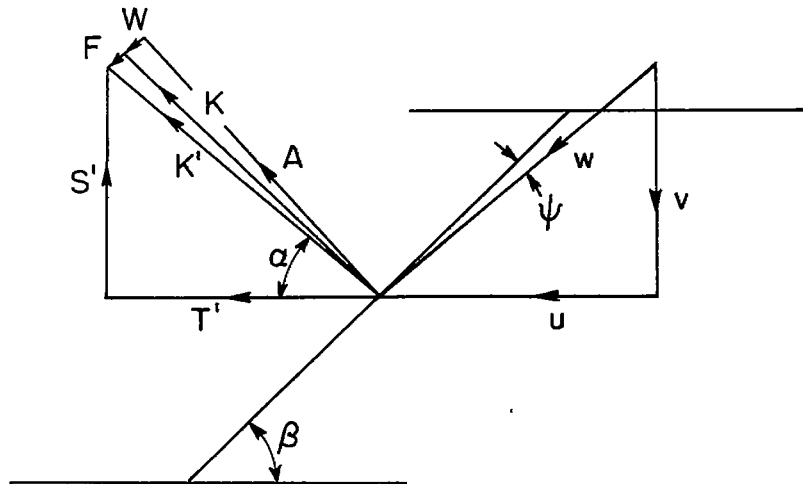
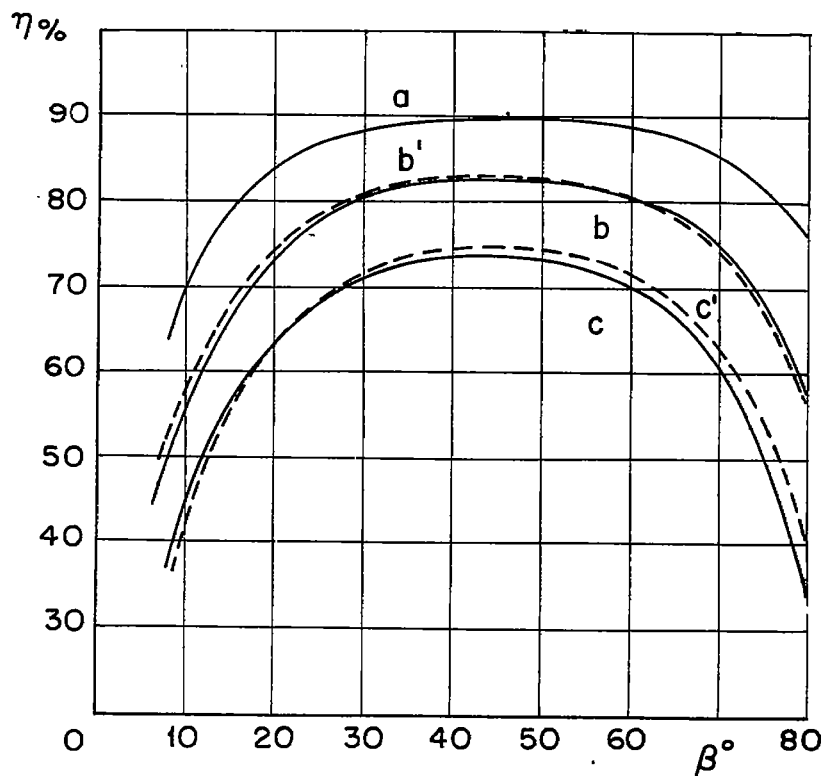


Figure 64.- Allowance for friction.



- (a) No friction.
- (b) With friction. $M = 1.40$, $\psi = 30^\circ$.
- (b') With friction. $M = 1.40$, $\psi = 2.65^\circ$.
- (c) With friction. $M = 2.50$, $\psi = 30^\circ$.
- (c') With friction. $M = 2.50$, $\psi = 4.11^\circ$.

Figure 65.- Cascade efficiency.

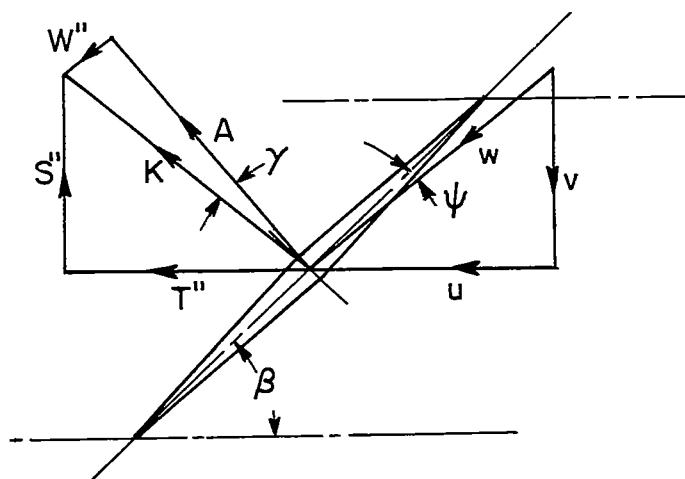


Figure 66.- Allowance of finite thickness ratio.

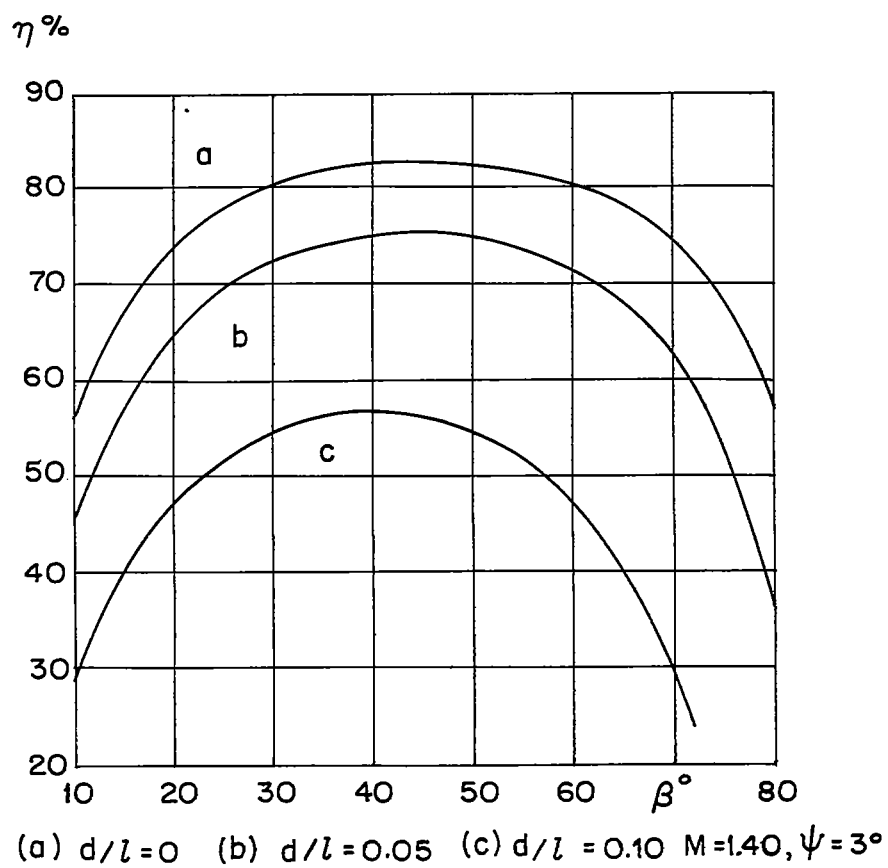


Figure 67.- Efficiency of cascade of double-wedge profiles.

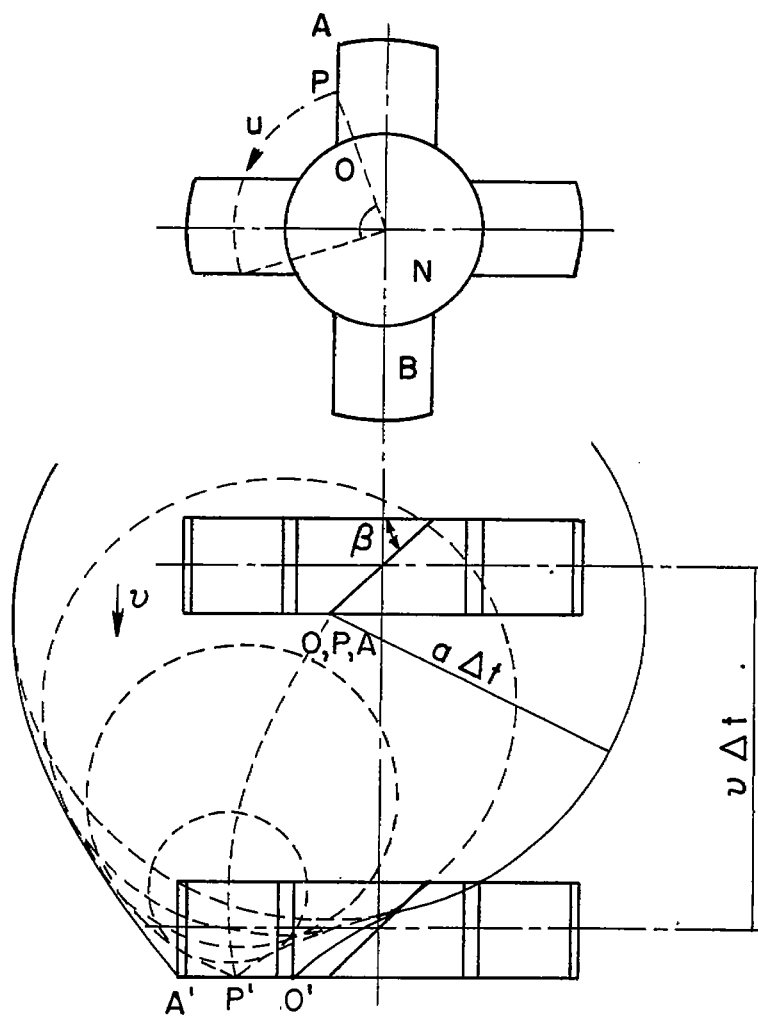


Figure 68.- Area disturbed by leading edge of a blade assumed as flat plate.

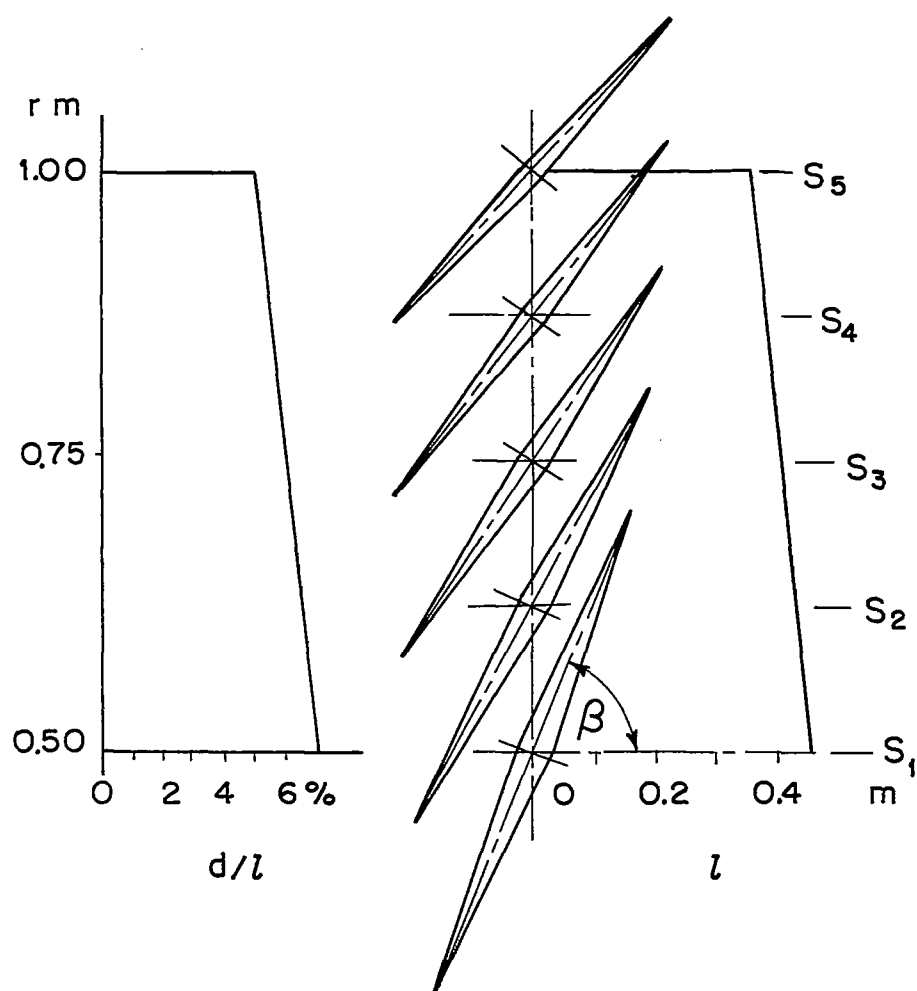


Figure 69.- Blade chord, maximum thickness, stagger, and location of cross sections.

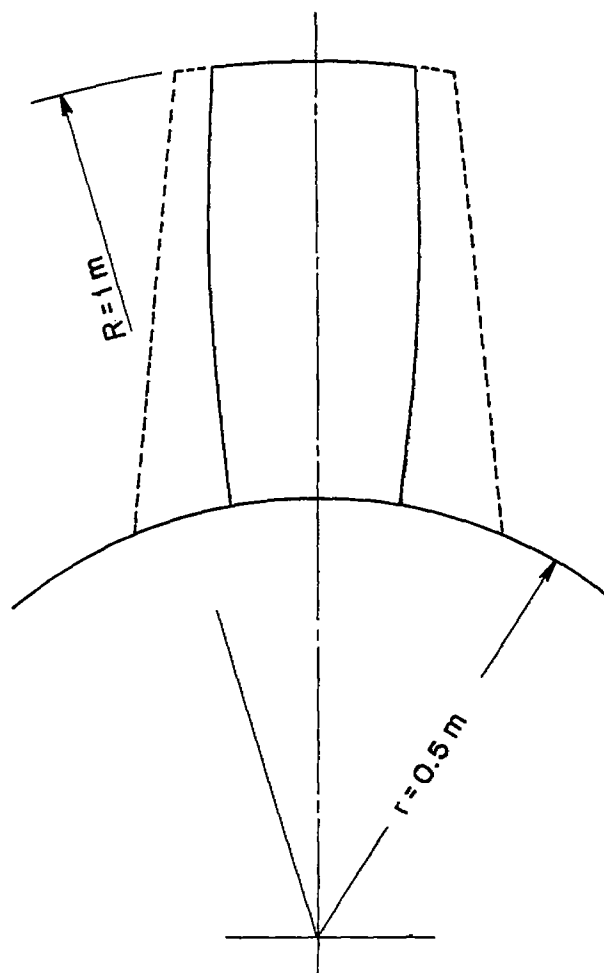
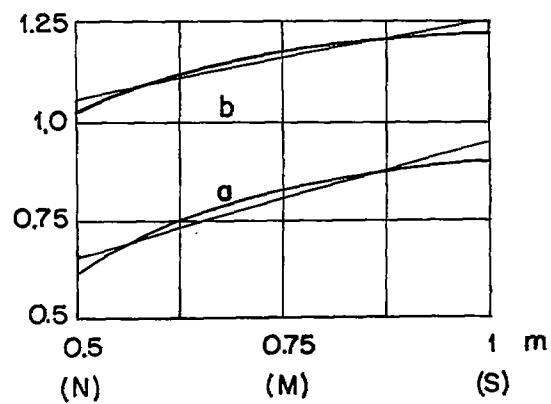


Figure 70.- Blade form, blade form without angular rotation.



(a) $dS/dr \times 10^{-3} \text{ kg/m}$. (b) $dD/dr \times 10^{-3} \text{ kg}$.

Figure 71.